5-2022

The roles of PON2 in mitochondrial physiology, lung tumor cell proliferation, and lung tumorigenesis.

Aaron Whitt
University of Louisville

Follow this and additional works at: https://ir.library.louisville.edu/etd

Part of the Cancer Biology Commons, Laboratory and Basic Science Research Commons, and the Other Pharmacology, Toxicology and Environmental Health Commons

Recommended Citation

THE ROLES OF PON2 IN MITOCHONDRIAL PHYSIOLOGY, LUNG TUMOR
CELL PROLIFERATION, AND LUNG TUMORIGENESIS

By

Aaron Whitt
B.S., Morehead State University, 2010
M.S., University of Louisville, 2019

A Dissertation
Submitted to the Faculty of the
School of Medicine of the University of Louisville
in Partial Fulfillment of the Requirements
for the Degree of

Doctor of Philosophy
in Pharmacology and Toxicology

Department of Pharmacology and Toxicology
University of Louisville
Louisville, Kentucky

May 2022

THE ROLES OF PON2 IN MITOCHONDRIAL PHYSIOLOGY, LUNG TUMOR
CELL PROLIFERATION, AND LUNG TUMORIGENESIS

By

Aaron Gregory Whitt
B.S., Morehead State University, 2010
M.S., University of Louisville, 2019

A Dissertation Approved on

March 29, 2022

By the following Dissertation Committee:

_____
Chi Li, Ph. D.

_____
Levi Beverly, Ph. D.

_____
Geoffrey Clark, Ph. D.

_____
Brian Clem, Ph. D.

_____
Robert Mitchell, Ph. D.

DEDICATION

     This dissertation is dedicated to my family, friends, educators, and colleagues who lent me the support necessary to achieve my ambitions: First and foremost, my wife, Kelly, whose endless love and encouragement empowers me on a daily basis; To my family, for their unwavering confidence in my abilities; To my friends, for providing solace and celebration; To current and former faculty members, for sparking and fortifying my curiosity; To my colleagues, for their technical and conceptual assistance. Without these contributions, this project would have been impossible.

ACKNOWLEDGMENTS

ABSTRACT

THE ROLES OF PON2 IN MITOCHONDRIAL PHYSIOLOGY, LUNG TUMOR

CELL PROLIFERATION, AND LUNG TUMORIGENESIS

Aaron Whitt

March 29, 2022

Paraoxonase 2 (PON2) is an intracellular, multifunctional enzyme with near-ubiquitous tissue distribution. Within cells, PON2 is localized to mitochondria and endoplasmic reticulum (ER), where it mitigates the formation of reactive oxygen species (ROS). PON2's chief enzymatic function is its lactonase activity, through which it catalyzes the hydrolysis of a bacterial quorum-sensing molecule, N-(3-oxododecanoyl)-l-homoserine lactone (C12), effectively disrupting bacterial intercellular communication and protecting against infection. C12 is produced by the opportunistic pathogen *Pseudomonas aeruginosa* and has been shown to disrupt various aspects of eukaryotic host cell physiology and evoke apoptotic cell death through the activity of PON2. Additionally, PON2 has garnered growing attention for its potential role in human cancers. Recent research has demonstrated that PON2 confers apoptotic resistance to tumor cells *in vitro* and is upregulated in a variety of solid and hematologic cancers. However, the detailed mechanisms by which PON2 facilitates these phenotypes remains unclear. The

following dissertation explores PON2's influence on airway mitochondrial physiology in response to C12, lung tumor cell metabolism, and *in vivo* lung tumorigenesis. Herein, we demonstrate that below a cytotoxic threshold, C12 disrupts mitochondrial metabolism and network morphology to hinder the cell proliferation of murine tracheal epithelial cells in a PON2-dependent manner. Furthermore, we show that loss of PON2 expression selectively impairs lung adenocarcinoma cell proliferation by exacerbating the production of ROS and compromising cellular bioenergetics. Finally, we examined PON2's role in lung tumorigenesis *in vivo* using a variety of implanted and spontaneous tumor models to show that PON2 plays a limited role in murine lung tumor development. Taken together, these findings highlight PON2's diverse roles in the context of pulmonary physiology.

TABLE OF CONTENTS

LIST OF FIGURES

CHAPTER 1

INTRODUCTION

1. Paraoxonases

The Paraoxonase (PON) family of enzymes comprises 3 evolutionarily ancient and structurally homologous members (PON1, PON2, and PON3) which exert antioxidant activity in a variety of contexts [1], [2]. The PONs are encoded in a gene cluster on the long arm of chromosome 7 (7q21.3-22.1) in humans and are highly conserved among mammals, with between 80 and 95% identity in both amino acid and nucleotide sequence [3]. Molecular studies have revealed PON2 is the oldest of the three and gave rise to PON1 and PON3 through gene duplication events [4], [5]. PON1 was first of the three discovered and was named for its ability to hydrolyze paraoxon, the toxic metabolite of the organophosphate insecticide parathion [6]. Despite their namesake, PON2 and PON3 are unable to hydrolyze paraoxon but retain the name based on their sequence identity to PON1 [1]. These enzymes all possess lactonase and arylesterase activities but differ in both catalytic efficiency and variety of substrates [1]. While the PONs exert activity against numerous exogenous compounds, no endogenous substrates have been identified. Enzymatic activity and tissue localization are summarized in Figure 1.
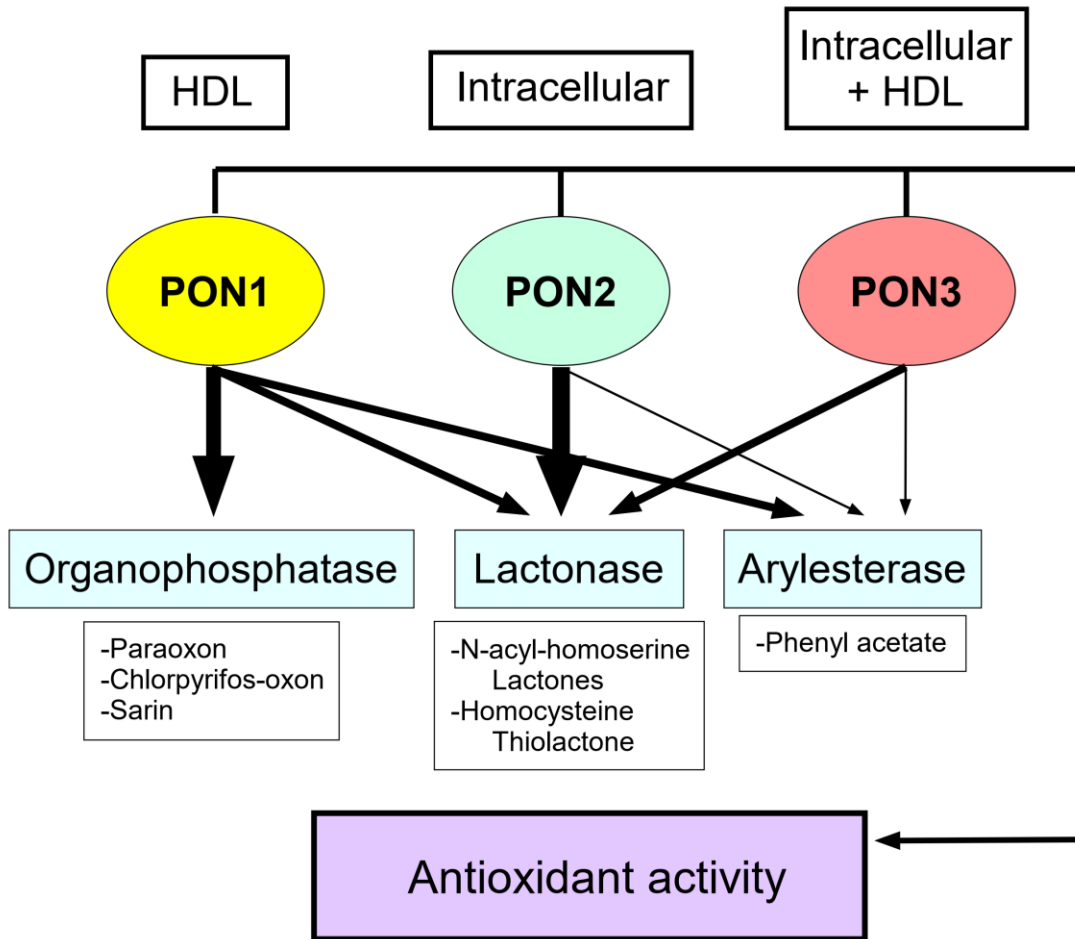
Figure 1.1. Summary of PON enzymatic activity and tissue localization.

1.1.1 PON1

PON1 was first described in a 1953 report by Aldridge, who highlighted PON1's ability to hydrolyze paraoxon, the toxic metabolite of the organophosphate insecticide parathion [7]. While PON1's primary enzymatic function is its organophosphatase activity, it also possesses lactonase and arylesterase capabilities [1]. Research conducted in the past decades has expanded to reveal PON1's antioxidant functions in the context of atherosclerosis, innate immunity, and cancer [8]. The *PON1* gene encodes a 43 kDa protein consisting of 354 amino acids [9] which is synthesized by the liver and secreted into circulation, where it tightly associates with high-density lipoprotein (HDL) particles in plasma [10]. PON1's primary function in serum is to prevent and reverse the oxidation of low-density lipoproteins (LDL), which can accumulate in the vascular endothelium and drive the formation of atheromatous plaques [11]. The anti-atherogenic role of PON1 has been extensively demonstrated using cell-based systems and PON1-deficient mice [9], [11]–[13]. Furthermore, studies on human PON1 polymorphisms have implicated a number of single nucleotide polymorphisms (SNPs) in the coding and promoter regions of the *PON1* gene with susceptibility to cardiovascular disease. [14]. This substantial and growing body of work has highlighted PON1 as a potential biomarker and possible molecular target for oxidative vascular damage [15].

PON1 lactonase activity is an important factor in innate immunity. One class of molecules, the acyl-homoserine lactones (AHLs), are substrates for PON1 and are used by various opportunistic pathogens to coordinate their gene expression

profiles in accordance with population density. PON1 is capable of hydrolyzing the lactone ring present in AHLs to an inactive form, effectively disrupting bacterial quorum sensing and protecting the host against bacterial infection [16].

Additional research has explored the relationship of PON1's ability to reduce oxidative stress and mitigate inflammation and its relationship to human cancers. For instance, Marchesani et al. investigated PON1's role in prostate cancer in a population of Finnish men and discovered a SNP of PON1, I102V, was positively correlated with disease incidence. [17]. Another SNP, L55M, was found in a separate study to be associated with an increased risk of breast cancer development in post-menopausal women [18]. PON1's role in lung cancer was explored using the cancer genome atlas (TCGA) database, lung cancer cell lines, and tissue biopsies from patients with lung cancer to demonstrate that PON1 promotes cell survival to stimulate tumor growth and progression [19]. Additionally, the influence of the common PON1 Q192R polymorphism was described in a meta-analysis of numerous human cancers, which revealed a mixed role of PON1 and cancer growth [20]. Despite these observations, further work is needed to elucidate PON1's role in tumorigenesis and cancer progression.

1.1.2 PON3

PON3 is the least studied and most recently identified member of the paraoxonase family of enzymes, although interest in its biology is increasing. PON3 is a 40kDa protein and shares similarity to PON1 in that it is mainly synthesized by the liver and is secreted into plasma in association with HDLs. In

contrast to PON1, PON3 is also synthesized by the kidney, albeit to a lesser degree [21]. In circulation, PON3 expression is lower than PON1, although PON3 combats lipid peroxidation of LDL particles at two orders of magnitude higher than PON1 [21], [22]. From circulation, PON3 may be taken up by cells and reside intracellularly, where it localizes to endoplasmic reticulum (ER) and mitochondria [23], [24]. Studies have revealed that PON3 is capable of preventing and reversing the oxidation of LDL in plasma and diminishing the formation of superoxide anion (O_2^-) in mitochondria and ER, thus implicating its activity in protecting against atherosclerosis, neurodegenerative disorders, diabetes, and cancer [3], [6], [25].

Based on PON3's association with HDL in plasma and its antioxidant properties, the majority of PON3 research has focused on its role in atherosclerosis. While human data are scarce, promising links have been established with regards to the anti-atherogenic potential of PON3 activity *in vitro* and in animal studies. A study by Rosenblat et al. demonstrated that the addition of purified PON3 to mouse peritoneal macrophages from ApoE^{-/-} mice diminished lipid peroxide formation at baseline, and following addition of the oxidant $CuSO_4$ [26]. Further, PON3 expression is stable in response to mitochondrial-mediated oxidative stress or oxidized-LDL [21], [27]. This observation is in contrast to PON1 and PON2, whose expression changes in response to various physiological stimuli, and suggests that PON3 may provide a baseline protection against atherogenic insults [21]. Overall, the relationship between PON3 antioxidant activity in macrophages, association with HDL, and oxidative stress warrants further investigation.

1.1.3 PON2

PON2 is a 43 kDa transmembrane protein [28] with near-ubiquitous tissue expression. Unlike its family members, PON2 is found exclusively within cells and [25] and is localized to membrane fractions of mitochondria, ER, and nuclear lamina [29]. PON2 shares antioxidant and anti-inflammatory characteristics with other PONs, such as preventing and reversing oxidative damage to LDL [25]. In addition, PON2 also mitigates oxidative stress in mitochondria and ER (Figure 1.2). Due to its widespread tissue distribution and subcellular localization, PON2 is involved in numerous (patho)physiological processes, including atherosclerosis, innate immunity, cancer, neurodegenerative disorders, and type 2 diabetes mellitus (T2DM).

1.1.3.1 PON2 and Atherosclerosis

The majority of PON2 biological research has highlighted its role as a protective factor against the development of atherosclerosis. While PON2 is the only paraoxonase that does not associate with HDL particles in plasma, this enzyme protects against vascular damage via its antioxidant activity in vascular endothelial cells and macrophages [8] and in mice maintained on a high-fat diet [30]–[32]. The first study to investigate PON2's role in atherosclerosis in mice was carried out by Ng et al., who reported that mice deficient in PON2 developed larger atherosclerotic lesions than their wild type counterparts [32]. Paradoxically, PON2-deficient mice had lower serum levels of very low-density lipoprotein (VLDL) and LDL, which are known to contribute to atherogenesis. However, VLDL and LDL
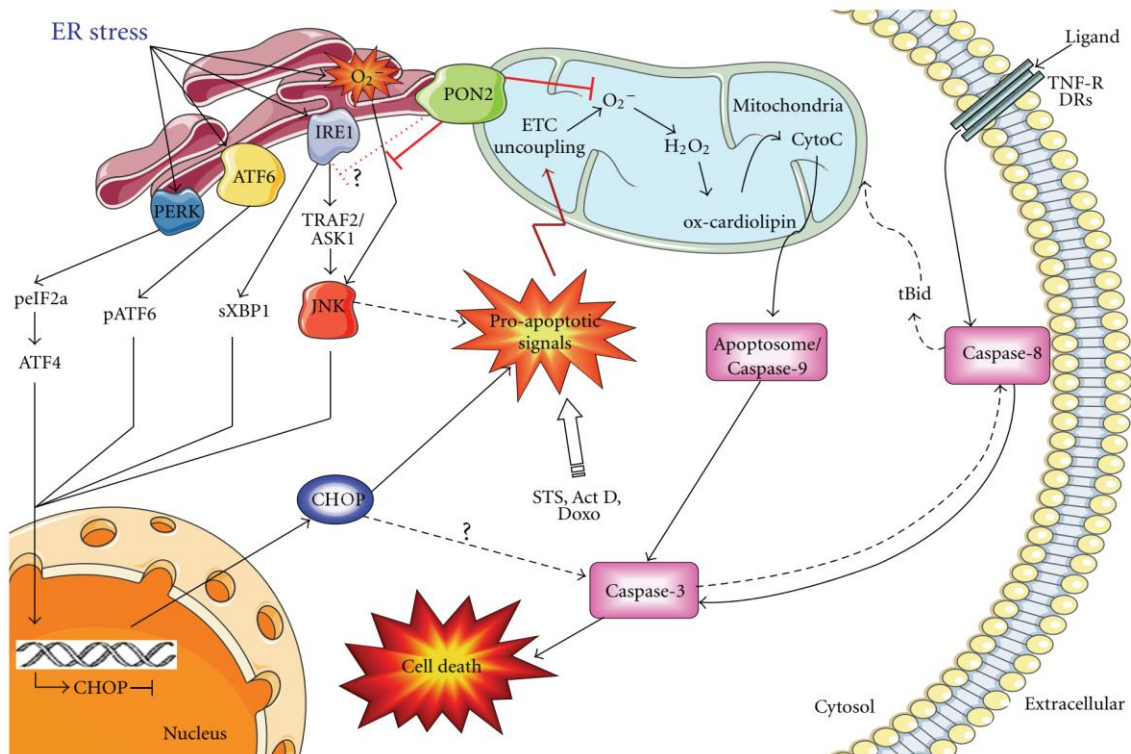
Figure 1.2. PON2 promotes cell survival through its antioxidant effects in mitochondria and ER. PON2 inhibits the production of superoxide (O_2^-) in mitochondria, preventing the formation of H_2O_2, release of cytochrome c into cytosol, and activation of caspases. In ER, PON2 reduces O_2^- production, preventing ER-stress mediated activation of the intrinsic apoptotic signaling cascade (Adapted from Witte et al., 2012.)

particles isolated from PON2-deficient mice were significantly more inflammatory to monocytes *in vitro* compared to their wild type counterparts [32]. Later studies conducted by Devarajan et al. expanded these findings using PON2-deficient mice crossed to hyperlipidemic ApoE$^{-/-}$ mice to demonstrate that PON2 protected against atherosclerotic plaque formation by reducing the mitochondrial formation of reactive oxygen species (ROS) at complex III of the electron transport chain (ETC) [31]. The same group later demonstrated that PON2 modulates ER stress by stabilizing calcium homeostasis in macrophages, ultimately promoting cellular survival [30]. These studies, taken in conjunction with abundant *in vitro* observations, demonstrate PON2's critical role in the mitigation of oxidative stress-induced atherosclerosis.

1.1.3.2 PON2 and Cancer

Over the past decade, PON2's role in human cancers has garnered increasing attention. Early work in this context hypothesized PON2 may contribute to neoplastic growth due to its ability to mitigate oxidative stress in mitochondria and ER; indeed, its activity within tumor cells serves to promote cellular survival and confer resistance to traditional chemotherapeutics [8], [25], [33]. The current body of evidence of PON2's involvement in neoplastic disease is growing, but restricted to a small number of cancer types. Nevertheless, these reports highlight PON2 as a potentially important pro-tumorigenic factor worthy of further study.

A study by Frank et al. was the first recorded implication of PON2 in the context of cancer. In this study, researchers investigated the gene expression

patterns of patients with Philadelphia chromosome-positive (Ph[+]) chronic myelogenous leukemia (CML) who were non-responsive to the kinase inhibitor imatinib [34]. The purpose of the study was to identify genes that mediated primary resistance to imatinib, as acquired resistance was well-documented at the time. Leukocyte RNA was isolated from Ph+ patients with CML classified as either responders or non-responders, converted to cDNA, and analyzed using microarray hybridization technology. In patients classified as non-responders, major expression changes to genes involved in oxidative stress, apoptosis, and DNA repair were identified [34]. This analysis revealed that PON2 was one of the most significantly-altered changes in expression in non-responders vs. responders. In addition, the researchers identified over 100 genes that contributed to acquired imatinib resistance in Ph[+] patients with CML. This is the first published report, to our knowledge, implicating PON2 in neoplastic disease.

Among other early studies implicating PON2 in human cancer, Kang et al. sought to identify prognostic indicators in patients with high-risk pediatric acute lymphoblastic leukemia (ALL). [35]. Researchers monitored relapse-free survival (RFS) in patients with ALL, separating their cohort into low- and high-RFS populations. DNA microarray data and cytometric measures were integrated to determine gene expression profiles capable of predicting RFS. The study identified 38 genes strongly correlated with RFS, including PON2 expression. These data revealed that patients with high PON2 expression experienced relapse earlier compared to patients with low PON2 expression [35] and was among the first studies to implicate PON2 in promoting carcinogenesis.

An early work by Altenhofer et al. established mechanistic insight into PON2's functionality in mitochondria. The central objective of this study was to explore whether the O_2^- scavenging activity of PON2 at the mitochondrial inner membrane would promote tumor cell survival [36]. Mitochondria are the primary source of O_2^- within cells, which dismutates (either spontaneously or via superoxide dismutase [SOD]) to H_2O_2. In turn, H_2O_2 can induce cell death by triggering the release of cytochrome c from mitochondria and caspase activation through the intrinsic apoptotic cascade [37]. Additionally, these investigators used a site-directed mutagenesis approach to demonstrate that the antioxidant activity of PON2 was independent of its lactonase activity. [36]. While this research was conducted using the human endothelial cell line E.A.hy 926 (and not tumor cell lines), it was the first report suggesting a pro-tumorigenic role for PON2.

This same group of researchers published a subsequent report detailing a dual role for PON2 in tumorigenesis [38]. The purpose of this study was to explore PON2's influence on redox homeostasis and ER stress pathways in tumor cells and how modulation of these organelles impacted tumor cell apoptotic signaling. PON2 expression was evaluated in tissue samples from over 400 patients with cancer, which revealed >2 fold upregulation of PON2 in tumors from uterus, liver, kidney, lymphoid tissues, or urinary bladder compared to normal adjacent tissues. Further, tumors from thyroid gland, prostate, pancreas and testis were upregulated approximately 1.5-fold [38]. In this study, all tumor tissues of a given subtype were combined, as well as normal samples from the same tissue, obscuring insight into pair-wise comparisons of the same patient. Therefore, it is possible that PON2

upregulation may have been missed in specific tumor types due to inter-patient variability with baseline PON2 expression. Next, researchers explored how PON2 expression alters cellular apoptotic signaling in the context of cancer. Using a variety of normal and tumor cell lines with high (ectopic overexpression) or low (RNA interference; RNAi) PON2 expression, researchers evaluated the response to various cytotoxic chemotherapeutic agents and demonstrated that PON2 promotes cell survival and drug resistance phenotypes. Conversely, loss of PON2 expression sensitizes cells to cytotoxic agents [38]. Mechanistically, this study demonstrates that PON2 prevents activation of CHOP (CCAAT/-enhancer-binding protein homologous protein) by mitigating ER stress, preventing activation of the intrinsic apoptotic cascade. [38]. Taken together, these observations demonstrate that PON2 is upregulated in a variety of human cancers and promotes apoptotic resistance in response to traditional cytotoxic chemotherapeutics.

Further work established a protective role for PON2 in promoting cell survival in oral squamous cell carcinoma (OSCC) cells exposed to ionizing radiation. [39]. The study by Kruger and colleagues demonstrated that PON2 expression positively correlated with radiotherapy resistance in various OSCC cell lines. In agreeance with previous studies, the OSCC cells that overexpress PON2 undergo less cell death than those with lower PON2 expression, whereas RNAi-mediated knockdown of PON2 restored sensitivity to irradiation [39]. A subsequent study by the same group revealed that PON2 expression was regulated through the Wnt/β-catenin pathway in OSCC cells [40]. Using computational biology, liquid chromatography-mass spectrometry (LC-MS) based proteomics, and a siRNA

assay screen, sites in the PON2 gene promoter were identified which are bound by transcription factors involved in Wnt/β-catenin signaling. This hypothesis was validated using traditional biochemical approaches in which ligands and upstream transcription factors in the Wnt/ β-catenin were shown to directly upregulate PON2 expression [40]. Further, PON2 expression was found to be positively correlated to OSCC relapse and β-catenin expression in tumor samples from 32 patients with OSCC. While regulatory cross-talk between Wnt/β-catenin and PON2 has not been explored in other cancer contexts, it expands our current mechanistic insight into how tumor cells may exploit PON2's anti-apoptotic influence.

Recently, PON2 was identified in an integrative genomics study of pancreatic ductal adenocarcinoma (PDAC) by Nagarajan et al [41]. Once identified *in silico* and validated in an initial screen, PON2 was knocked down via shRNA-mediated RNAi and was shown to prevent metastasis of PDAC cells in multiple *in vivo* models [41]. Further *in silico* analysis coupled with chromatin-immunoprecipitation (ChIP) assays also revealed transcriptional repression of PON2 by p53, which was not previously reported. Intriguingly, this study also demonstrated that PON2 expression may modulate glucose uptake by stimulating GLUT1-mediated glucose transport. This work reveals a regulatory pathway by which PON2 promotes tumor survival and metastasis in the context of PDAC. It is currently unknown whether these observations may be extended to other types of neoplastic growth, or whether PDAC is a contextual requirement for these interactions.

Largely, this body of work provides a cohesive lens through which PON2's pro-tumorigenic role may be viewed. Although the complete mechanisms and regulatory network interactions are still being investigated, our knowledge to date indicates PON2 provides apoptotic resistance to tumor cells by minimizing ROS-induced ER stress and mitochondrial dysfunction. This antioxidant activity enables various tumor cells to overcome cytotoxic insults including chemotherapeutics [34], [38] and irradiation [39], [40], and may serve to promote the metastatic spread of cancer through the body [41]. Additionally, PON2 receives and exerts regulatory control through commonly-dysregulated oncogenic networks, such as the Wnt/β-catenin pathway [40] and p53 [41]. In conjunction with large-scale studies that have demonstrated that PON2 is upregulated in numerous and diverse tumor types [38], [42], these considerations necessitate further study of PON2's oncogenic contribution in other neoplastic tissues and cells.

1.1.3.3 PON2 and neurodegenerative disease

Neurodegeneration is the process through which neurons in the central and/or peripheral nervous tissue undergo progressive loss of structure or function, leading to pathological sensory and motor deficits. Neurodegenerative disorders affect approximately 50 million people worldwide and represent a significant public health burden. The most significant risk factor to the development of neurodegeneration is age—a growing concern as global life expectancy is projected to increase. PON2 expression in mouse brain tissue peaks during infancy and declines throughout adulthood, suggesting a potential neuroprotective

role of PON2 in developing mice [43], [44]. Recent work has also suggested that PON2 plays a protective role in the context of Alzheimer's disease (AD) and Parkinson's disease (PD), the first and second most prevalent neurodegenerative disorders, respectively [45].

AD is characterized by the accumulation of the amyloid-β peptide into extracellular plaques and hyperphosphorylated tau proteins into intracellular neurofibrillary tangles, resulting in a progressive loss of brain function [46]. Numerous potential etiologies have been identified, including chronic inflammation and oxidative stress [46]. A common polymorphism of PON2, Ser311Cys, was positively correlated in patients with AD in Asian and Caucasian populations [47]–[49], suggesting a possible link between PON2's ability to mitigate oxidative stress and inflammation in the brain. Further, modulating the expression of PON2 in CNS tissue has received attention as a novel neuroprotective approach in AD [45]. In particular, Quercetin, a flavonoid phytochemical with antioxidant properties, has shown promise as an anti-AD agent *per se* [50] and has been highlighted for its ability to upregulate PON2 in mouse striatal astrocytes and neurons *in vitro* [51]. Furthermore, striatal astrocytes from PON2$^{+/+}$ mice pretreated with quercetin were protected from the ROS-inducing agents H_2O_2 and 2,3-dimethoxy-1,4-naphthalenedione (DMNQ) compared to astrocytes from PON2$^{-/-}$ mice [51].

PD is the progressive loss of dopaminergic neurons in the substantia nigra pars compacta region of the brain, which leads to deficiency in striatal dopamine, culminating in disruptions of motor and cognitive function [52]. While both genetic and environmental factors have been identified as contributing to PD, specific

etiologies remain largely unknown. At the cellular level, PD pathogenesis is characterized by the cytotoxic aggregation of misfolded α-synuclein protein and ROS production from impaired mitochondrial respiration [53]. Giordano et al. demonstrated that PON2 mRNA and protein expression is highest in dopaminergic regions of the brain, including the nucleus accumbens, substantia nigra, and striatum [43]. Further, PON2 expression was elevated in mouse brain tissues from female compared to male mice—an interesting observation considering the prevalence of PD is higher in males. Additional work by Parsanejad and colleagues demonstrated that PON2 stabilizes neurons in response to oxidative stress and/or deficiency in DJ-1 [54], a gene identified in some cases of familial PD [55].

1.1.3.4 PON2 and Type II Diabetes Mellitus

PON2 is speculated to contribute to type II diabetes mellitus (T2DM) based on the role of oxidative stress and inflammation in the pathophysiology of this disease. Despite reports demonstrating that PON2 polymorphisms (A148G and S311C) contribute to T2DM development and severity [56]–[58], a recent meta-analysis failed to observe this correlation [59]. However, research efforts continue to further delineate this relationship.

1.1.3.5 Regulation of PON2 expression

PON2 expression is controlled at the transcription and post-translation level in response to various stimuli, including oxidative stress, hormones, non-steroidal anti-inflammatory drugs (NSAIDs), and phytochemicals [60], [61]. Insights into

modulating PON2 expression and activity could play important roles in the treatment, prevention, and management of various pathophysiologies.

1.1.3.5.1 Transcriptional regulation

Transcription of PON2 mRNA is regulated by a variety of endogenous and exogenous factors. For instance, multiple studies have demonstrated that oxidative stress and cholesterol content are capable of modulating PON2 expression. In J774A.1 murine macrophages, cellular oxidative stress exerts a bi-phasic response on PON2 expression [62]; i.e. the addition of antioxidants or free radical-generating compounds leads to upregulation of PON2 protein and prevents the release of O_2^- and subsequent formation of lipid peroxides. Similarly, PON2 was upregulated in mouse peritoneal macrophages isolated from ApoE$^{-/-}$ mice in response to treatment with various oxidants, as well as oxidized LDL [26]. In human macrophages differentiated from THP-1 monocytes, PON2 expression is promoted in response to urokinase plasminogen activator (uPA) through a multi-step pathway in which ROS is produced by NADPH oxidase, which activates ERK1/2, thereby stimulating translocation of sterol regulatory binding protein-2 (SREBP-2) to the nucleus, and culminating in transcriptional activation of the *PON2* gene [63]. In intestinal Caco2 cells, an oxidizing cellular environment decreases PON2 expression [64], suggesting contextual requirements for modulation of PON2 expression that may prove important in atherogenesis.

1.1.3.5.2 Post-translational modifications (PTMs)

Recent work has begun to elucidate the role of post-translation modifications (PTMs) in PON2 activity. Specifically, N-glycosylation and ubiquitination have been reported as potentially important modulators of PON2 activity. A study by Altenhofer and colleagues demonstrated that N-glycosylation at two positions, Asn254 and Asn323, were required for PON2 catalytic activity [36]. Similarly, Stoltz et al. reported that the common Ser311Cys polymorphism resulted in reduced glycosylation and impaired PON2 lactonase function [65]. However, a study employing recombinant PON2 purified from *E. coli* yielded conflicting results showing that PON2 retained enzymatic activity in the absence of glycosylation [66]. The same study identified Lys168 as a site of ubiquitination following treatment with the quorum-sensing molecule N-(3-oxododecanoyl)-l-homoserine lactone (C12) that resulted in impaired enzymatic activity [66], which was later validated using intact cells [67]. Together, this growing body of research is highlighting the varied mechanisms that govern PON2 status within cells.

CHAPTER 2

PON2 MEDIATES MITOCHONDRIAL DYSFUNCTION IN TRACHEAL

EPITHELIAL CELLS IN RESPONSE TO THE QUORUM SENSING MOLECULE

N(-3-OXODODECANOYL)-L-HOMOSERINE LACTONE

2.1 INTRODUCTION

Pseudomonas aeruginosa is a gram-negative bacterium among the most common causes of nosocomial pneumonia in the United States [68]. The highest risk factors for opportunistic *P. aeruginosa* infection include severe burns, neutropenia, and Cystic Fibrosis (CF) [69]. In a majority of patients with CF, lung colonization of *P. aeruginosa* exacerbates declining lung function through chronic inflammation and progressive loss of lung tissue, eventually resulting in death [70], [71]. This bacterium constitutively synthesizes and secretes the freely-diffusible quorum sensing molecule N-(3-oxododecanoyl)-l-homoserine lactone (C12) to coordinate its gene expression profiles according to population density [72].

The primary role of C12 is to facilitate the phenotypic switch of *P. aeruginosa* from its free-swimming, planktonic morphology to its distinct biofilm architecture, in which multicellular clusters (microcolonies) are encapsulated in a protective extracellular matrix comprised of polysaccharides and DNA [73]. Once

formed, biofilm infections exhibit up to 1000-fold increased resistance to antibiotic therapies compared to their planktonic counterparts [74]. The exact concentrations of C12 in established infections are contested, but are estimated to reach high micromolar concentrations near biofilms [75]–[77]. Beyond its role in bacterial intercellular communication, C12 also modulates eukaryotic host cell physiology [78]. Numerous studies have demonstrated C12's ability to trigger apoptosis [79]–[85], alter immune cell signaling (reviewed in [78]), and disrupt epithelial barriers [86]–[89]. The pro-apoptotic effects of C12 have been extensively documented in multiple cell types and predominantly occur through the intrinsic (mitochondrial) cell death pathway. In mitochondria, C12 freely diffuses across lipid bilayers into the mitochondrial matrix and induces the release of cytochrome c from the mitochondrial intermembrane space into the cytosol, activates Caspase 9, and culminates in cell death [85], [90], [91].

Schwarzer and colleagues revealed that the cytotoxic effects of C12 are mediated by PON2 [83]. As a lactonase, PON2 hydrolyzes the lactone ring of C12 to an open-ring carboxylic acid derivative (C12-COOH). This metabolite is more polar than C12 and is therefore sequestered within cells, making PON2 an important factor in disrupting *P. aeruginosa* quorum sensing [83], [92]. However, an unfortunate ramification of this quorum quenching activity is that C12-COOH accumulates in mitochondria and ER and leads to activation of early events in the intrinsic apoptotic cascade [90].

Based on observations by our laboratory and published reports, we sought to investigate how PON2 mediates alterations to mitochondrial network

morphology and bioenergetics in airway epithelial cells upon exposure to physiological concentrations of C12. To this purpose, we examined PON2's influence on mitochondrial network morphology and respiration using a novel cell line, SV-40 immortalized primary tracheal epithelial cells (TECs), isolated from mice with normal PON2 expression and those harboring homozygous PON2 deletion. The results of this study suggest PON2 serves as a fulcrum upon which airway integrity is balanced against quorum quenching. In this regard, clearance of C12 serves to disrupt the formation of *P. aeruginosa* biofilms at the cost of cellular proliferation and survival.

2.2. MATERIALS AND METHODS

2.2.1 Reagents and antibodies

Dulbecco's Modified Eagle's Medium (DMEM), penicillin/streptomycin, trypsin, and L-glutamine were obtained from Mediatech (Manassas, VA); fetal bovine serum was purchased from Gemini (Broderick, CA); Bronchial Epithelial Cell Growth Medium (BEGM) and SingleQuots were purchased from Lonza (Walkersville, MD); Ham's F12 and Amphotericin B (250 µg/mL) were purchased from Gibco (Dublin, Ireland); Pronase was purchased from Roche (Indianapolis, IN); Lipofectamine 3000 transfection reagents, propidium iodide, and β-Mercaptoethanol were purchased from Thermo Fisher (Waltham, MA); N-(3-oxododecanoyl)-homoserine lactone (C12), polybrene, Y-27632 (inhibitor of Rho-associated, coiled-coil containing protein kinase [ROCK]), N-[N-(3,5-

Difluorophenacetyl-L-alanyl)]-(S)-phenylglycine t-butyl ester (DAPT; inhibitor of γ-secretase), crude pancreatic DNase I, bovine serum albumin, and puromycin were purchased from Sigma-Aldrich (St. Louis, MO). Plasmid mCherry-Mito-7 was a gift from Michael Davidson (Addgene plasmid # 55102). Antibodies (Abs) for western blots were anti-β-actin mAb (A5441; Millipore Sigma; Burlington, MA), anti-PON3 mAb (ab109964; Abcam; Cambridge, England), anti-Mouse PON2 pAb (ABIN1573944; antibodies-online.com; Atlanta, GA), peroxidase-conjugated goat anti-rabbit IgG (65-6120; Thermo Fisher) and peroxidase-conjugated goat anti-mouse IgG (65-6520; Thermo Fisher).

2.2.2 Animal studies

Animals were housed in an AALAC- (Association for Assessment and Accreditation of Laboratory Animal Care) accredited pathogen-free barrier facility. All procedures were approved by the University of Louisville Institute for Animal Care and Use Committee (IACUC). Fertilized C57BL/6J-Tyrc-2J (i.e. B6 Albino; Jackson Laboratory; Bar Harbor, ME) embryos were co-injected with Cas9 mRNA and a sgRNA targeted to exon 3 of the mouse PON2 gene. Treated mouse embryos were implanted into a pseudopregnant female mouse to resume gestation. Viable F_0 pups were weaned, and genotypes were determined by sequencing at the PON2 locus. An F_0 pup was identified to be heterozygous for a single base-pair insertion in exon 3 that resulted in an early termination codon. Heterozygous mice were backcrossed to wild type C57BL/6J mice (Jackson) for 5 generations to reduce genetic heterogeneity and retain the mutant PON2 allele.

Mice were then selectively bred to generate wild type, heterozygous, and homozygous-mutant (PON2-KO) genotypes. Genotyping of mice was carried out at the University of Louisville genomics core facility by sequencing mouse tail DNA. Body weights of C57BL/6J wild type and PON2-KO mice were recorded biweekly from 1 month of age until 3 months, at which time heart, lungs, liver, kidneys, and spleen were dissected and weighed.

2.2.3 Primary mouse embryonic fibroblasts (MEFs) isolation and culture

Primary MEF cells were isolated and cultured according to a published protocol [93]. Briefly, embryos were aseptically dissected from wild type or PON2-KO female C57BL/6J mice at 13 days following observation of a copulation plug. After removing embryonic brain, heart, and liver, remaining tissue was finely minced using sterile scissors and incubated in 0.25% trypsin-EDTA for 10 min at 37°C. The resultant mixture was thoroughly agitated with a pipette and incubated for an additional 10 min at 37°C. Primary MEF medium (DMEM supplemented with 10% FBS, 100 units/mL penicillin, 100 µg/mL streptomycin, and 0.1mM β-Mercaptoethanol) was added to quench trypsin and mixed using a pipette. Larger fragments were allowed to sink to tube bottom for 10 min, after which cell suspension was plated in 15 cm plates, incubated at 37°C overnight, and refreshed with warm medium the following day. After 2 days, primary MEF cells were collected by trypsinization and resuspended in cryopreservation medium (10% DMSO in FBS), whereupon cells were aliquoted and stored in 2mL cryovial tubes at -140°C for long-term storage.

2.2.4 Lentivirus production

The cDNA of SV40-Large-T was cloned into the vector pCDH-CMV-MCS-EF1α-copGFP (System Biosciences; Palo Alto, CA) to generate plasmid pCDH-CMV-SV40-Large-T-EF1α-copGFP. The plasmid identity was validated by sequencing. For lentivirus production, the package cell line HEK293T was transfected with the plasmid pCDH-CMV-SV40-Large-T-EF1α-copGFP using Lipofectamine 2000 transfection reagent (Thermo Fisher). Medium containing lentivirus was collected 48–72 h after transfection.

2.2.5 Isolation, immortalization, and culture of primary tracheal epithelial cells (TECs)

Primary mouse tracheal epithelial cells (TECs) were isolated from male wildtype and PON2$^{-/-}$ C57BL/6J mice 6-8 weeks of age as previously described [94], [95]. To reduce terminal differentiation of TECs and improve cell yield per trachea, isolated TECs were cultured in medium supplemented with 5 µM DAPT (γ-secretase inhibitor) and 10 µM Y-27632 (ROCK inhibitor) [96]. Following 7 days of culture, TECs isolated from wild type or PON2-KO mice were immortalized via infection using SV40-Large-T lentiviral supernatant supplemented with 10 µg/ml polybrene. Stable cell lines were self-selected after 14 days of serial passage as non-immortalized TECs reached replicative senescence. Primary TECs were cultured in BEGM supplemented with SingleQuots, DAPT, and Y-27632; Immortalized TECs were cultured in DMEM containing 10% FBS, 100 units/mL penicillin, and 100 µg/mL streptomycin. All cell lines were cultured in a 5% CO_2

humidified incubator at 37°C. The cells were passaged at 1:5–1:10 dilutions and were continuously cultured no longer than 3 weeks.

2.2.6 Western Blot analysis

Frozen mouse organ tissue samples were resuspended in equal volumes of tissue protein extraction reagent (Thermo Fisher) supplemented with protease inhibitors (cOmplete; Roche) and phosphatase inhibitors (PhosSTOP; Roche). Following homogenization and centrifugation, protein concentration was determined by bicinchoninic acid (BCA assay) (Thermo Fisher). Whole cell extracts of cultured cells were prepared using RIPA buffer (Thermo Fisher) supplemented with protease inhibitors (cOmplete; Roche). For mouse organ tissue, 10 μg of total protein was used; for TECs, 30 μg of total protein. All samples were electrophoresed in 4–12% Bis/Tris gels (Bio-Rad; Hercules, CA). Separated proteins were transferred to a polyvinylidene difluoride (PVDF) membrane (Millipore) and incubated with respective primary or secondary antibodies diluted with 10% (w/v) nonfat dry milk (Bio-Rad) in blocking buffer (1X phosphate-buffered saline [PBS] with 0.2% Tween-20). The enhanced chemiluminescence detection system (Thermo Fisher) was used to detect proteins.

2.2.7 Detection of PON2 enzymatic activity

Tissue lysates from mouse liver and small intestine and whole cell lysates from immortalized primary MEFs were prepared according to published methods [97], [98] with minor modifications. Mouse organs were harvested and thoroughly

rinsed with 1X PBS, flash-frozen in liquid N_2, and stored at -80°C. Immediately prior to analysis, organ tissue was thawed on ice, to which an equal volume of lysis buffer (25 mM Tris/HCl containing 1 mM $CaCl_2$, supplemented with protease inhibitors [cOmplete; Roche] and phosphatase inhibitors [PhosSTOP; Roche]) was added. Tissue was sonicated on ice for 1 min. Lysates were centrifuged at 14,000 x g and 4°C for 10 min. Supernatant protein concentration was determined using the BCA assay (Thermo Fisher). Final protein concentration was adjusted to 2 µg/µL in lysis buffer.

Primary MEFs ($1*10^6$) were seeded into 10 cm tissue culture plates and cultured for 24 h. Following trypsinization, cell number was determined using a hemocytometer. Cells ($1*10^6$) were centrifuged at 300 x g and resuspended in 1 mL ice-cold 1X PBS. Following an additional wash step, cells were centrifuged at 5000 x g and 4°C for 5 min and supernatant was removed by aspiration. Cell pellets were stored at -80°C. Immediately prior to analysis, cell pellets were thawed on ice and resuspended in 100 µL lysis buffer. Cells were sonicated on ice for 10 sec. and lysates were centrifuged at 14,000 x g and 4°C for 10 min. Supernatant protein concentration was determined using the BCA assay (Thermo Fisher). Final protein concentration was adjusted to 2 µg/µL in lysis buffer.

Total protein (10 µg) from respective lysates was diluted to a final volume of 100 µL in 5 mM Tris/HCl (pH 7.4) containing 1 mM $CaCl_2$. Reactions were initiated with either 1% MeOH or 1% 5 mM C12 (in Methanol; final concentration 50 µM C12) and incubated at 37°C for 30 min. The reaction was stopped with 70 µL of ice-cold acetonitrile and immediately analyzed by liquid chromatography–

mass spectrometry (LC-MS) without further manipulation. LC-MS experiments were carried out at the University of Louisville medicinal chemistry core facility. A sample volume of 15 μL was injected into an Agilent 1260 HPLC system (Agilent; Santa Clara, CA) equipped with an Agilent 6224 Accurate-Mass Time-of-Flight MS utilizing electrospray ionization. The HPLC system was equipped with a Zorbax Extend-C18 column (1.8 μm, 2.1 x 50 mm; Agilent) with a mobile phase consisting of mass spectrophotometry grade water (with 0.1% formic acid and 0.1% methanol) and acetonitrile (with 0.1% formic acid) and operated in positive ion mode (3500 V V-Cap, 750 V OctRF Vpp, 65 V skimmer, 135 V fragmentor, 40 psi Nebulizer gas, 12 L/min drying gas, and 325°C gas temperature). Samples were eluted with a linear gradient of 5 to 100% acetonitrile at 0.3 mL/min over 10 min. Agilent software analysis suite was used to determine respective measured masses of spectrometry signals. The presence of a specific metabolite was determined by calculating the error value (in ppm) using the calculated exact mass (m_i) and the measured accurate mass (m_a) according to the following formula:

$$\frac{m_a - m_i}{m_i} * 10^6 = error\ (ppm)$$

An error value having an absolute value of less than 5 ppm was considered acceptable; i.e., a specific metabolite was present in the sample.

2.2.8 Real-time quantitative reverse transcription PCR

Total RNA was extracted from primary and immortalized TECs using the GeneJet RNA purification kit (Thermo Fisher) according to manufacturer's protocol. For each sample, 1 μg of RNA was reverse-transcribed to cDNA using

the GeneJet cDNA Reverse Transcription kit (Thermo Fisher) according to manufacturer's protocol. Gene expression was quantified using TaqMan gene expression reagents and the following probes (Thermo Fisher): KRT5 (Mm01305291_g1), Vimentin (Mm01333430_m1), SOX2 (Mm03053810_s1), and Trp53 (Mm00495788_m1); β-actin (Mm02619580_g1) served as internal control. Samples were pre-incubated for 50°C for 2 min, 95°C for 10 min, followed by 40 amplification cycles—95°C for 15 sec, amplification at 60°C for 1 min—in a StepOnePlus^{TM} Real-Time PCR System (Applied Biosystems, Foster City, CA). Data are mean ± SD of ΔC_T values from 3 independent experiments (n=3).

2.2.9 Cell death assays

TECs (7.5*10^3 cells/well) were plated in a 96-well tissue culture plate and cultured for 24h. Cells were incubated with medium containing 0.1% DMSO or C12 at the indicated concentrations. Following treatment with DMSO or C12, cells were trypsinized, pelleted, and resuspended in complete medium supplemented with 1 μg/ml propidium iodide (PI). Cell viability was measured by PI exclusion using flow cytometry (FACScalibur, Beckon Dickinson, San Jose, CA). The percentage of cell death was determined as 100 minus the percentage of viable cells.

2.2.10 Caspase-3/7 activity

Caspase-3/7 activity was measured using a Caspase-Glo assay kit (Promega, Madison, WI). This assay detects caspase activation by measuring cleavage of a proluminescent substrate containing a DEVD (Asp-Glu-Val-Asp)

amino acid sequence, resulting in the release of the luciferase substrate aminoluciferin and subsequent production of luminescence. TECs were plated in white-walled 96-well plates 24 h prior to treatment with either 0.1% DMSO or C12 at the indicated concentrations and incubated for 24 h at 37°C in a 5% CO_2 humidified incubator. Following incubation, an equal volume of Caspase-Glo reagent was added to each well and equilibrated for 1 h, at which point luminescence was quantified using a Gemini EM microplate spectrofluorometer (Molecular Devices, Sunnyvale, CA) according to manufacturer's protocol. Data are presented as mean ± SD fold-change relative luminescence units (RLU) of 3 independent experiments.

2.2.11 Cellular proliferation assays

Proliferation was assessed using a hemocytometer to count cells at 24, 48, and 72 hours. Immortalized TECs ($1*10^4$) were plated and cultured in 12-well plates. Results are from 3 independent experiments.

2.2.12 Measurement of mitochondrial respiration using the Seahorse XF analyzer

To assess mitochondrial respiration in immortalized TECs, the Mito Stress test assay was performed by measuring oxygen consumption rate (OCR) and extracellular acidification rate (ECAR) with a Seahorse XF analyzer. An initial experiment determined the optimal cell seeding density to be 10^4 cells/well in a XF96e microplate. Subsequent optimization experiments were performed to determine optimal drug concentrations to be used in future experiments: 1 µM

Oligomycin (ATP synthase inhibitor), 1.5 µM FCCP (mitochondrial decoupling agent), and 10/1 µM Antimycin A/Rotenone (inhibitors of Complex I and III, respectively). Using the optimized cell seeding density and assay conditions, we performed the Mito Stress test in both WT and PON2-KO TECs, which were plated in DMEM containing either 0.1% DMSO or 20 µM C12 and cultured for 24 h at 37°C in a 5% CO_2 humidified incubator. The following day, the medium was replaced with pre-warmed XF assay medium and equilibrated for 1 h at 37°C in a non-CO_2 incubator. The assay was performed on a Seahorse XF analyzer according to the manufacturer's protocol. The OCR and ECAR values were normalized to total protein in each well.

2.2.13 Mitochondrial membrane potential ($\Delta\psi_{mito}$) and morphology

To image $\Delta\psi_{mito}$ and morphology, cells were first cultured on 35 mm glass coverslips for 16-24 hours. The coverslips were then mounted in a recording chamber positioned on the stage of an inverted microscope (IX71; Olympus America Inc., Center Valley, PA). The chamber was continuously perfused throughout the experiment with Hank's Balanced Salt Solution containing TMRE (20 nM) at room temperature. Cells were visualized using a 60x PlanApo, 1.42 NA oil immersion objective and confocal images acquired using a VT-Infinity 3 (VisiTech International; Sunderland, UK). After a 20-minute equilibration period, TMRE was excited using the 488 nm line of a Krypton-Argon laser. The emitted fluorescence was filtered using a dual bandpass filter set and collected using MetaMorph Microscopy Automation and Image Analysis software (Molecular

Devices, LLC; San Jose, CA). For mitochondrial morphology, cells cultured on 35 mm glass coverslips were imaged 24 hours after transient transfection with the matrix-targeted fluorescent construct, mCherry-Mito-7 [99], using jetOPTIMUS® (Polyplus transfection, New York, NY) according to the manufacturer's instructions. Image analysis was performed using ImageJ software [100]. $\Delta\psi_{mito}$ was quantified by measuring the average background corrected fluorescence within individual cells, and mitochondrial morphology assessed in thresholded image sections by calculating the form factor [$perimeter^2/(4\pi \times area)$] and the aspect ratio (ratio between the major and minor axes of the ellipse equivalent to the object) as measures of elongation and interconnectivity, respectively, as described [101].

2.2.14 Statistical analysis

Data are presented as mean ± SD of 3 independent experiments, unless otherwise noted. Animal weight studies were carried out with 10 animals per sex per group. Organ weight results are 5 per sex per group. A Student's two-tailed unpaired t-test with p-value of < 0.05 was used to determine statistical significance. Seahorse XF experiments comprised 5 technical replicates and 3 biological replicates; statistical analysis was performed using GraphPad Prism software in which a two-way ANOVA with Tukey's multiple comparison test were used to determine statistical significance.

2.3 RESULTS

2.3.1 Generation of PON2-knockout mice

We generated PON2-knockout (PON2-KO) mice using a CRISPR/Cas9 approach to explore how PON2 expression mediates cellular physiology following treatment with C12 (Fig. 2.1A). Previous studies employed PON2-deficient mice generated by a gene-trap approach [32], which may allow for low levels of expression of the target gene [102]. In these studies, PON2 mRNA and protein expression was detected in brain, liver, lung, and stomach tissues [103]. Therefore, we sought to generate a novel PON2-knockout strain with no detectable PON2 expression. In collaboration with the University of Louisville genomics core facility, we employed a CRISPR/Cas9 approach to generate mice with systemic PON2 deletion. Fertilized Cb7Bl/6/TyrC2J mouse embryos were co-injected with Cas9 mRNA and a single guide RNA (sgRNA) targeted to exon 3 of the mouse PON2 gene, then were implanted into pseudopregnant female mice. Genomic DNA was isolated from 7-day old neonates and analyzed for insertion-deletion mutations by Sanger sequencing following PCR amplification. An individual neonate was identified that possessed a single nucleotide insertion in exon 3, resulting in an early termination codon. Following 5 generations of selective backcrossing to minimize genomic heterogeneity, mice were bred to generate wild type (WT; PON2$^{+/+}$), heterozygous (PON2$^{+/-}$), and homozygous knockout (PON2-KO; PON2$^{-/-}$) mice. PON2 genotypes were determined by PCR amplification of genomic DNA purified from mouse tail tissue and Sanger sequencing (Fig. 2.1B).
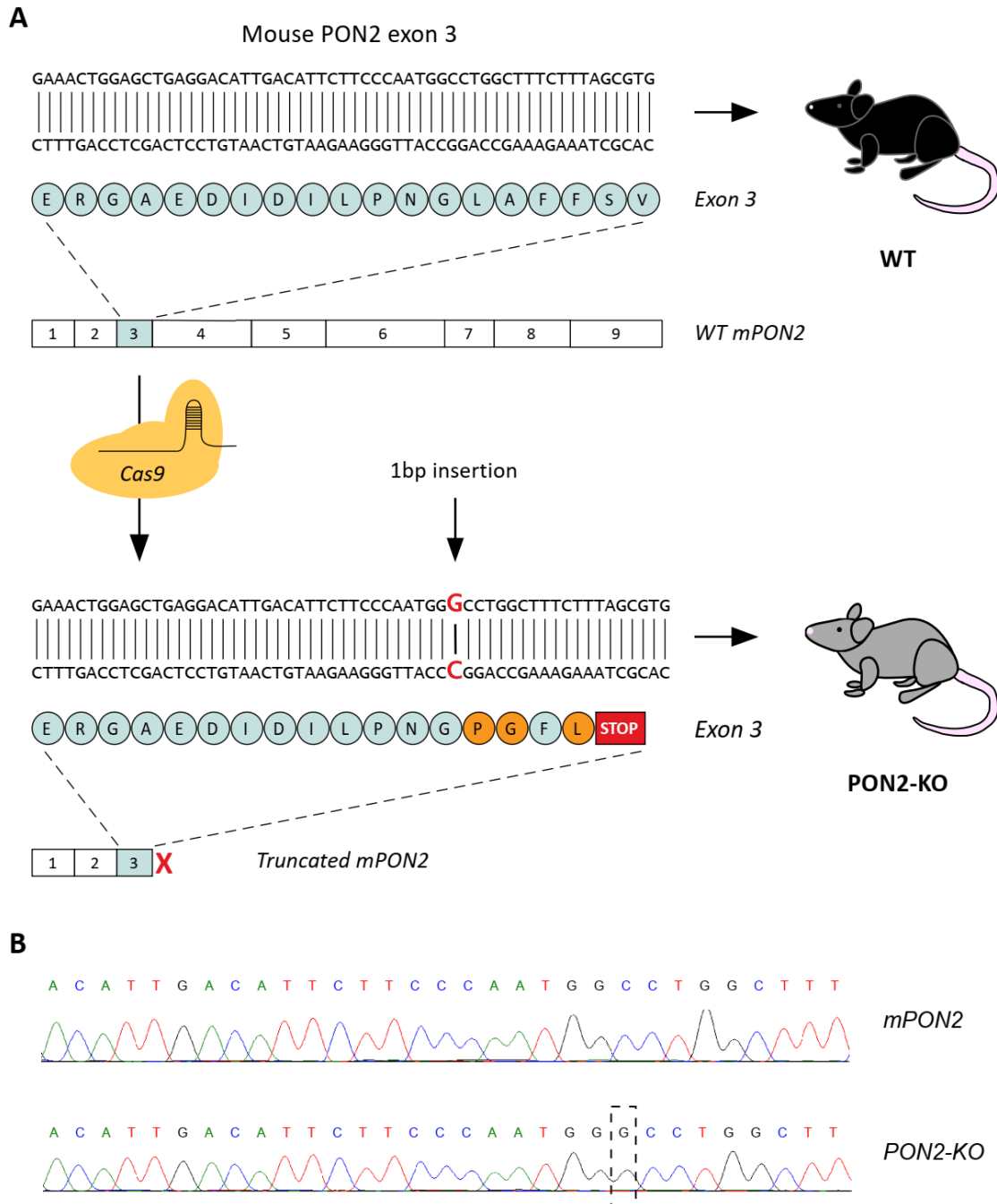
Figure 2.1. Generation of PON2-deficient mice. (A) CRISPR/Cas9 was used to generate a single nucleotide insertion in mPON2 exon 3 which resulted in an early termination codon. Mice harboring the mutant PON2 allele were backcrossed for 5 generations with wild type C57BL/6J mice, then selectively bred to generate heterozygous and homozygous PON2-KO mice. (B) Genotypes were confirmed by sequencing.

2.3.2 PON2 protein expression is absent in PON2-KO mice

We next sought to confirm that introducing an early termination codon into the PON2 genomic locus resulted in elimination of PON2 expression in mouse tissues. To this purpose, we collected tissues with the highest PON2 expression (lung, stomach, small intestine, and large intestine) and analyzed PON2 protein content by western blot analysis (Fig. 2.2). As predicted, PON2 expression was detected at the highest levels in all tissues from WT mice. We detected a decreased level of PON2 protein expression in tissues collected from heterozygous mice, which correlates with the number of intact PON2 alleles. Most importantly, no PON2 expression was detected in mice harboring 2 mutant PON2 alleles.

We hypothesized that PON3 may by upregulated in mice lacking PON2 expression in a compensatory manner, since the two enzymes overlap in their tissue distribution and enzymatic activity. To address this concern, we also determined PON3 protein expression by western blot analysis and found similar protein content in each genotype (Fig. 2.2), indicating that PON3 does not compensate for loss of PON2. Taken together, the results of these experiments demonstrate the systemic deletion of PON2 in homozygous mutant mice.
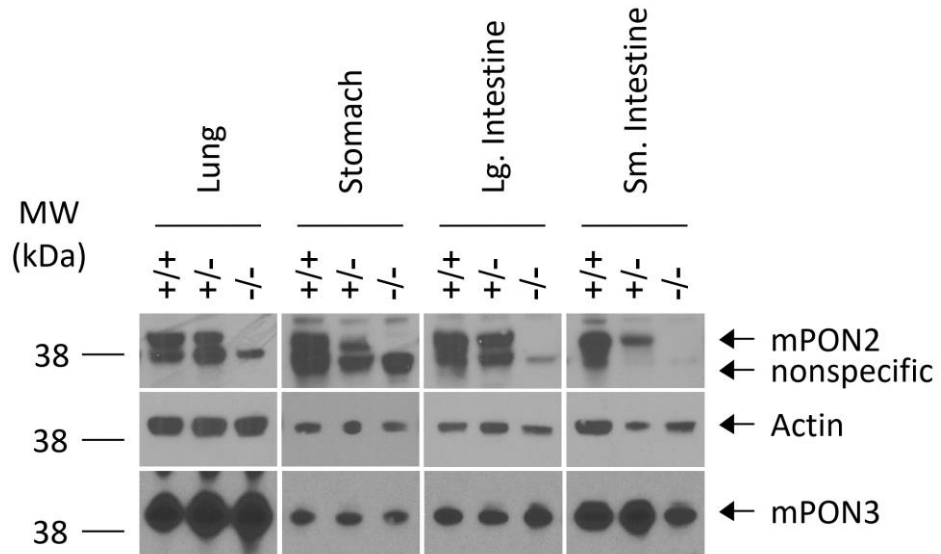
Figure 2.2. PON2 and PON3 expression in tissues from wild type, heterozygous, and homozygous PON2-knockout mice. Mouse PON2 and PON3 expression was determined by western blot analysis in lung, stomach, large intestine, and small intestine. Actin band shown as a control. Representative immunoblots are shown.

2.3.3 Functional assessment of PON2 activity in mouse tissues and primary cells

PON2's primary enzymatic function is its lactonase activity [1], by which lactone ring moieties are opened via hydrolysis of the ester bond. Previous work has established that PON2 hydrolyzes the bacterial quorum sensing molecule N-3-Oxododecanoyl)-L-homoserine lactone (C12) to a carboxylic acid derivative (C12-COOH). Therefore, production of C12-COOH serves as a useful surrogate of PON2 lactonase activity *in vitro* [97], [98]. To functionally confirm loss of PON2 expression, we measured PON2 lactonase activity in tissue and cells isolated from wild type (WT) and PON2-KO mice by liquid chromatography-mass spectrometry (LC-MS; Fig. 2.3 & 2.4). PON2 activity was assessed in lysates prepared from small intestine tissue and primary MEF cells. Lysates were incubated with either methanol (vehicle control) or 50 μM C12 for 30 min and analyzed by LC-MS. The presence of a specific metabolite was determined by calculating the error value (in ppm) as described in Materials and Methods (section 2.2.7). An error value with an absolute value of less than 5 ppm was considered acceptable; i.e., a specific metabolite was detected. Error values for each sample are summarized in Table 1.

As expected, the peak corresponding to C12 was present in all treated samples, and absent in vehicle control lysates (Fig. 2.3B & C; Fig. 2.4). The calculated exact mas of C12 is 298.2013 g/mol, and measured accurate masses for each sample fell within the acceptable threshold of less than 5 ppm. C12-COOH (calculated exact mass is 316.2118 g/mol) was detected in all lysates from WT animals at relatively high abundance, whereas this metabolite was absent in PON2-KO lysates prepared from small intestine tissue and primary MEF cells

(chromatograms for each sample are depicted in Fig. 2.4). Taken together, these results demonstrate PON2 lactonase activity is absent in tissues and cells from mice deficient in PON2 expression.
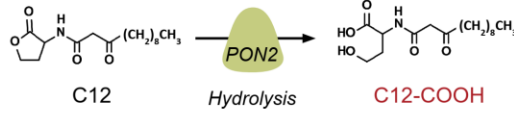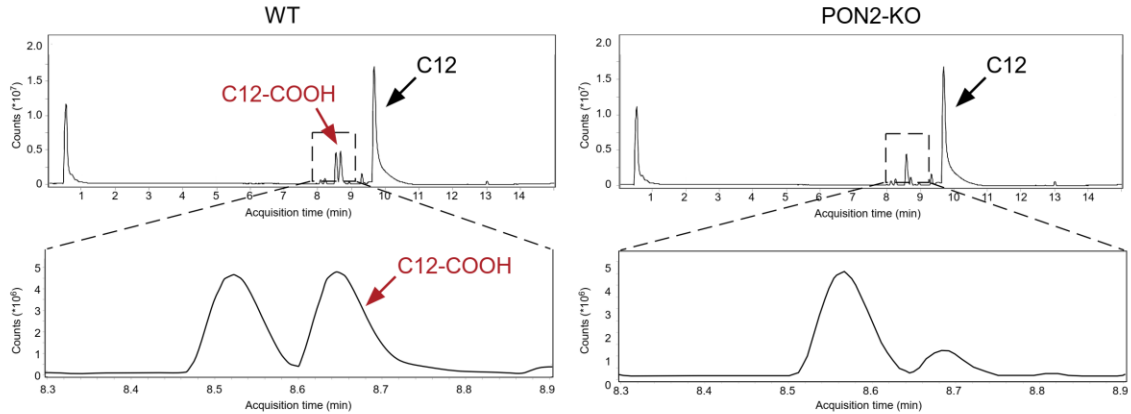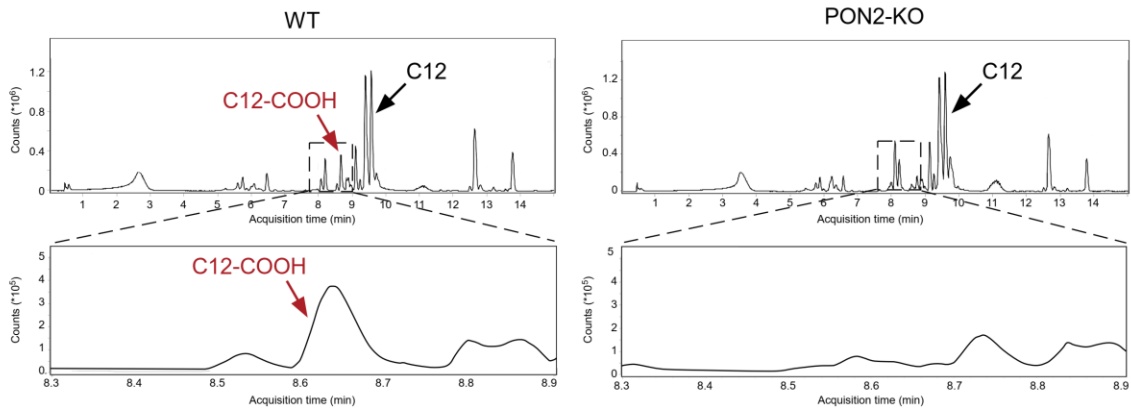
Figure 2.3. Tissues and cells from PON2-KO mice are devoid of PON2 lactonase activity. (A) PON2 catalyzes the hydrolysis of C12's lactone ring to a carboxylic acid derivative (C12-COOH). Representative UV spectrogram showing the PON2-dependent production of C12-COOH in lysates prepared from (B) small intestine and (C) primary MEF cells.
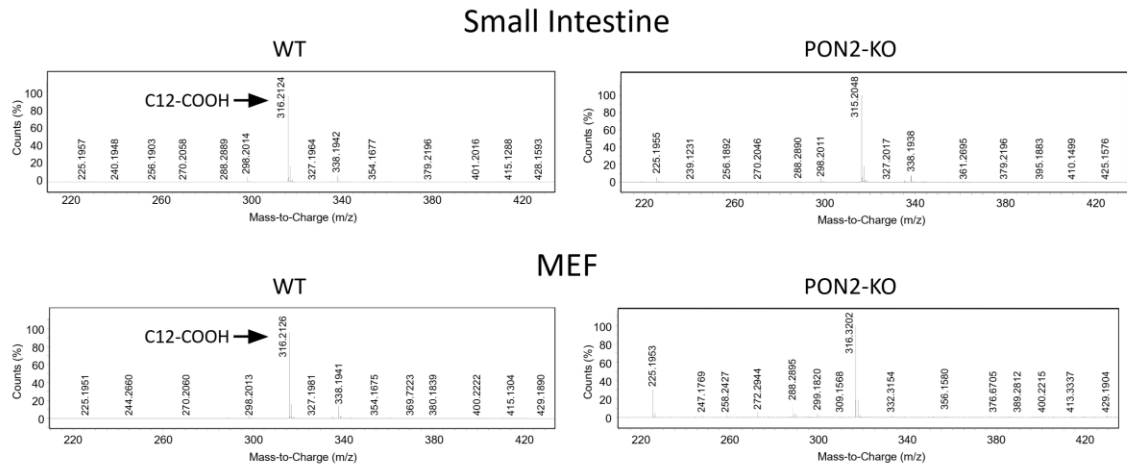
Figure 2.4. LC-MS chromatograms of cell and tissue lysates treated with C12. Relative abundance data shown for lysates prepared from small intestine and primary MEF cells from WT or PON2-KO mice. Peak intensity values are not absolute, but are instead relative to the highest abundance metabolite in each sample. C12-COOH was detected in all WT samples and absent in PON2-KO samples.

Table 2.1. Summary of PON2 lactonase activity in mouse tissues and cells by LC-MS. Error values (in ppm) were calculated by using calculated exact mass (m_i) and measured exact mass (m_a) in grams. Values of |ppm| < 5 are considered to be acceptable, i.e., a given metabolite was detected.

Genotype	Metabolite	Small intestine [a]	MEF [a]
WT	C12	3.6888	3.6888
	C12-COOH	1.2650	2.2137
PON2-KO	C12	2.0121	4.0241
	C12-COOH	-3184.6*	347.24*

[a] Values represent Error (ppm)
* Values of |ppm| < 5 are considered acceptable

2.3.4 PON2 status does not alter normal mouse growth and organ development

To explore PON2's role in mouse growth and development, we measured body and organ weight in mice with or without PON2 expression during critical periods of early growth. Specifically, body weight was recorded for male (Fig. 2.5A) and female (Fig. 2.5B) mice biweekly from the ages of 4 to 12 weeks. No differences in body weight were observed in mice of either sex in WT vs. PON2-KO mice. Furthermore, we also investigated PON2's influence on organ development by determining the relative organ weight of vital organs (heart, lungs, kidneys, liver, and spleen) collected from male (Fig. 2.5C) and female (Fig. 2.5D) mice at 12 weeks of age. Regardless of PON2 status, no significant differences in relative organ weight were observed in mice of either sex. Together, these observations demonstrate that PON2 is dispensable for normal mouse growth and organ development.
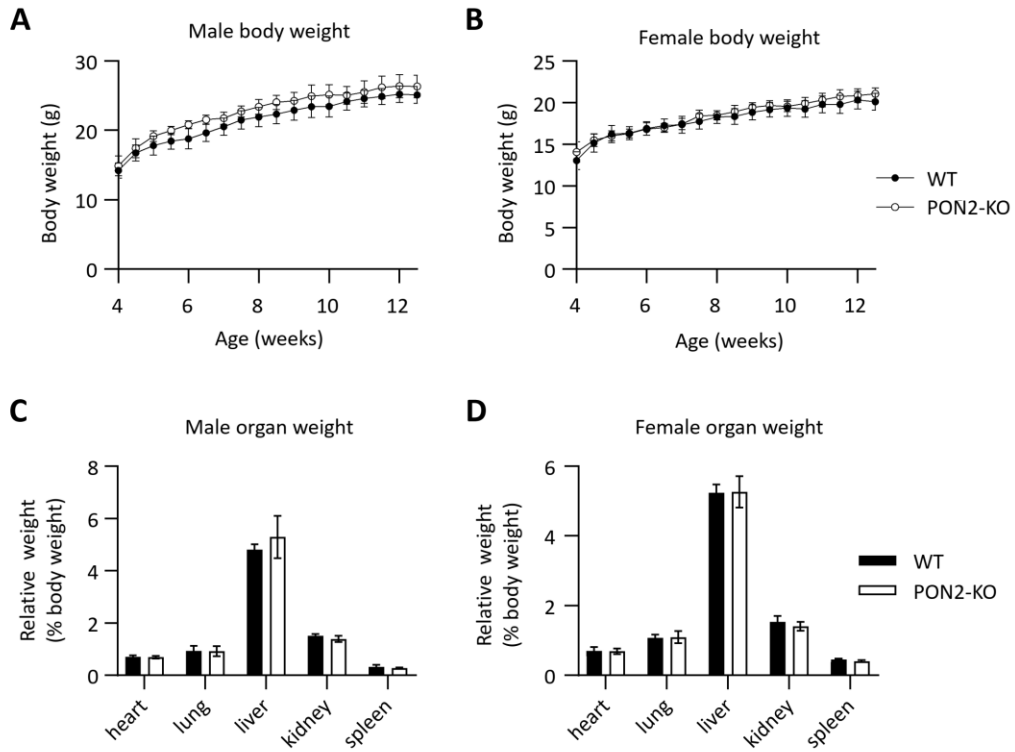
Figure 2.5. PON2 deficiency does not affect mouse body and organ weight.
Male (A) and female (B) mice 4 weeks of age with or without PON2 expression
were weighed biweekly for 8 weeks (n=10 per sex per group). At 12 weeks of age,
male (C) and female (D) organ weight was determined (n=5 per sex per group).

2.3.5 Generation and characterization of immortalized murine tracheal epithelial cells (TECs)

TECs are the main multipotent progenitor cell type in the murine lung and are capable of differentiating into all cell types comprising the murine airway [104]–[106]. Therefore, this cell type is physiologically relevant to *P. aeruginosa* infections: any disruption to TEC physiology *in vivo* could contribute to progressive loss of respiratory function during chronic infection. We sought to explore the PON2-mediated effects of C12 at physiological concentrations using primary TECs isolated from mice with or without PON2 expression. Primary TECs were isolated as previously described [94], [95] and cultured in the presence of ROCK and DAPT inhibitors according to a report by Eenjes and colleagues [96] to maximize cell yield. Once isolated, primary TECs reach replicative senescence after approximately 14 days in culture. We sought to overcome this practical limitation and expand the experimental utility of TECs through cellular immortalization. To this purpose, these cells were infected with lentivirus engineered to express SV40-Large T antigen as described by Lundberg et al. [107], which is a widely-used system of cellular immortalization via binding and inactivation of p53 and retinoblastoma (Rb) proteins.

The mammalian airway epithelium comprises numerous cell types necessary for respiration and host defense [108]. Distinct cellular populations correspond to the various compartments of the respiratory tract along the proximal-distal axis. In mice, the tracheobronchial epithelium predominantly consists of ciliated cells, secretory cells, and basal cells. Of these, basal cells are the primary

progenitor cell type capable of self-renewal and differentiation into other tracheobronchial epithelial cell lineages [105]. We evaluated cellular lineage markers of primary and immortalized TECs to observe any alterations in molecular phenotypes associated with immortalization with SV-40 Large-T antigen. To this purpose, we quantified mRNA expression of TEC basal cell markers: KRT5, SOX2, and TP63 [105], [109], and one marker of mesenchymal cells, Vimentin [110] (Fig. 2.6). Expression of tracheal epithelial markers KRT5, SOX2, and TP63 were similarly high in both primary and immortalized TECs, and low in primary MEF cells (used as negative controls), regardless of PON2 expression status. In contrast, Vimentin expression was low in primary and immortalized TECs, and high in primary MEF cells. Next, expression of PON2 in primary TECs, immortalized TECs, and primary MEF cells was examined by western blot, confirming PON2 deficiency in cells derived from PON2-KO mice (Fig. 2.7). Taken together, these observations demonstrate that TECs immortalized via transduction with SV40-Large-T antigen retain the expression profile of their primary counterparts.
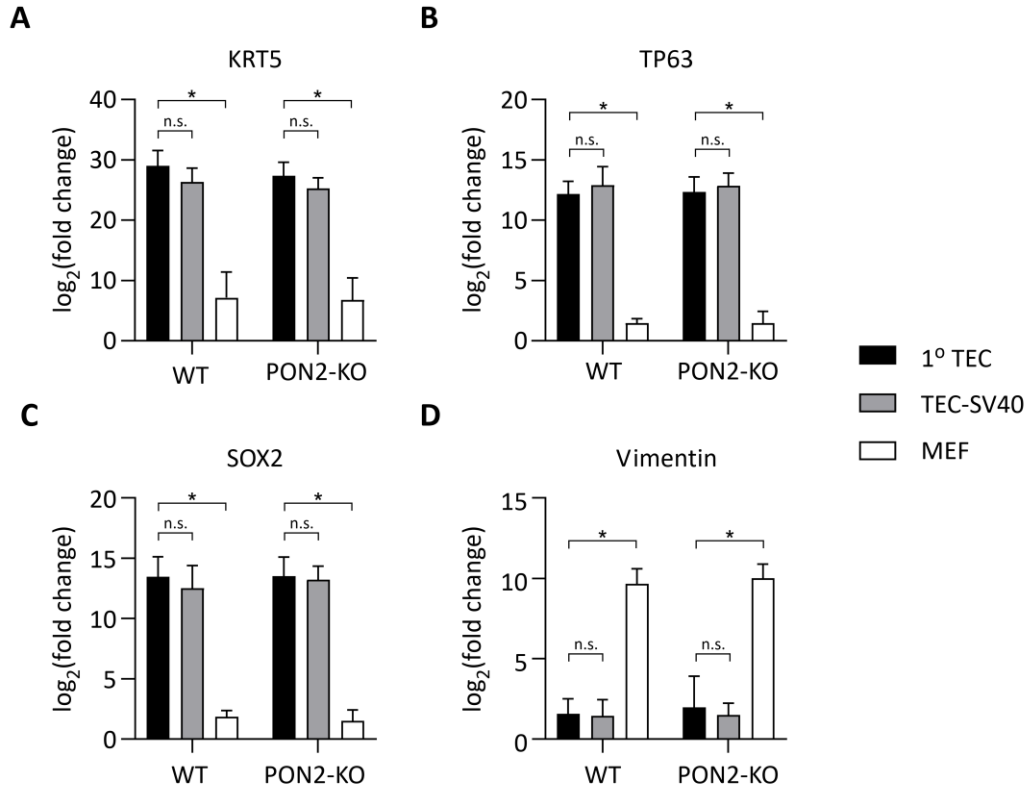
Figure 2.6. **Gene expression profile of SV40-immortalized TECs.** Expression of three basal epithelial cell markers, KRT5 (A), TP63 (B), and SOX2 (C), and one mesenchymal cell marker, Vimentin (D), was quantified by qRT-PCR (relative to Actin). Primary and immortalized TECs exhibit similarly high expression of KRT5, SOX2, and TP63, and low expression of Vimentin. In contrast, primary MEF cells express KRT5, SOX2, and TP63 at low levels, while vimentin expression is high. Data are mean $\log_2$(fold change) values ± SD from 5 independent experiments. Statistical significance was determined by two-way ANOVA: (n.s.) non-significant, (*) $p < 0.01$.
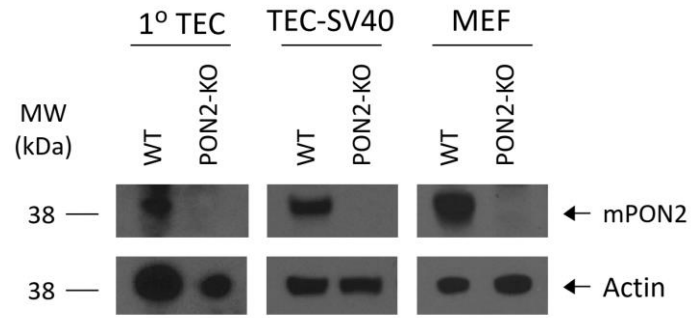
Figure 2.7. PON2 expression of primary TECs, immortalized TECs, and MEF cells. PON2 expression was assessed by western blot analysis in primary TECs, immortalized TECs, and primary MEF cells isolated from WT and PON2-KO mice. Actin shown as loading control.

2.3.6 PON2 mediates the cytotoxic and subtoxic effects of C12 in TECs

Our laboratory has previously demonstrated that PON2 is required for the cytotoxic effects of C12 in a variety of human and murine cell lines [83]–[85]. To investigate the PON2-mediated effects of C12 in the context of the mammalian airway, we treated WT and PON2-KO TECs with increasing concentrations and assessed cellular viability by propidium iodide (PI) exclusion via flow cytometry (Fig. 2.8A) as previously described [85]. The results of this analysis revealed that C12 exhibited a concentration-dependent increase to cytotoxicity in WT cells at concentrations above 20 µM. In contrast, TECs lacking PON2-KO expression were similarly viable at all concentrations of C12. Because C12 is known to induce cell death through activation of the intrinsic apoptotic cascade, we also quantified caspase 3/7 activation (Fig. 2.8B) as previously described [84], [85]. In accordance with the PI exclusion assay, we observed a similar concentration-dependent caspase 3/7 activation in WT TECs at concentrations of C12 above 30 µM, whereas caspase activation was unaffected in PON2-KO cells at all concentrations. Next, we cultured WT and PON2-KO TECs in subtoxic concentrations of C12 and monitored cellular proliferation every 24 h for 3 days (Fig. 2.8C & D). Significant impairment to cellular proliferation was observed in WT TECs treated with 20 µM C12 after 3 days. Conversely, proliferation of PON2-KO TECs was similar at each treatment condition. Taken together, these results corroborate the PON2-dependent manner by which C12 induces apoptotic cell death and highlight a previously-unreported finding that C12 impairs cellular proliferation at subtoxic concentrations, which is dependent on PON2 expression.
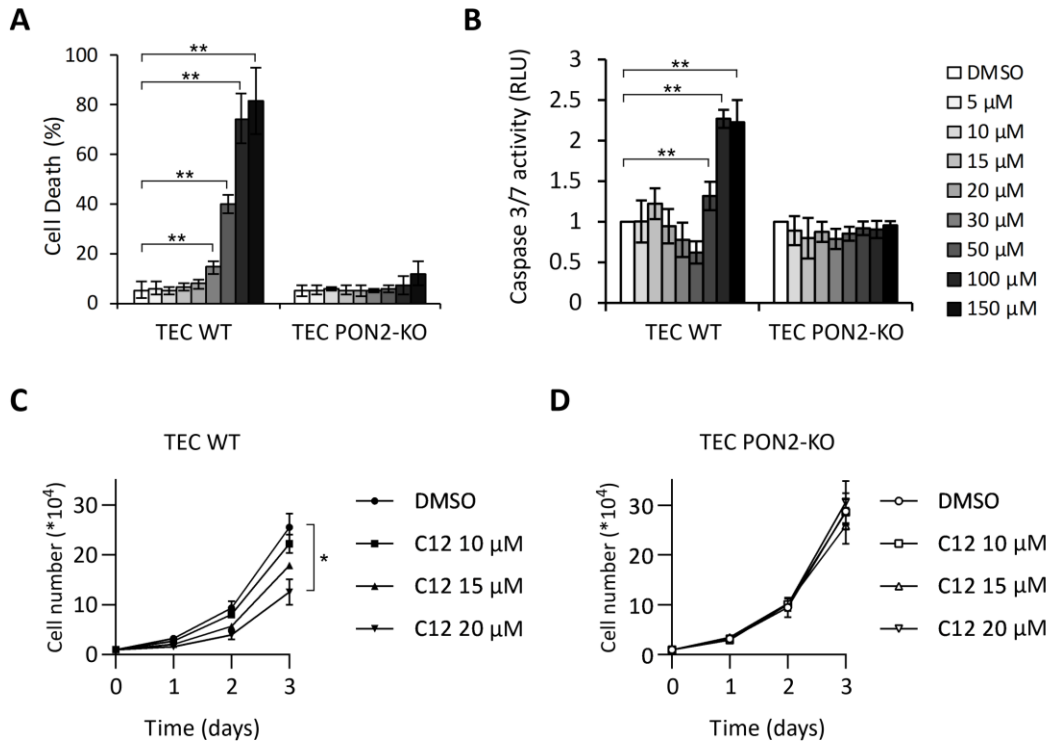
Figure 2.8. PON2 expression is required for the cytotoxic and subtoxic effects of C12. SV40-immortalized TECs were treated with increasing concentrations of C12 for 24 h, cell death was quantified via flow cytometry (A), and Caspase 3/7 activation was quantified by measuring fluorescence intensity (B). Cell proliferation was monitored for 3 days in WT (C) and PON2-KO (D) SV40-immortalized TECs cultured in the presence of subtoxic concentrations of C12. Data are mean ± SD from 3 independent experiments. An unpaired Student's t test was used to determine statistical significance. (*) $p < 0.05$ (DMSO vs 20 µM C12),

2.3.7 PON2 mediates disruptions to mitochondrial membrane potential in response to C12

Previous work has identified mitochondria as one of the primary targets of C12 [78]. Mitochondrial potential ($\Delta\psi_{mito}$) and network morphology are key indicators of mitochondrial health essential for cellular survival and proliferation. We sought to explore the mechanisms by which subtoxic and cytotoxic concentrations of C12 impact cellular viability and proliferation. Because maintenance of $\Delta\psi_{mito}$ is essential for mitochondrial integrity, we examined PON2's role in modulating $\Delta\psi_{mito}$ in response to C12. We first labeled WT and PON2-KO TECs with the membrane potential-dependent dye tetramethylrhodamine ethyl ester (TMRE) followed by treatment with DMSO or C12 (Fig. 2.9). Changes to $\Delta\psi_{mito}$ were monitored at the single-cell level by time-lapse confocal microscopic imaging of TMRE-labeled live cells. Next, $\Delta\psi_{mito}$ was quantified by comparing the ratio of average background-corrected TMRE fluorescence intensity pre- and 25 minutes post-treatment (Fig. 2.9B & C). Mitochondria in WT cells treated with either DMSO or 20 µM C12 were similarly polarized, as indicated by TMRE fluorescence intensity. Conversely, treatment with the highest concentration C12 (100 µM) reduced TMRE fluorescence, indicative of less-polarized mitochondria. Importantly, no significant changes to $\Delta\psi_{mito}$ were observed in PON2-KO TECs treated with either 20 or 100 µM C12 (Fig. 2.9C), again reinforcing the PON2-dependent manner by which C12 modulates TEC physiology. Together, these results indicate that C12 triggers PON2-dependent acute $\Delta\psi_{mito}$ depolarization at cytotoxic, but not subtoxic, concentrations.
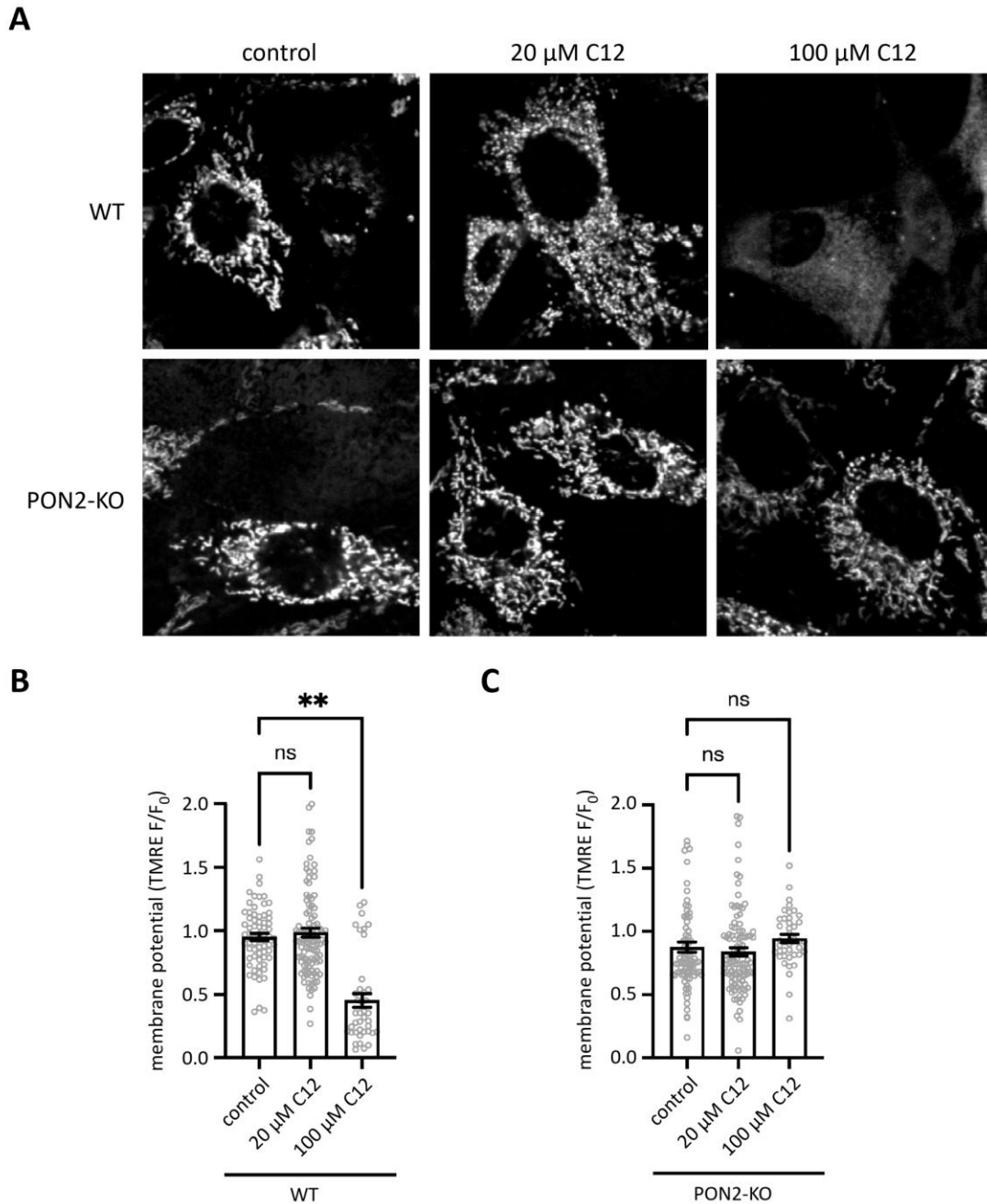
Figure 2.9. C12 disrupts mitochondrial membrane potential ($\Delta\psi_{mito}$) in WT but not PON2-KO cells. (A) Representative confocal images showing TMRE fluorescence in WT and PON-KO cells after 25-minute treatment with vehicle control (DMSO) or the indicated concentration of C12. (B, C) Summary data of $\Delta\psi_{mito}$ (TMRE F/F$_0$) in WT and PON-KO cells after a 25-minute treatment with vehicle control or C12 (mean ± SD; **P<0.001; ANOVA). Measurements were collected from more than 40 cells per treatment.

2.3.8 C12 induces mitochondrial fission in PON2-dependent manner

Another key indicator of mitochondrial health and function is mitochondrial network morphology. In the previous experiments investigating the effects of C12 on $\Delta\psi_{mito}$, we observed (qualitative) disruptions to mitochondrial network morphology in WT TECs following treatment with C12 (Fig. 2.9A). Since TMRE is a $\Delta\psi_{mito}$-dependent dye, we were unable to quantify network morphology in depolarized mitochondria from WT TECs treated with the highest concentration of C12. To overcome this limitation and explore C12's role in altering mitochondrial morphology, we employed an alternate strategy in which TECs were transiently transfected with the matrix-targeted fluorescent protein mCherry-mito-7, which has been used to study the morphology of single mitochondria [99]. Mitochondrial morphology was evaluated in WT or PON2-KO TECs treated with 20 or 100 µM C12 by calculating the form factor and the aspect ratio as measures of elongation and interconnectivity, respectively. Compared to DMSO-treated cells, the mitochondria in WT TECs treated with 20 or 100 µM C12 were less elongated and interconnected (Fig. 2.10). In contrast, mitochondria in PON2-KO TECs maintained their morphology, regardless of treatment, demonstrating that C12 disrupts mitochondrial network morphology in a PON2-dependent manner at both subtoxic and cytotoxic concentrations. Furthermore, these data are consistent with the mitochondrial morphology changes in TEC cells treated with 20 µM C12 as measured by TMRE fluorescence (Fig. 2.11). Taken together, our studies indicate that PON2 mediates acute disruptions to mitochondrial integrity and structure in response to both subtoxic and cytotoxic concentrations of C12.
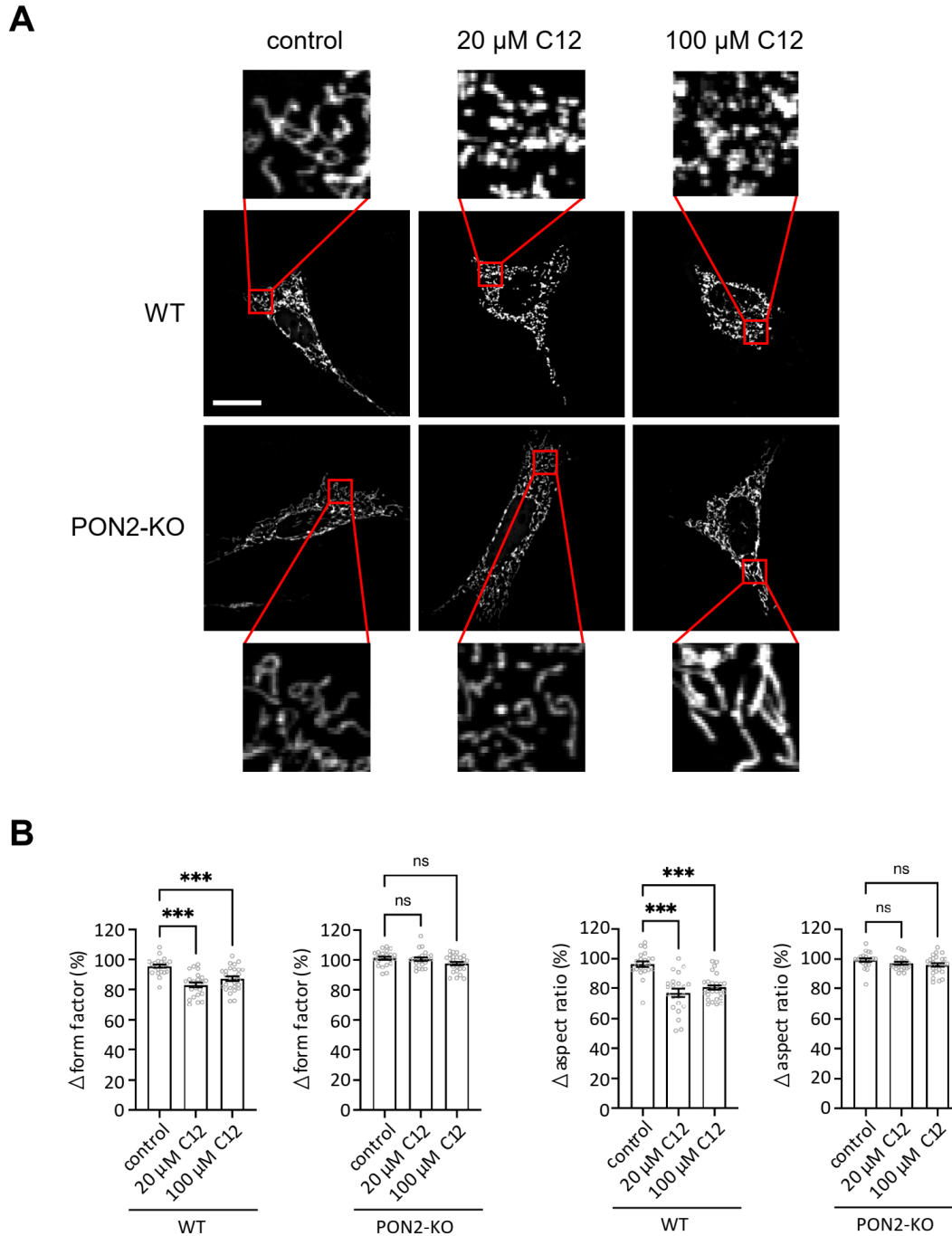
Figure 2.10. C12 disrupts mitochondrial morphology in WT but not PON2-KO cells. (A) Representative confocal images showing mCherry fluorescence in WT and PON-KO cells after 25-minute treatment with vehicle control (DMSO) or the indicated concentration of C12. Mitochondrial morphology in WT and PON2-KO cells assessed by form factor **(D)** and aspect ratio **(E)** after treatment with C12 (**$P<0.001$; ANOVA). Measurements were collected from greater than 40 cells per treatment.
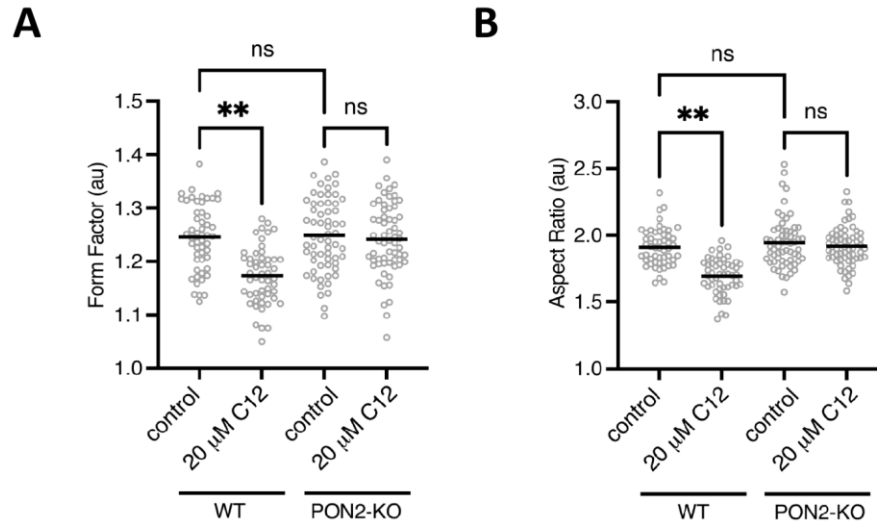
Figure 2.11. PON2 mediates disruptions to mitochondrial network morphology in response to C12 as assessed by TMRE fluorescence. Mitochondrial morphology was quantified in TMRE-stained WT and PON2-KO TECs following 25-minute treatment with vehicle control (DMSO) or 20 µM C12 as assessed by form factor (A) and aspect ratio (B). (Horizontal bar denotes mean; **P<0.001; ANOVA). Measurements were collected from greater than 40 cells per treatment.

2.3.9 C12 disrupts mitochondrial respiration and promotes aerobic glycolysis

While a number of studies have demonstrated that high concentrations of C12 reduce mitochondrial respiration [111], [112] and electron transport chain activity [113] in cells showing early signs of apoptosis, PON2's role in mediating mitochondrial function in response to subtoxic concentrations of C12 remains unknown. To address this knowledge gap, we utilized the Seahorse XF Mito Stress test to monitor changes in mitochondrial respiration in response to a subtoxic concentration of C12 (Fig. 2.12). WT or PON2-KO TECs were cultured with either DMSO or 20 µM C12 for 24 h, and oxygen consumption rate (OCR) and extracellular acidification (ECAR) were quantified using the Seahorse XF bioanaylzer. Using this approach, we observed that C12 impaired key metrics of mitochondrial activity in WT cells, basal respiration (Fig. 2.12B), maximal respiration (Fig. 2.12C), ATP production (Fig. 2.12D), and spare respiratory capacity (Fig. 2.12E). No changes to non-mitochondrial oxygen consumption (Fig. 2.12F) or proton leak (Fig. 2.12G) were observed. Further, ECAR was significantly increased in the C12-treated WT cells compared to their vehicle-control treated counterparts (Fig. 2.12H). In contrast to these observations, OCR and ECAR values were unaltered in PON2-KO TECS. These results demonstrate that treatment with a subtoxic concentration of C12 impairs key facets of oxidative metabolism and promotes aerobic glycolysis in a PON2-dependent manner.
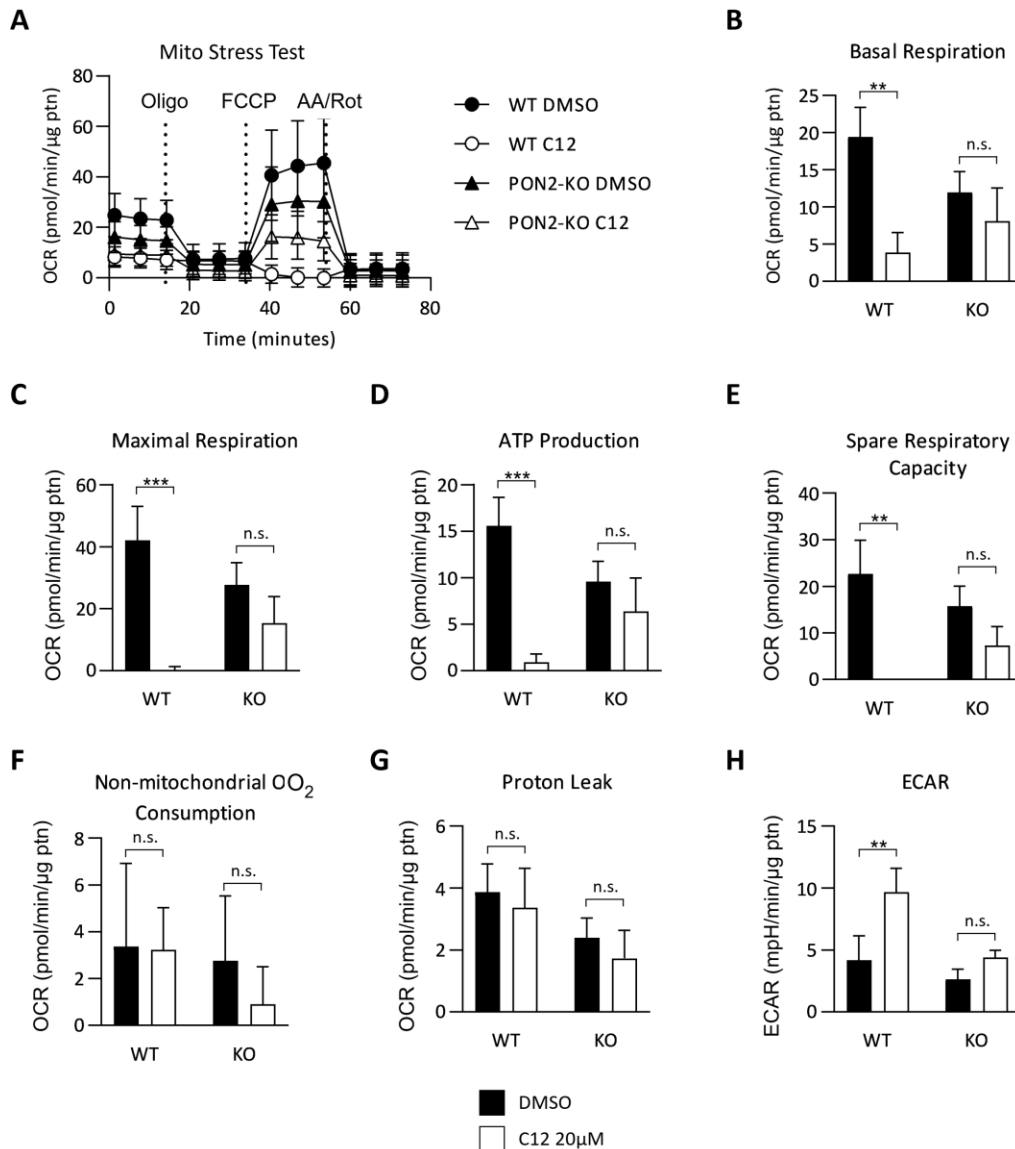
Figure 2.12. Treatment with C12 decreases oxygen consumption and increases extracellular acidification in a PON2-dependent manner. Mitochondrial function was assessed using the Seahorse XF Mito Stress test assay. (A) Oxygen consumption rate (OCR) was quantified in TEC-SV40 cells with or without PON2 expression following 24 h treatment with 20 µM C12. OCR values were used to determine basal respiration (B), maximal respiration (C), ATP production (D), spare respiratory capacity (E), non-mitochondrial O2 consumption (F), and proton leak (G). (H) Extracellular acidification rate (ECAR) was quantified under the same conditions. Data are mean ± SD of 3 independent experiments, 5 technical replicates per group. Statistical significance was determined by two-way ANOVA with Tukey's multiple comparison test. (*) $p < 0.05$, (**) $p < 0.01$, (***) $p < 0.005$ compared to vehicle-treated WT.

2.4 DISCUSSION

Clinicians face increasing challenges in treating patients with chronic *P. aeruginosa* infections due to a steady rise in antibiotic-resistant strains of this bacterium [69]. Therefore, understanding the mechanisms underlying *P. aeruginosa* infections is critical to expand future treatment options for susceptible patients. Beyond its role in bacterial intercellular communication, earlier work has established C12's role in modulating immune responses and inducing apoptotic cell death in a variety of eukaryotic cells [79]–[82]. Further, the intracellular lactonase PON2 is required for C12's effects in host cells [83], [84]. However, little attention has been given to how concentrations of C12 present in active infections of *P. aeruginosa* alter mitochondrial function in the host airway. While the exact concentrations of C12 in patients with *P. aeruginosa* are contested, estimates range from nanomolar to low micromolar in patient sputum samples [76], [77], [114]. Therefore, it is likely that concentrations of C12 at or near biofilms are significantly higher *in vivo*. The majority of published reports investigating C12's role in modulating eukaryotic physiology have used concentrations that evoke apoptotic cell death and are likely not relevant to infected patients. With this consideration in mind, we directed our attention to lower concentrations of C12 which may alter host physiology without triggering apoptosis. Here, we demonstrate that C12 disrupts mitochondrial respiration and biogenesis through the enzymatic activity of PON2, resulting in impaired cellular proliferation of key airway progenitor cells. While work by several groups has explored the role of C12

on mitochondrial function using other types of cells undergoing apoptosis [111]–[113], this is the first report, to our knowledge, demonstrating that PON2 mediates the effects of subtoxic concentrations of C12 in mammalian airway cells, the primary site of *P. aeruginosa* infections.

We first generated PON2-knockout animals using a CRISPR-Cas9 approach (Fig. 2.1) and confirmed loss of PON2 by genomic sequencing (Fig. 2.1B), western blot analysis (Fig. 2.2), and enzymatic assay (Fig. 2.3-4; Table 2.1). PON2 expression does not appear to impact the normal growth and development of mice of either sex, as demonstrated by body and organ weight studies (Fig. 2.5). Since PON2 is implicated in numerous disease states, including atherosclerosis, neurodegenerative disorders, and cancer, PON2-deficient mice may serve as a potentially useful experimental tool in future studies into PON2 biology.

The central research objective in this study was to explore how PON2 expression modulates airway epithelial cell physiology in response to various concentrations of C12 using a physiologically-relevant experimental approach. To this end, we sought to use primary TECs from mice with or without PON2 expression. This experimental system was limited by the replicative senescence of primary TECs in culture, therefore, we generated immortalized TECs to expand their utility in this investigation. The cellular phenotype of immortalized TECs was validated by measuring expression of cell lineage markers commonly present in basal airway epithelial cells *in vivo* (Fig. 2.6). Given that SV40-immortalized TECs retain phenotypic markers characteristic of their primary counterparts, these cells

may provide a useful platform to expand our understanding of PON2's influence on tracheal epithelial physiology in the future.

The influence of C12 on cellular metabolism has been investigated in earlier studies [111]–[113]. However, these effects were observed in cells treated with C12 at or above physiological concentrations that induced cellular events distinctive of apoptotic cell death, including depolarization of $\Delta\psi_{mito}$ [112], increased concentration of cytosolic Ca^{2+} [113], release of cytochrome c into the cytosol [111], and activation of caspases [111], [113]. In accordance with these observations, PON2 is required for apoptotic cell death of TECs treated with increasing concentrations of C12 (Fig. 2.8A-B). Below 30 µM, C12 failed to reduce TEC viability (Fig. 2.8A), whereas a concentration of 20 µM was sufficient to slow cellular proliferation (Fig. 2.8C), indicating that C12 can impair cellular metabolism at subtoxic concentrations. While WT TECs treated with a subtoxic concentration of C12 maintained $\Delta\psi_{mito}$ (Fig. 2.9), PON2-dependent reductions of oxidative metabolism were observed. Specifically, C12 impaired key aspects of oxidative respiration in mitochondria, including basal respiration, maximal respiration, ATP production, and spare respiratory capacity (Fig. 2.12). We also observed a concomitant PON2-dependent increase in extracellular acidification, likely due to enhanced production of H^+ ions from glycolysis. These results suggest that C12 diminishes mitochondrial respiratory activity required for energy production, thereby promoting a shift to aerobic glycolysis to maintain baseline cellular functions.

Mitochondria exist in a dynamic network within cells and alter their shape continuously through the fusion, fission, and motility processes in response to intracellular energy demands and stress [115]. In the present study, we observed rapid, PON2-dependent changes to mitochondrial network morphology in response to subtoxic and cytotoxic concentrations of C12 (Fig. 2.10 & 2.11). At a higher concentration (100 μM), C12 induced acute $\Delta\psi_{mito}$ dissipation, considered an early indicator of intrinsic apoptotic cell death [116]. These results are consistent with TEC viability data (Fig. 2.8) as well as earlier work by our laboratory demonstrating that C12 acts through mitochondria to activate the intrinsic apoptotic cascade at higher concentrations [82]–[85]. At a subtoxic concentration of C12 (20 μM), cells maintained $\Delta\psi_{mito}$, while mitochondria were less elongated and interconnected, indicators of mitochondrial fission (Fig. 2.10 & 2.11). Mitochondrial fission has established roles in mediating cellular survival, proliferation, and apoptotic cell death. While fission is required to generate new mitochondria, it may also serve as a quality control measure to trigger selective mitophagy and salvage mitochondria in response to stress or damage [117]. It is conceivable that cells treated with subtoxic concentrations of C12 undergo mitochondrial fission to eliminate damaged mitochondria, maintain $\Delta\psi_{mito}$ and basic cellular functions, albeit at the cost of impaired cellular proliferation to avoid catastrophic cell death. However, once damages caused by a high concentration of C12 (100 μM) reach a critical threshold, i.e., "the point of no return", mitochondria lose $\Delta\psi_{mito}$, triggering the apoptotic cell death signaling cascade.

Changes in the expression of regulatory proteins governing mitochondrial physiology have been linked to the effects of C12 on mitochondrial morphology [111], [112]. In response to C12, fibroblasts and intestinal epithelial cells alter expression of proteins involved in mitochondrial structural organization, oxidative phosphorylation, and stress responses [111]. Likewise, in human lung epithelial cells, high concentrations of C12 reduce expression of peroxisome proliferator-activated receptor-γ coactivator-1α (PGC-1α), a principal regulator of mitochondrial biogenesis [112]. Regulation of protein expression normally occurs at multiple steps of signal transduction, and the biological events reflective of these signaling cascades are largely observed hours following C12 incubation when signs of apoptosis, such as $\Delta\psi_{mito}$ depolarization, are evident. In the present study, mitochondrial morphology changes were detected within 25 minutes following exposure of a subtoxic concentration of C12 (Fig. 2.10 & 2.11), which is unlikely to be caused by changes in expression of key protein regulators of mitochondrial structure and function. Therefore, the observed induction of mitochondrial fission is likely an acute response to C12 to maintain cellular functions required for cell survival and proliferation. Mechanistically, the effects of C12 on mitochondrial morphology are mediated by PON2. As a lactonase localized in mitochondria, PON2 is capable of hydrolyzing C12 into a carboxylic acid that accumulates within mitochondria and causes acidification of the mitochondrial matrix [90]. Therefore, one possible scenario is that C12-COOH is capable of directly inducing a stress response in mitochondria, resulting in alterations to mitochondrial network dynamics. Alternatively, PON2 is known to associate with the mitochondrial

electron carrier coenzyme Q10 (CoQ10) to cleave oxidized mitochondrial lipids and prevent the production of superoxide [30], [31]. Thus, another possibility is that C12 interrupts the protein-protein interaction between PON2/CoQ10, thereby destabilizing electron transport activity, mitochondrial redox potential, and Ca^{2+} homeostasis required for mitochondrial integrity. Future studies are warranted to further expand our understanding into the mechanisms that underly the C12-induced modulation of mitochondrial biogenesis through PON2.

CHAPTER 3

PON2 ENHANCES MITOCHONDRIAL BIOENERGETICS TO PROMOTE LUNG
ADENOCARCINOMA PROLIFERATION

3.1 INTRODUCTION

Lung cancer remains the leading cause of cancer deaths in the United States and worldwide [118]. Adenocarcinoma of the lung is the most common histological subtype and accounts for 40% of all lung cancer diagnoses—a relative frequency which is increasing [119]. Despite shared morphology, lung adenocarcinoma tumors are highly heterogeneous at the genetic and cellular level, complicating therapeutic intervention [120]. As a consequence of variability within and among tumors, patients with lung adenocarcinoma frequently exhibit or develop resistance to chemotherapeutic agents [120]. Treatment options have expanded in recent years beyond traditional chemotherapeutics to include molecular-targeted therapies and immune checkpoint inhibitors [121]. However, the prognosis of patients with lung adenocarcinoma remains dismal. Therefore, it is imperative to continue identifying molecular vulnerabilities to improve therapeutic outcomes for patients with lung adenocarcinoma.

As an intracellular enzyme with wide tissue distribution and antioxidant activity, Paraoxonase 2 (PON2) has received increasing attention for its role in promoting apoptotic escape in tumor cells. A recent large-scale study demonstrated that PON2 is overexpressed at the mRNA and protein levels in numerous human tumors [42], perhaps due to its stabilizing effect on cancer cells [38]. Novel insights into PON2 function have uncovered that PON2 promotes metabolic phenotypes favorable to certain cancer cells. For instance, loss of PON2 expression impaired glucose uptake and ATP production in a murine model of B-cell acute lymphoblastic leukemia (B-ALL) by disrupting glucose transporter 1 (GLUT-1) membrane localization [122]. Furthermore, PON2 mRNA expression was inversely correlated with B-ALL patient prognosis [122]. Similar observations were reported in the context of pancreatic ductal adenocarcinoma (PDAC), in which PON2 promoted GLUT1 membrane localization and inhibited AMP-activated protein kinase (AMPK) mediated cellular starvation response, thereby promoting anoikis and metastasis in a murine model of PDAC [41]. Conversely, a tumor suppressor role for PON2 was identified in the context of ovarian cancer (OC) [123]. In this study, high PON2 expression blunted OC cellular proliferation and xenograft tumor growth in mice through inhibition of insulin like growth factor-1 (IGF-1) expression and signaling [123]. Thus, PON2 expression likely modulates different aspects of cellular physiology depending on the molecular context of its activity within cells.

Given the unclear conditional requirements of PON2 activity in cancer, we sought to investigate the influence of PON2 expression and lactonase activity in

lung adenocarcinoma cellular proliferation, cell cycle progression, ROS generation, extracellular nutrient uptake, and cellular bioenergetics.

3.2 MATERIALS AND METHODS

3.2.1 Cell lines and reagents

Dulbecco's Modified Eagle's Medium (DMEM), penicillin/streptomycin, trypsin, and L-glutamine were obtained from Mediatech (Manassas, VA); Glucose-free DMEM was purchased from Thermo Fisher (Waltham, MA) fetal bovine serum was purchased from Gemini (Broderick, CA); Bronchial Epithelial Cell Growth Medium (BEGM) and SingleQuots were purchased from Lonza (Walkersville, MD); and propidium iodide was purchased from Invitrogen (Carlsbad, CA). N-(3-oxododecanoyl)-homoserine lactone (C12), polybrene, puromycin, and [U-^{13}C]-glucose were purchased from Sigma-Aldrich (St. Louis, MO). Antibodies (Abs) for western blot were anti-β-actin mAb (A5441; Millipore Sigma; Burlington, MA), anti-Human PON2 mAb (ab183710; Abcam; Cambridge, England), anti-Mouse PON2 pAb (ABIN1573944; antibodies-online.com; Atlanta, GA), peroxidase-conjugated goat anti-rabbit IgG (65-6120; Thermo Fisher; Waltham, MA) and peroxidase-conjugated goat anti-mouse IgG (65-6520; Thermo Fisher).

3.2.2 Cell culture

HEK-293T, A549, and NCI-H1299 cell lines were purchased from ATCC (Manassas, VA). Human bronchia/tracheal epithelial (HBE) immortalized by

telomerase and SV40 large T antigen were obtained from Professor Barrett Rollins (Harvard Medical School). HBE cells were cultured in BEGM supplemented with SingleQuots. All other cells were cultured in DMEM containing 10% FBS, 100 units/mL penicillin, and 100 µg/mL streptomycin. All cell lines were cultured in a 5% CO_2 humidified incubator at 37°C. Cells were passaged at approximately 1:5–1:10 dilutions and were continuously cultured no longer than 3 weeks. Stocks come from thawed vials frozen at passage two following receipt from ATCC and were authenticated by ATCC cell bank using the Short Tandem Repeat (STR) profiling.

3.2.3 Plasmids

Control double nickase plasmid (SC-437281) and PON2 CRISPR/Cas9 plasmid (SC-403181-NIC) were purchase from Santa Cruz (Santa Cruz, CA). Control double nickase plasmid comprises a pair of plasmids, each with D10A mutant Cas9 nuclease and a non-targeting 20nt scramble gRNA. One plasmid in the pair contains a puromycin-resistance gene, the other plasmid in the pair contains a GFP as selection markers. PON2 CRISPR/Cas9 knockout plasmid comprises 2 pooled plasmids, each encoding the Cas9 nuclease, a 20nt PON2-specific gRNA, with puromycin-resistance or GFP as selection markers. The selected gRNA is targeted to exon 3 of the PON2 genomic locus and designed to trigger a site-specific double strand break (DSB). Control shRNA plasmid-A (SC108060), murine PON2-shRNA plasmids (sc-62839-SH) and human PON2-shRNA plasmids (SC62838-SH) were purchased from Santa Cruz. Control shRNA

plasmid-A encodes a non-specific scramble shRNA; PON2-shRNA plasmid comprises 3 lentiviral vector plasmids with 19-25nt shRNAs targeted to PON2. Each shRNA plasmid utilizes puromycin resistance as a selection marker. Lentiviral helper plasmids pMDLg/pRRE (12251), pRSV.Rev (12253) and pMD2.G (12259) were purchased from Addgene (Watertown, MA). Retroviral helper plasmids pUMVC (8449) and pMDLg/pRRE (12251) were also acquired from Addgene. The identities of each plasmid were verified by sequencing.

The retroviral infection expression vector pBabe-Ires-mKate2 was generated by replacing EGFP cDNA in the plasmid pBabe-Ires-EGFP [83] with mKate2 cDNA in the vector pmKate2-C acquired from Evrogen (Farmingdale, NY). Human wild-type hPON2 cDNA or lactonase-deficient mutant hPON2(H114Q) cDNA [83] was cloned into pBabe-Ires-mKate2 to generate pBabe-hPON2(WT)-Ires-mKate2 or pBabe-hPON2(H114Q)-Ires-mKate2. The plasmid identities were validated by sequencing.

3.2.4 Generation of cells with reduced PON2 expression by RNA interference

To produce lentivirus, HEK-293T cells ($1.5*10^6$) were plated in 6 cm tissue culture plates, cultured for 24 h, then transfected with control shRNA plasmid-A (SC108060) or PON2-shRNA plasmids (SC62838) along with the lentiviral helper plasmids pMDLg/pRRE, pRSV.Rev and pMD2.G using Lipofectamine2000® transfection reagent (Thermo Fisher). Tissue culture medium containing lentiviral particles was collected 48- and 72-hours following transfection and was filtered through a sterile syringe filter with 0.4 μM polyethersulfone membrane (VWR;

Radnor, CA). A549, NCI-H1299, HEK-293T, and HBE cells were seeded 24 h prior to lentiviral infection in 6-well tissue culture plates. For lentiviral infection, culture medium of plated cells was replaced with medium containing lentiviral particles supplemented with 10 μg/mL polybrene; infection was repeated 24 h later. The day following second infection, puromicyin (final concentration 5 μg/mL) was added to culture medium to eradicate uninfected cells. For all subsequent experiments, cells were cultured in medium containing 1 µg/mL puromycin. PON2 protein expression in bulk population infected cells was examined by western blot analysis.

3.2.5 CRISPR-Cas9-mediated knockout of endogenous PON2 expression

NCI-H1299 cells ($2*10^6$) were plated in 10-cm tissue culture plates and cultured for 24 hours. Control double nickase plasmid (SC-437281) and PON2 CRISPR/Cas9 plasmid (SC-403181-NIC) were transfected into NCI-H1299 cells using Lipofectamine2000® transfection reagent (Thermo Fisher) according to manufacturer's protocol. Puromycin (5 µg/mL) was added to culture medium to select against untransfected cells 24 h following transfection. Cells were maintained in culture medium with 5 µg/mL puromycin for 3 weeks to allow stably-transfected cells to proliferation. Fluorescence-activated cell sorting (FACS; MoFlo, Beckman Coulter, Brea, CA) was used to establish single clones of stably-transfected cells by seeding GFP-positive cells into individual wells of 96-well tissue culture plates containing medium supplemented with 5 µg/mL puromycin. Western blot analysis was then used to detect PON2 expression in clonal cell lines.

For subsequent experiments, clonal cells were cultured in medium containing 1 µg/mL puromycin.

3.2.6 Re-expression of wild type or lactonase-deficient PON2

For retrovirus production, HEK-293T cells were transfected with the empty retroviral vector pBabe-Ires-mKate2, pBabe-hPON2(WT)-Ires-mKate2 or pBabe-hPON2(H114Q)-Ires-mKate2 along with the helper plasmids pUVMC and pMDG2.0 using Lipofectamine2000® transfection reagent (Thermo Fisher). Retroviral supernatant was collected 48-72 hours following transfection with the addition of 10 µg/ml polybrene (Sigma) to increase infection efficiency. NCI-H1299 CRISPR-PON2 cells (0.2×10^6) were cultured in a 6-well tissue culture plate for 24 hours. The culture medium of plated cells was replaced with the retrovirus-containing medium. hPON2(WT), hPON2(H114Q), or the control mKate2 alone was expressed by retroviral infection. The expression of PON2 was determined by western blot.

3.2.7 Western blot analysis

Whole cell extracts of HBE, HEK-293T, LLC, A549, and NCI-H1299 cells were prepared using RIPA buffer (Thermo Fisher) supplemented with protease inhibitors (cOmplete; Roche). Protein concentration was measured by bicinchoninic acid (BCA assay) (Thermo Fisher). Total protein (30 µg) was electrophoresed in 4-12% Bis/Tris gels (Bio-Rad; Hercules, CA). Separated proteins were transferred to a polyvinylidene difluoride (PVDF) membrane

(Millipore) and incubated with indicated primary or secondary antibodies in blotting buffer (1X phosphate-buffered saline [PBS] with 0.2% Tween-20 and 10% (w/v) non-fat dry milk (Bio-Rad). The enhanced chemiluminescence detection system (Thermo Fisher) was used to detect proteins as previously described [84]. ImageJ software (NIH, Bethesda, MA) was used to quantify optical density (OD) values of immunoblot bands.

3.2.8 Cell death assays

LLC or NCI-H1299 cells were plated at a density of $7.5*10^3$ cells/well in 96-well culture plates and cultured overnight. The following day, culture medium was replaced with DMEM containing 0.1% DMSO or C12 at the indicated concentrations and cells were culture for 24h. Cells were collected by trypsinization and incubated in medium supplemented with 1 µg/mL propidium iodide (PI). Cell viability was measured by PI exclusion using flow cytometry (FACScalibur, Beckon Dickinson, San Jose, CA). The percentage of cell death was determined as 100 minus the value of cell viability measurement.

3.2.9 Cellular proliferation experiments

Proliferation was quantified by counting cells every 24 h for 96 h using a hemocytometer. Cells were plated at an initial density of $1.5*10^4$ cells/well in 12-well culture plates.

3.2.10 Cell cycle analysis

A549 or NCI-H1299 cells ($5*10^5$) were centrifuged at 300 x g for 5 minutes and washed twice with 500 µl 1X PBS. Cells were then fixed overnight in 1 ml 70% ethanol in 1X PBS. After centrifugation (300 x g for 5 minutes), cells were washed twice with 1X PBS and resuspended in 500 µl 1X PBS. Cells were incubated with 50 U RNase A (Qiagen; Valencia, CA) at 37°C for 1 hour. PI (5 µg) was added to each sample and incubated for an additional 30 min at 37°C, after which PI stain intensity was measured using flow cytometry (FACScalibur).

3.2.11 NMR sample preparation

NCI-H1299 CRISPR-vector or CRISPR-PON2 (6×10^5) cells were plated in 15-cm cell culture dishes in regular DMEM medium containing unlabeled glucose. Cells were cultured for 24 h and medium was replaced with glucose-free DMEM medium containing 10% glucose-free FBS and 5 mM [U-^{13}C]-glucose. Glucose-free fetal bovine serum was acquired by dialyzing against 1 x PBS three times using 12-14 kDa cutoff dialysis membrane. The culture medium was collected, frozen in liquid nitrogen, and stored at -80°C at 0, 24, 48 and 72 h time points. At 72 h, Cells were treated with trypsin, pelleted by centrifugation, and washed 3 times with 20 mL ice-cold 1X PBS. Cell pellets (7×10^6) were frozen in liquid nitrogen and stored at -80°C. To extract metabolites, 200 µl growth medium sample was mixed with 200 µl 40% ice cold trichloroacetic acid (TCA) and 300 µl 10% TCA was added to cell pellets. Samples were centrifuged and lyophilized as previously described [124], [125].

3.2.12 NMR analysis

The lyophilized extracts for medium and cells were dissolved in 100% D_2O (0.35 mL) and loaded into a 5 mm Shigemi NMR tube (Sigma-Aldrich). DSS (2,2-Dimethyl-2-silapentane-5-sulfonate sodium salt) was added to the samples at a final concentration of 50 nM to serve as a ^1H reference standard. NMR spectra were recorded at 14.1 T on a Varian Inova spectrometer (Palo Alto, CA) equipped with a 5 mm inverse triple resonance cold probe at 20°C. 1D NMR spectra were recorded with an acquisition time of 2 s and a recycle time of 5 s. Concentrations of metabolites and ^{13}C incorporation were determined by peak integration of the ^1H NMR spectra referenced to the DSS methyl groups, with correction for differential relaxation, as previously described [124], [126]–[128].^1H Spectra were typically processed with zero filling to 131 k points, and apodized with an unshifted Gaussian and a 0.5 Hz line broadening exponential. ^{13}C profiling was achieved using 1D ^{13}C-edited HSQC ^1H spectra recorded with a recycle time of 1.5 s, with ^{13}C GARP decoupling centered at 80 ppm (1JCH set to 150 Hz) and during the proton acquisition time of 0.15 s.

TOCSY spectra were recorded with a mixing time of 50 ms and a B1 field strength of 8 kHz with acquisition times of 0.573 s in t_2 and 0.036 s in t_1. The fids were zero filled once in t_2, and linear predicted and zero filled to 4096 points in t_2. The data were apodized using a squared cosine bell function in both dimensions. Specific ^{13}C isotopomers and fractional incorporation of ^{13}C were determined by comparing the areas or volume of satellite peaks with the total integrated area or

volume, with appropriate corrections for differential relaxation as previously described [124], [126]–[128].

3.3. RESULTS

3.3.1 PON2 is upregulated following oncogenic transformation

A growing number of studies have implicated PON2 as a potential modulator of oncogenesis. An early study by Witte et al. first demonstrated that PON2 protein expression was upregulated in a variety of solid and hematological tumors, including lung cancers [38]. More recently, Shakhparonov et al. expanded these insights using RNA and DNA sequencing analysis from over 10,000 cancer patients to reveal that mRNA expression of PON2 is elevated in patients with non-small cell lung carcinoma (NSCLC) [42]. However, PON2's role in the context of lung tumorigenesis has not been investigated further.

To elucidate the mechanisms by which PON2 may influence lung cancer cell survival and proliferation, our laboratory previously analyzed PON2 expression in human bronchial epithelial (HBE) cells following transformation with oncogenic Hras^{G12V} using western blot analysis (Fig. 3.1A). The results of this analysis demonstrated that Ras-mediated transformation was sufficient *per se* to induce upregulation of PON2 protein expression. To further investigate this phenomenon, PON2 expression was also evaluated in samples acquired from 11 patients with NSCLC (Fig. 3.1B & C,) by western blot analysis. PON2 expression was analyzed

in both tumor and normal adjacent lung tissues in each patient to allow pair-wise comparisons. This approach enabled our laboratory to explore how PON2 expression changed in response to oncogenic stimuli. To this purpose, optical density (OD) values of individual PON2 and actin (loading control) bands were quantified using ImageJ software (NIH) for each tumor and normal lung tissue sample. Relative PON2 expression was determined by calculating the ratio of PON2:actin OD values to account for variations in baseline PON2 expression among patients. Finally, the ratio of relative PON2 expression was calculated in tumor vs. normal lung samples for each patient (Fig. 3.1C), which revealed that PON2 was overexpressed in 8 of 11 patients with NSCLC and slightly decreased in the remaining 3. Furthermore, relative PON2 expression was similarly high in all tumor samples, while highly-variable in normal lung tissues. The discrepancy in normal lung tissue expression could be due to variations in premalignant lesions among patients [129] and warrant further investigation. Overall, the results of these experiments suggest a correlation between PON2 expression and malignant transformation in the lung.

Figure 3.1. PON2 is upregulated in oncogenically-transformed cells and lung tumor tissues. (A) Expression of PON2 in normal and ras-transformed HBE cells was determined by western blot analysis. Actin shown as loading control. (B) PON2 expression in non-small cell lung carcinoma was detected by western blot in tumor (T) and normal adjacent lung tissue (N) samples from 11 patients with NSCLC. Samples 1–4, 6, 8, 9, 11 were from adenocarcinoma patients, whereas samples 5, 7, 10 were from squamous cell carcinoma patients. (C) Immunoblot band intensities were quantified using ImageJ software (NIH). Values are ratios of relative PON2 expression (normalized to actin band intensities) in tumor:normal tissues. Values > 1 signify PON2 expression is higher in tumor compared to corresponding normal adjacent lung tissue.

3.3.2 PON2 promotes cell proliferation in Lewis lung carcinoma (LLC) cells.

Work by our laboratory and others has demonstrated that PON2 promotes cellular survival and chemotherapy resistant phenotypes in a variety of cells [36], [38], [40]. Therefore, we sought to explore how PON2 may impact cellular proliferation using murine lung cancer cells. We hypothesized that PON2 played an important physiological function in malignant lung cells, given its upregulation in tumor samples from patients with NSCLC. To test this hypothesis, we assessed cell proliferation by counting cells every 24 h for 96 h using a hemocytometer as described in Materials and Methods using Lewis lung carcinoma (LLC) cells (Fig. 3.2). Cells were stably-transfected to express either control- or PON2-shRNA and expression of PON2 was confirmed by western blot analysis (Fig. 3.2A). To confirm knockdown of PON2 function we performed a cell viability assay in which LLC control- and PON2-shRNA cells were treated with increasing concentrations of C12, a specific inducer of PON2-mediated cell death (Fig. 3.2B). As expected, cells lacking PON2 expression were resistant to the cytotoxicity of C12 at all concentrations. In contrast, control-shRNA cells exhibited a concentration-dependent decrease in cell viability in a similar manner as the parental LLCs. Next, we monitored cellular proliferation in LLCs with or without PON2 expression (Fig. 3.2C). Intriguingly, knockdown of PON2 expression impaired LLC proliferation compared to cells expressing the control-shRNA. These results highlight an important role for PON2's ability to modulate cell proliferation in these oncogenically-transformed cells.
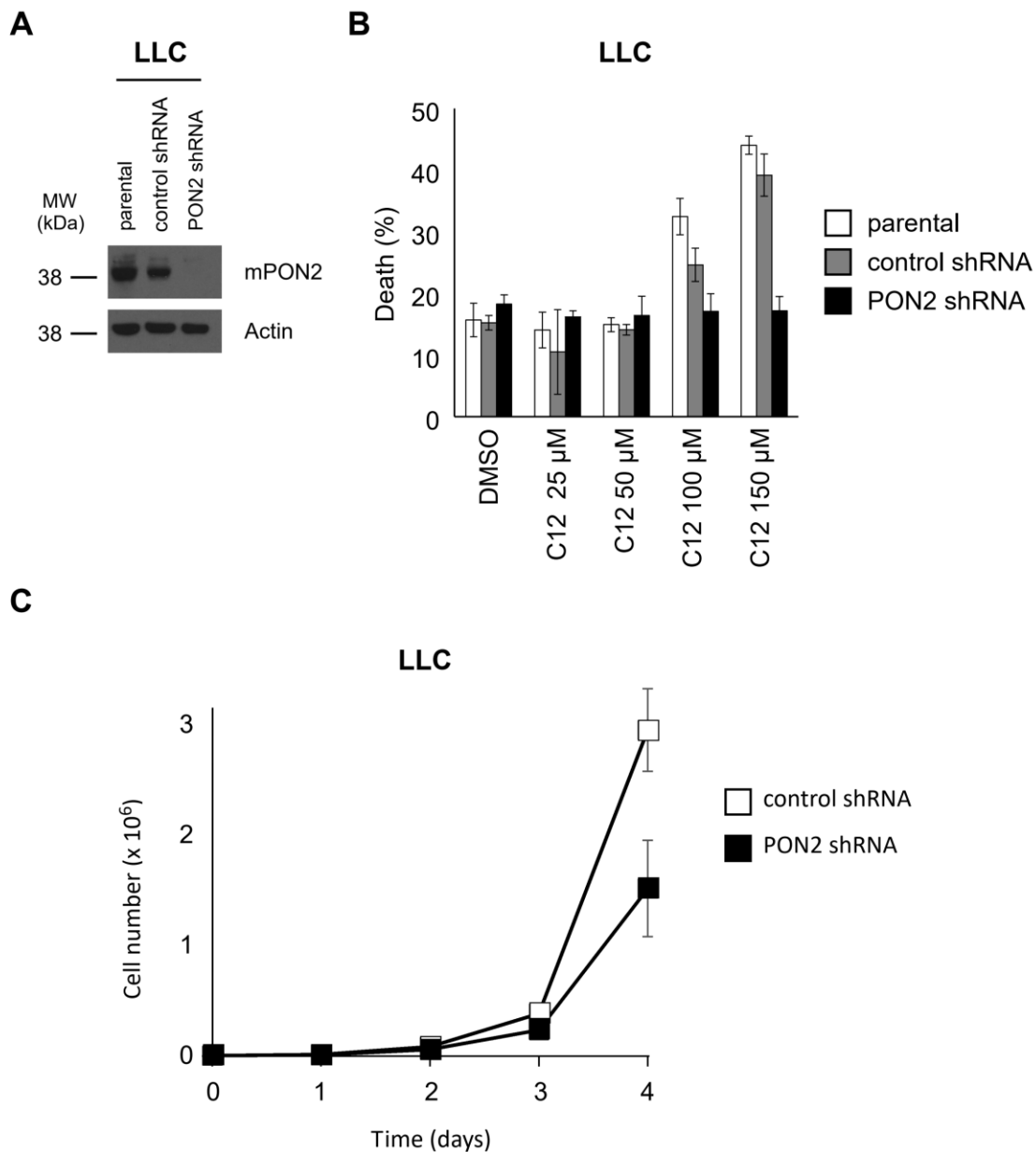
Figure 3.2. Loss of PON2 expression impairs murine lung cancer cell proliferation. (A) PON2 expression was detected by western blot analysis in LLC parental, non-targeted shRNA, or PON2-shRNA cells. (B) Cell viability was determined by PI exclusion via flow cytometry in parental, control-shRNA, and PON2-shRNA in response to increasing concentrations of C12. (C) Cell proliferation was measured by cell counting over a 4 day period in control- and PON2-shRNA LLC cells. Data are mean ± SD of three independent experiments.

3.3.3 PON2 is required for human lung adenocarcinoma cell proliferation

To exclude the possibility that PON2 activity may only modulate the cell physiology of murine cells, we also investigated PON2's role in the context of two human lung adenocarcinoma cell lines, A549 and NCI-H1299 cells. As before, we employed an RNAi approach to reduce PON2 expression in A549 cells, which were transduced to express either a control- or PON2-specific shRNA. For NCI-H1299 cells, we utilized a CRISPR-Cas9 approach to disrupt endogenous PON2 expression (see 3.2.5- Materials and Methods). Briefly, cells were transfected with a plasmid encoding Cas9 (D10A) Nickase and either a 20 nt non-targeting gRNA, or a 20 nt gRNA targeted to exon 3 of the *PON2* gene. Stably-transfected clonal NCI-H1299 CRISPR-vector and CRISPR-PON2 cells were generated and PON2 status was confirmed by Sanger sequencing and western blot analysis. A similar CRISPR-Cas9 approach was attempted in A549 cells but was unsuccessful, likely due to high copy number of the *PON2* gene as a result of genomic instability.

Western blot analysis was used to analyze PON2 expression in A549 and NCI-H1299 cells (Fig. 3.3A & C), which confirmed efficient shRNA-mediated knockdown of PON2 expression in A549 cells (Fig. 3.3A) and undetectable PON2 expression in clonal CRISPR-PON2 NCI-H1299 cells (Fig. 3.3C). Furthermore, expression of the CRISPR-vector alone did not alter endogenous expression of PON2 (Fig. 3.3C).

Next, we monitored cell proliferation in A549 and NCI-H1299 cells with normal or reduced PON2 expression as before (Fig. 3.3B & D). Similar to murine LLC cells, loss of PON2 expression in A549 and NCI-H1299 cells resulted in

impaired cellular proliferation over the 4-day period. Furthermore, proliferation was similar between clones of the same type in NCI-H1299 cells, further validating PON2's role in regulating their proliferation. These results are in agreeance to observations in LLC cells and demonstrate that PON2 promotes the proliferation of human lung adenocarcinoma cells.
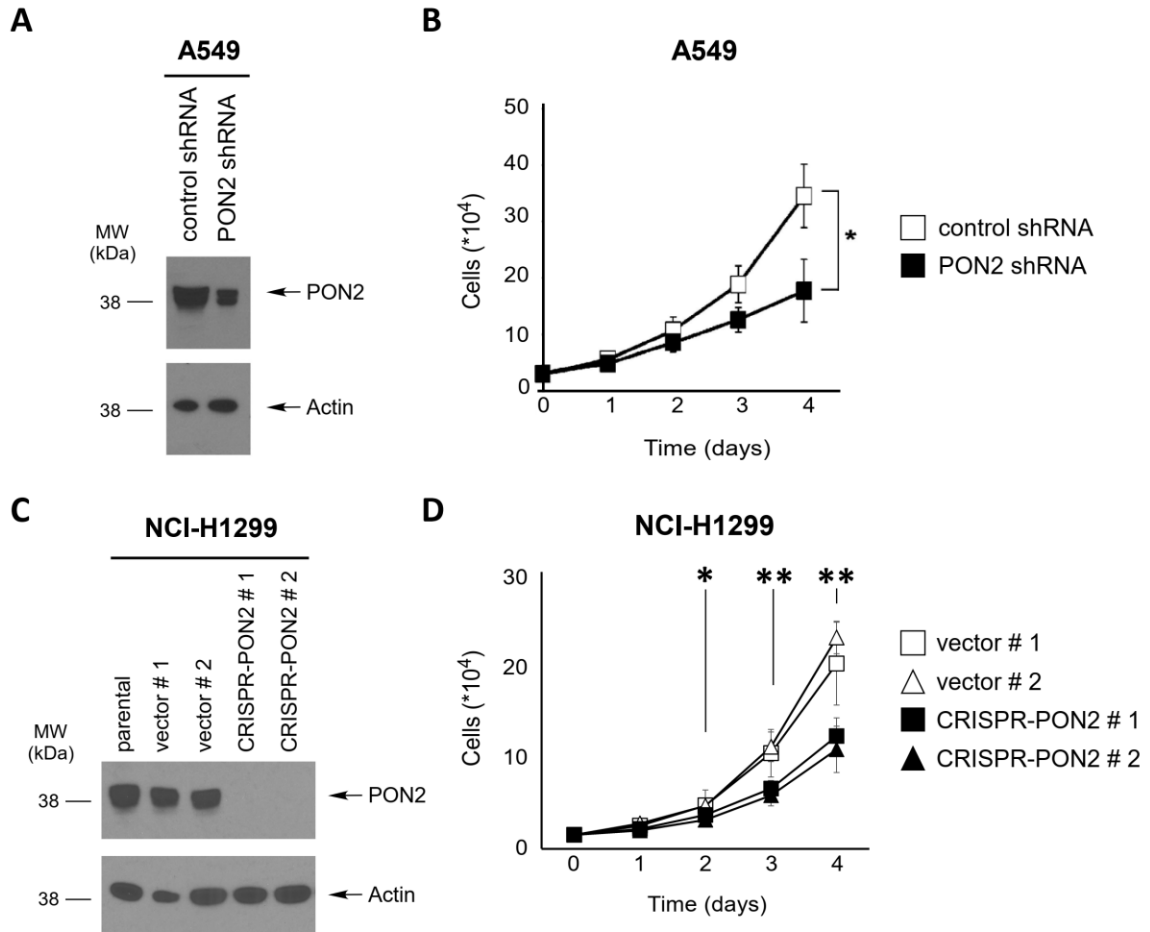
Figure 3.3. PON2 is required for human lung adenocarcinoma cellular proliferation. PON2 expression was reduced in A549 and H1299 cells by RNAi or using a CRISPR-Cas9 approach, respectively. (A)Western blot analysis demonstrates PON2 knockdown in A549 cells expressing a control- or PON2-specific shRNA. (B) A549 PON2-shRNA cells proliferated at a slower rate than their control counterparts. (C) PON2 expression was analyzed by western blot in parental and clonal H1299 cells expressing an empty vector or a CRISPR-PON2 construct. (D) Cell proliferation in H1299 cells was determined by cell counting. Both CRISPR-PON2 clonal H1299 cells proliferated slower than clonal vector cells. Data are mean ± SD of three independent experiments. (*) $p < 0.05$, (**) $p < 0.01$ by Student's unpaired t-test.

3.3.4 PON2 is expendable for non-transformed cellular proliferation

We next sought to explore PON2's role in non-transformed cellular proliferation. For this purpose, HBE and HEK-293T cells were engineered to express either a scrambled non-specific shRNA or a PON2-specific shRNA. Western blot analysis was used to determine knockdown efficiency (Fig. 3.4A), which revealed a robust decrease in endogenous PON2 levels in HBE and HEK-293T cells expressing the PON2-shRNA. Cell proliferation was assessed as previously described herein. The results of this analysis revealed that control- and PON2-shRNA cells proliferated at the same rate in HBE and HEK-293T cells (Fig. 3.4B). Together, these observations suggest that PON2 expression does not govern the proliferation of non-transformed cells. That loss of PON2 expression impaired oncogenically-transformed murine and human lung adenocarcinoma cell proliferation highlights PON2 as a potentially-selective target against lung cancer cell growth.
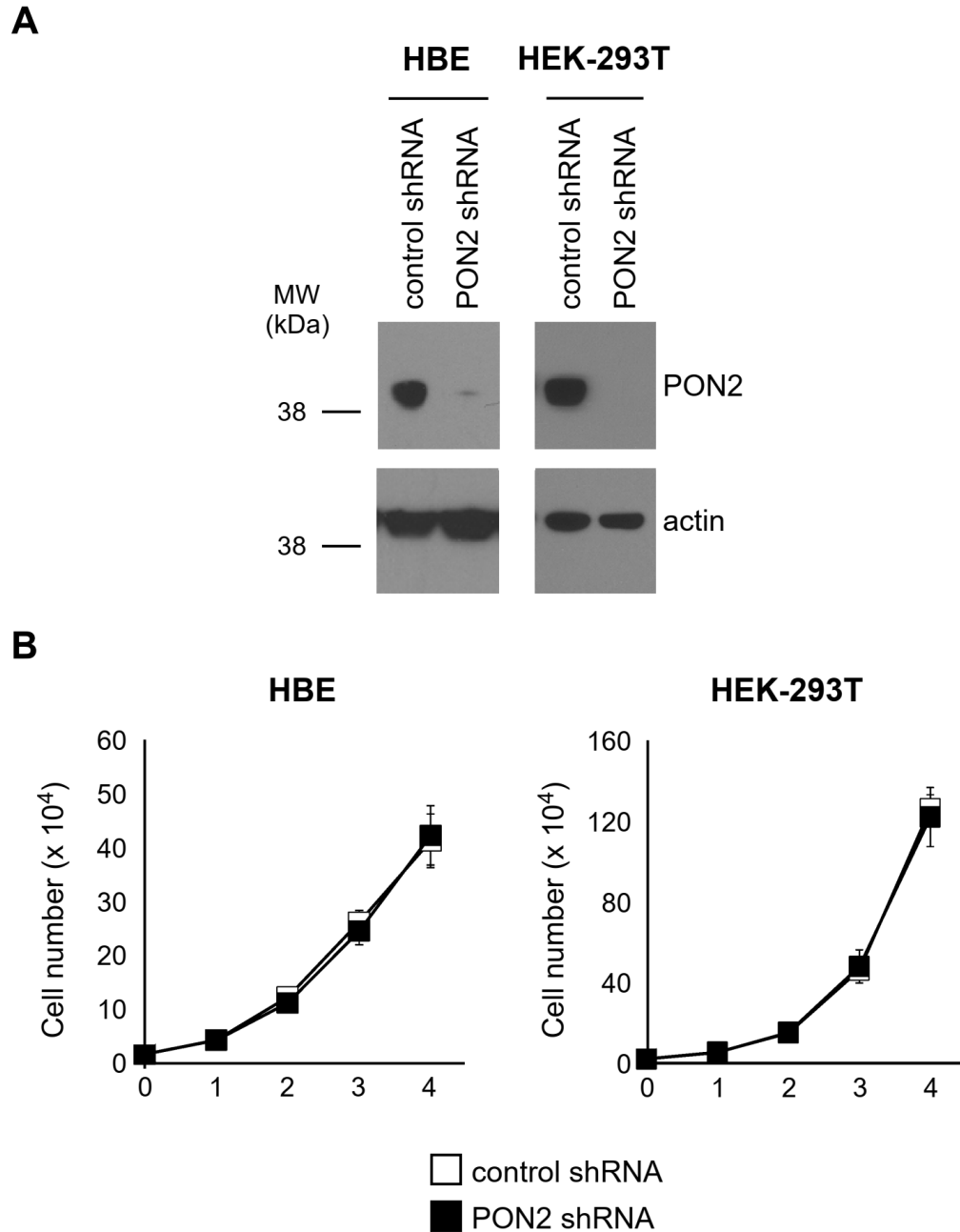
Figure 3.4. Normal cell proliferation is unaffected by PON2 expression. (A) Western blot analysis was used to demonstrate RNAi-mediated knockdown in HBE and HEK-293T cells expressing either a non-targeted control shRNA or a shRNA targeted to the PON2 gene. (B) Cell proliferation was measured by counting cells daily over the course of 4 days. Data are mean ± SD of three independent experiments.

3.3.5 PON2 mediates cell proliferation independent of lactonase activity in NCI-H1299 cells.

As a multi-functional enzyme, the extent to which PON2's physiological roles are mediated by its various enzymatic activities has not been fully explored. A report by Altenhofer et al. demonstrated PON2 scavenged ROS independent of its lactonase activity in cells expressing a lactonase-deficient mutant PON2-H114Q [36]. We sought to elucidate whether PON2 lactonase activity was required to promote lung adenocarcinoma cell proliferation. To this purpose, we generated NCI-H1299 CRISPR-PON2 cells expressing either an empty vector, wild type human PON2 (hPON2-WT), or mutant PON2-H114Q lacking lactonase activity. Western blot analysis was used to confirm that WT or mutant PON2 was re-expressed at similar levels to parental cells (Fig. 3.5A) prior to further experimentation. Next, PON2 re-expression and lactonase activity was functionally confirmed using a cell death assay (Fig. 3.5B). The lactonase activity of PON2 is required for the cytotoxic effects of C12, therefore, NCI-H1299 cells were treated with increasing concentrations of C12 and cell death was measured by PI positivity via flow cytometry. The results of this analysis revealed that cells expressing wild type PON2 normally (parental and CRISPR-vector) or by re-expression (hPON2-WT) were sensitive to C12 cytotoxicity in a concentration-dependent manner (Fig. 3.5B). Conversely, cells lacking PON2 expression (CRISPR-PON2 parental and empty vector) or expressing a lactonase-deficient mutant PON2 (PON2-H114Q) were resistant to C12 cytotoxicity, regardless of concentration. These observations functionally confirm PON2 expression and lactonase status in NCI-H1299 cells.

To explore PON2 lactonase activity as a potential modulator of cell proliferation, cell numbers of CRISPR-PON2 empty vector, hPON2-WT, and hPON2-H114Q cells were monitored as previously described (Fig. 3.5C). As expected, re-expression of wild type PON2 was sufficient to increase cell proliferation compared to empty-vector cells lacking PON2 expression. Further, proliferation of cells expressing hPON2-H114Q was similar to the hPON2-WT cells, indicating that the lactonase activity of PON2 is not required to promote NCI-H1299 proliferation.
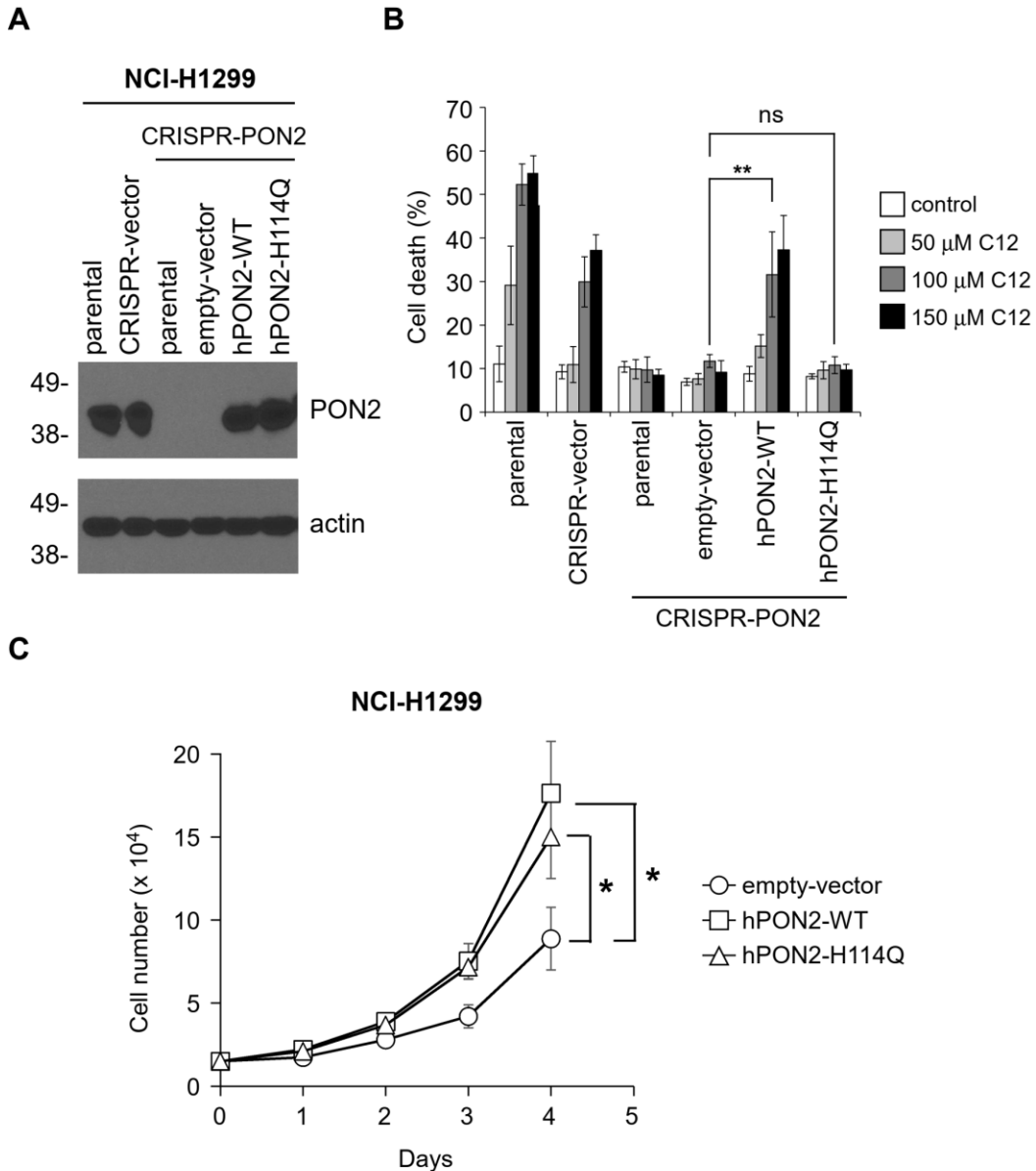
Figure 3.5. PON2 promotes NCI-H1299 proliferation independent of its lactonase activity. (A) Western blot analysis was performed to determine PON2 expression in parental H1299, CRISPR-vector, CRISPR-PON2, as well as CRISPR-PON2 cells engineered to express an empty vector, wild type human PON2 (hPON2-WT), or a lactonase-deficient mutant PON2 (hPON2-H114Q). (B) Cell viability was analyzed by PI exclusion assay in H1299 cells treated with increasing concentrations of C12. Re-expression of wild type, but not mutant (H114Q), PON2 restores the cytotoxicity of C12. (C) Re-expression of PON2 increases cell proliferation regardless of lactonase activity. Data are mean ± SD or three independent experiments. (*) $p < 0.05$, (**) $p < 0.01$ by Student's t-

3.3.6 Loss of PON2 expression arrests lung adenocarcinoma cell cycle

progression in G1 phase.

We next sought to explore the consequence of reduced PON2 expression on lung adenocarcinoma cell cycle progression. To this purpose, the DNA content of A549 and NCI-H1299 cells with normal or reduced PON2 expression was analyzed by flow cytometry of PI-stained cells (Fig. 3.6). In A549 cells, PON2 knockdown cells had a higher percentage of cells in G1 phase compared to their control counterparts. Further, a lower proportion of the PON2-shRNA cells were in S phase of the cell cycle than in the control-shRNA cells. No differences were observed in the proportion of A549 cells in G2 phase. Similar results were observed in the NCI-H1299 cells. The CRISPR-vector cells had a lower percentage of cells in G1 phase and a higher percentage in S phase than the CRISPR-PON2 cells. As in A549 cells, no changes were observed in the proportion of NCI-H1299 cells in G2 phase. Taken together, these results demonstrate that loss of PON2 expression results in G1 cell cycle arrest in lung adenocarcinoma cells.
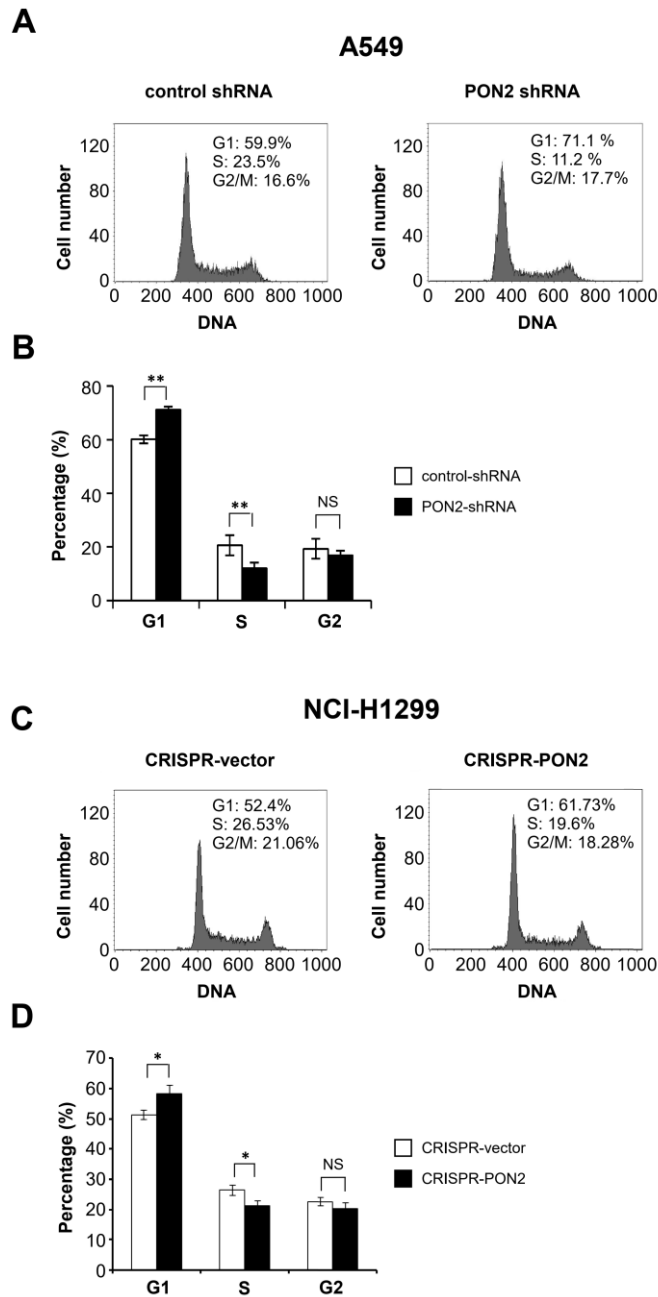
Figure 3.6. Lung adenocarcinoma cells with reduced PON2 expression are arrested in G1 of the cell cycle. DNA content was measured by flow cytometry of PI-stained A549 (A) and H1299 (C) cells. Data shown in (A) and (C) were analyzed using FloJo software to determine cell cycle stages of A549 (B) and H1299 (D) cells. In both A549 and H1299 cells, reducing PON2 expression yielded a higher percentage of cells in G1 and lower percentage of cells in S phase. Data are mean ± SD of three independent experiments. (*) p < 0.01, ns = not significant. Student's unpaired t-test.

3.3.7 PON2 deficiency accelerates ROS production in lung adenocarcinoma

cells.

Much research into PON2 biology has established an antioxidant role for PON2 within cells [1], [31], [33], [130], [131]. Managing the intracellular production and propagation of oxidative species is paramount to tumor cell survival and proliferation [132]. Therefore, we hypothesized that disrupting PON2 expression may result in redox imbalance within lung adenocarcinoma cells. To test this hypothesis, we analyzed ROS production in A549 and NCI-H1299 cells with normal or reduced PON2 expression via the DCF assay. In this assay, cells are treated with the non-fluorescent cell permeant compound 2',7'-dichlorodihydrofluorescein diacetate (H_2DCFDA), which is oxidized to the fluorescent molecule 2',7'-dichlorofluorescein (DCF), the production of which serves as an indicator of ROS formation. PON2 expression was reduced by RNAi in both A549 and NCI-H1299 cells, and DCF fluorescence was analyzed over the course of 2 hours (Fig. 3.7A & B). Reducing PON2 expression led to an increased rate of DCF fluorescent accumulation in both cell types (Fig. 3.7C & D), suggesting that the antioxidant activity of PON2 may serve a protective role in lung adenocarcinoma cells.
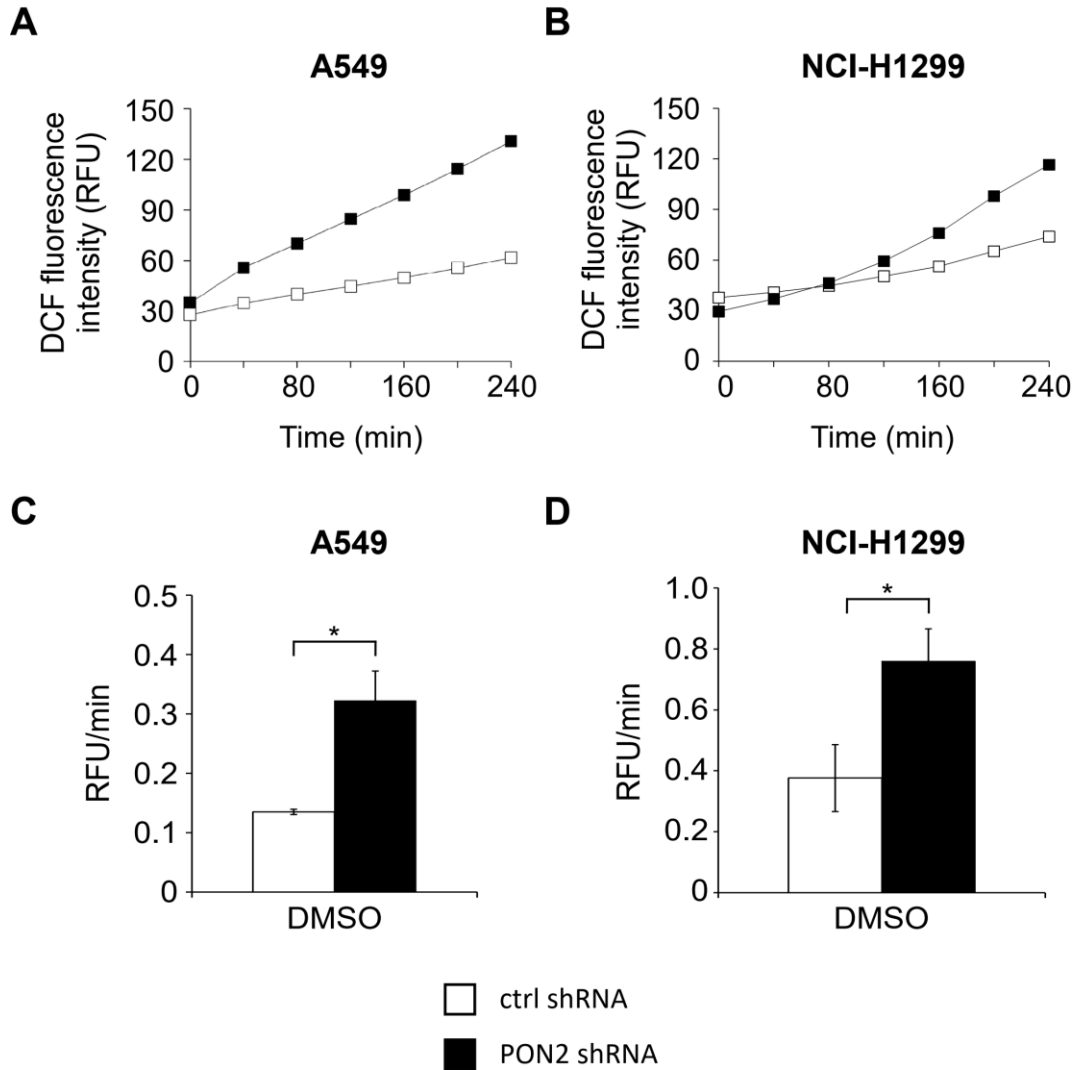
Figure 3.7. PON2 deficiency accelerates ROS production in lung adenocarcinoma cells. DCF fluorescence intensity was measured over 2 hours as an indicator of ROS production in A549 (A) and NCI-H1299 (B) cells expressing a non-specific control shRNA or PON2-specific shRNA. Representative kinetics shown. Rate of ROS production was calculated as RFU/min in A549 (C) and NCI-H1299 (D) cells. Reducing PON2 expression increases the rate of ROS production in both lung adenocarcinoma cell lines. Data are mean ± SD or three independent experiments. (*) p < 0.01 by Student's unpaired t-test.

3.3.8 Evaluating PON2's role in cellular metabolism using stable isotope-resolved metabolomics (SIRM).

Based on the central role for PON2 in lung adenocarcinoma cell proliferation established herein, we hypothesized that loss of PON2 expression was detrimental to lung adenocarcinoma cellular metabolism. Therefore, we sought to investigate PON2's influence on cellular bioenergetics using a stable isotope resolved metabolomics (SIRM) approach. SIRM is a technique used to trace the incorporation of stable isotope tracer molecules into key metabolic intermediates whose identity is determined by high-resolution nuclear magnetic resonance (NMR) or mass spectrometry. In the present study, we employed NMR to track the flow of [U-^{13}C]-glucose through oxidative metabolic networks to understand PON2's influence on key metrics of cellular metabolism, including glycolysis, TCA cycle, pyrimidine biosynthesis, and pentose phosphate pathway (PPP) activity (Fig. 3.8). In the present study, NCI-H1299 cells with or without endogenous PON2 expression were cultured in the presence of 5 mM [U-^{13}C]-glucose for 72 h (Fig. 3.8A). Aliquots of extracellular medium were collected at 24 h intervals and analyzed by one-dimensional Heteronuclear Single Quantum Coherence (1D-HSQC) analysis to measure the abundance of extracellular metabolites. At the end of the 72 h incubation period, intracellular metabolites were quantified by two-dimensional total correlation spectroscopy (TOCSY) analysis to measure the flow of [U-^{13}C]-glucose through key pathways of oxidative metabolism (Fig. 3.8B).
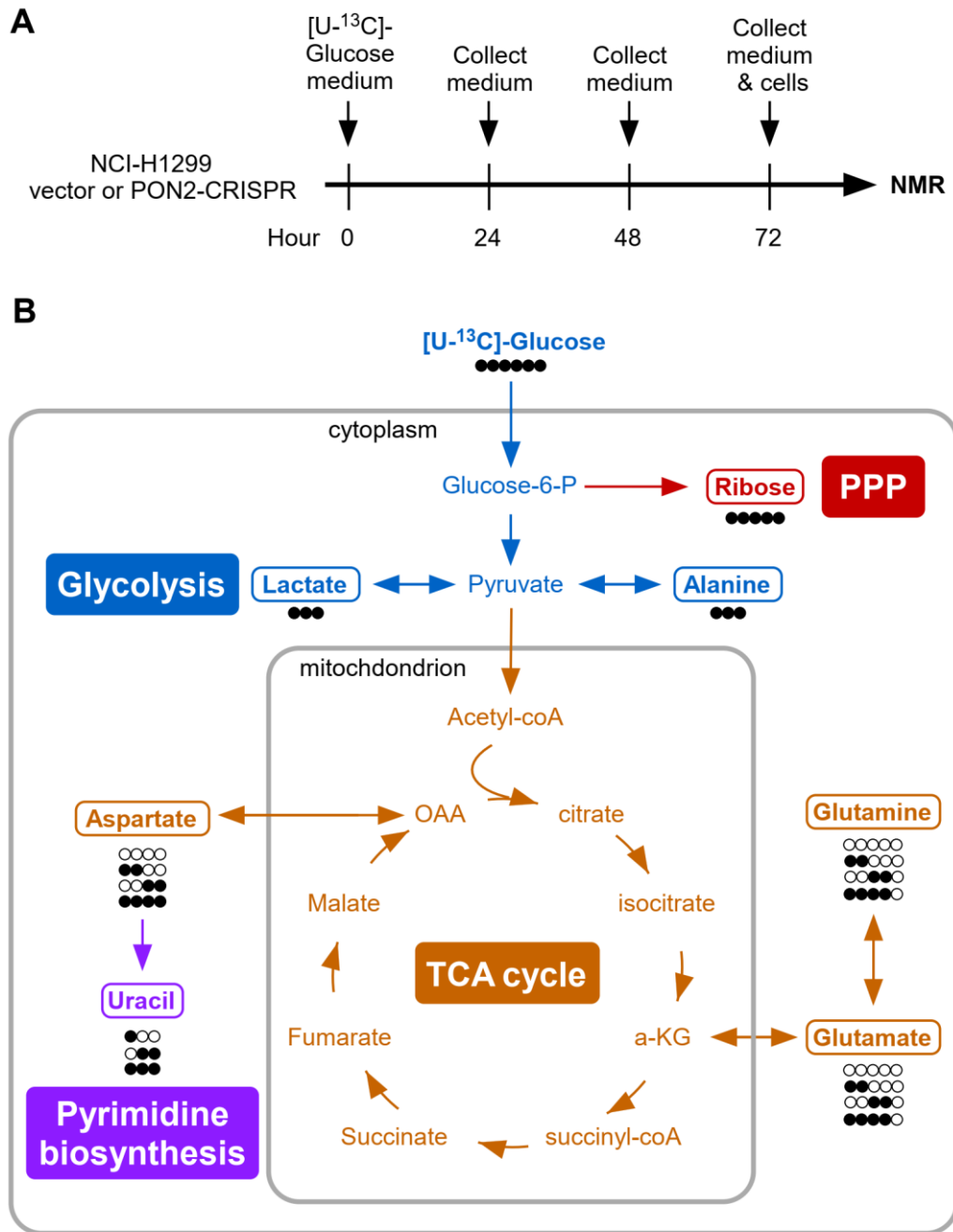
Figure 3.8. Investigating PON2's role in cellular bioenergetics using a stable isotope-resolved metabolomics (SIRM) approach in NCI-H1299 cells. (A) Schematic depiction of SIRM study using NCI-H1299 cells with or without endogenous PON2 expression. (B) The illustration of carbon flow from [U-^{13}C]-glucose into major intracellular metabolites through several metabolic processes, including glycolysis, TCA cycle, pentose phosphate pathway, malate/aspartate shuttle, and biosynthesis of pyrimidine nucleotides. Expected ^{13}C isotopomers of metabolites are shown with open circles representing ^{12}C and filled circles representing ^{13}C. Complex labeling patterns are a result of scrambling at the succinate step and subsequent turns of the TCA cycle

89

3.3.9 PON2 deficiency disrupts extracellular glucose consumption and lactate production in lung adenocarcinoma cells.

To evaluate our hypothesis that PON2 expression may modulate lung adenocarcinoma cellular metabolism, we first analyzed the abundance of key extracellular metabolites in the growth medium of NCI-H1299 cells cultured in the presence of [U-^{13}C]-glucose using 1D-HSQC analysis. At time 0 h, the peaks corresponding to ^{13}C-glucose, valine, and threonine were detected in the culture medium (Fig. 3.9A). Analysis of the extracellular medium following 72 h incubation revealed different analyte profiles corresponding to PON2 status (Fig. 3.9B & C). The peak corresponding to ^{13}C-glucose was detected in 72 h samples prepared from CRISPR-PON2, but not CRISPR-vector cells, indicating that PON2 promotes depletion of extracellular glucose. Further, the abundance of ^{13}C-lactate was higher in CRISPR-vector samples at 72 h, indicating that loss of PON2 expression impairs lactate secretion. The essential amino acids valine and threonine were detected at similar abundances, regardless of PON2 status. Metabolite abundances over time were plotted for samples and a linear regression was applied to visualize the rate of metabolite depletion and production (Fig. 3.10). In agreement with observations made at 72 h alone, loss of PON2 expression reduced the rate of ^{13}C-glucose consumption (Fig. 3.10A) and ^{13}C-lactate (Fig. 3.10B) production, while valine and threonine depletion were unaltered (Fig. 3.10C & D).
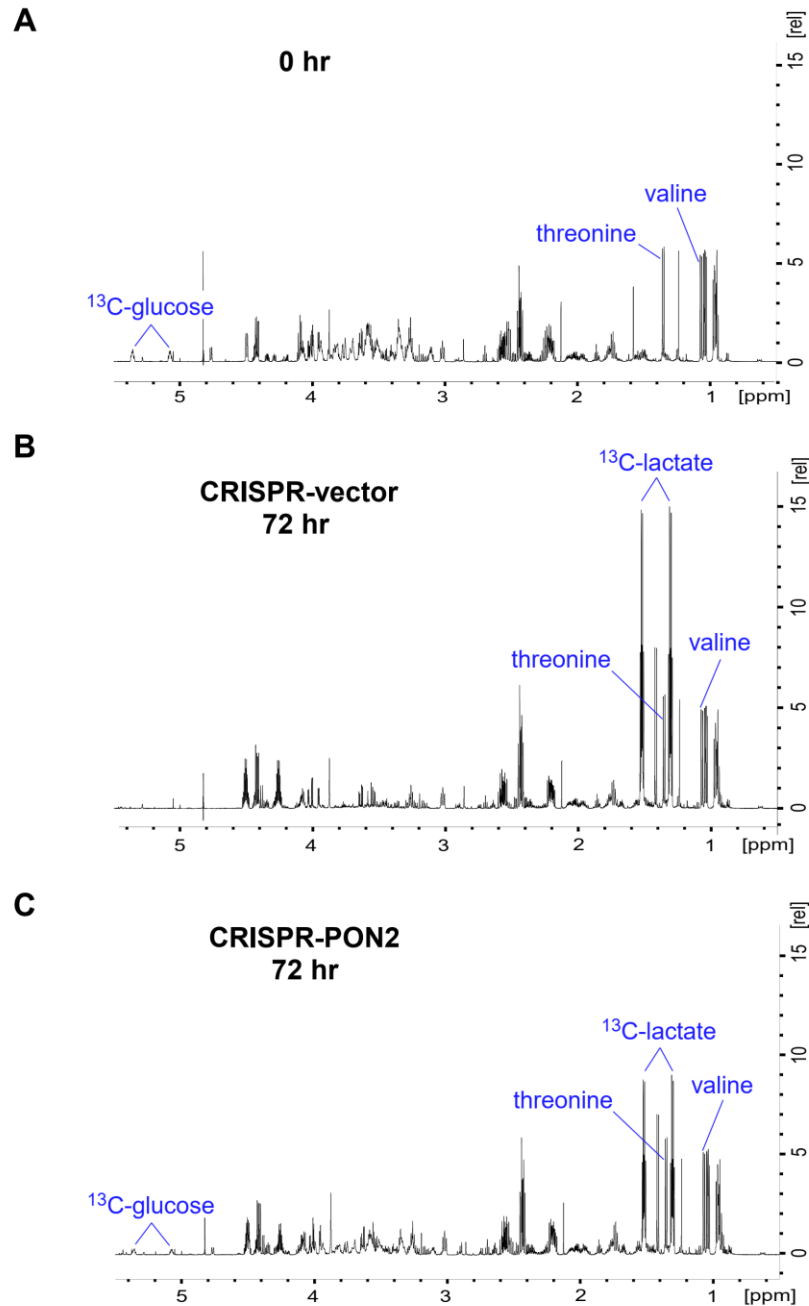
Figure 3.9. Key extracellular metabolites assessed by one-dimensional high-resolution NMR analysis. CRISPR-vector and CRISPR-PON2 NCI-H1299 cells were cultured in medium containing (U-^{13}C)-glucose, which was collected at time 0 h, and every 24 h thereafter. The metabolites in the medium samples were detected by 1D ^{1}H-^{13}C HSQC. The representative spectra of the medium collected at 0 (A) and 72 h (B & C) time points are shown. The key metabolites, including ^{13}C-glucose, ^{13}C-lactate, threonine, and valine, are highlighted in blue.

A ¹³C-glucose

B ¹³C-lactate

C Valine

D Threonine

☐ CRISPR-vector
■ CRISPR-PON2
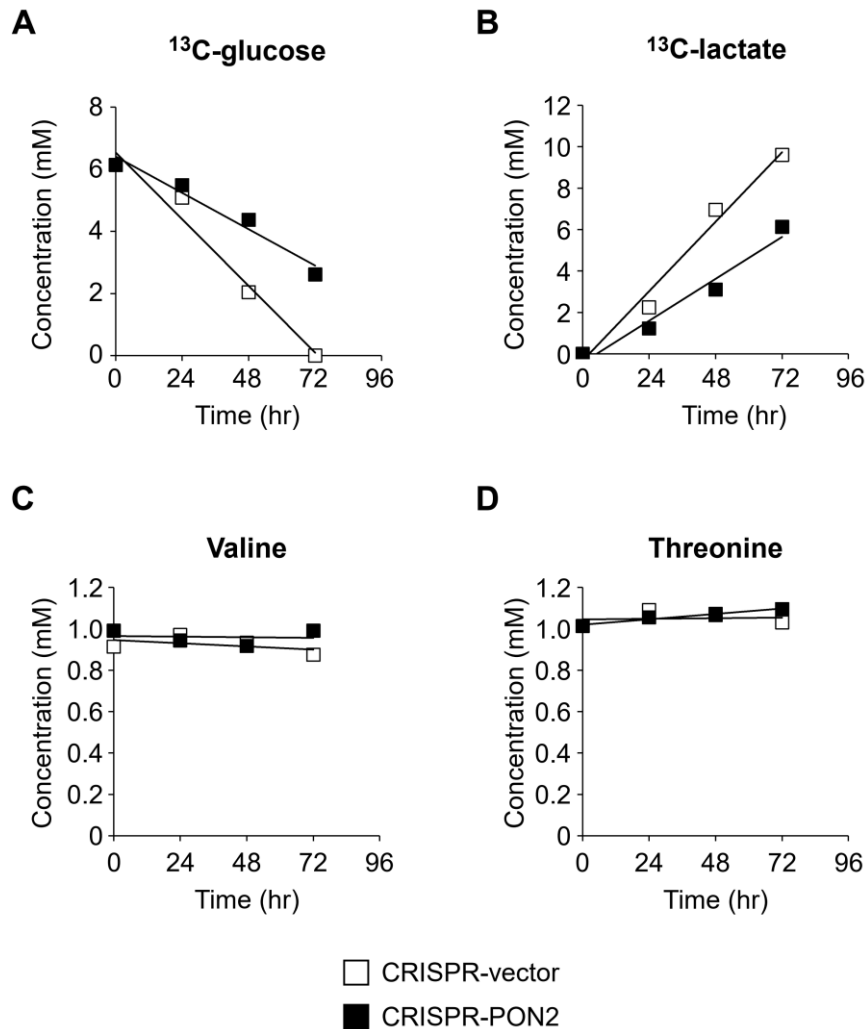
Figure 3.10. PON2 deficiency impairs extracellular glucose consumption and lactate production in NCI-H1299 cells. Vector and PON2-CRISPR NCI-H1299 cells were culture in radiolabeled glucose for 72 h. Key extracellular metabolites, including ¹³C-glucose, ¹³C-lactate, valine, and threonine were quantified by one-dimensional NMR HSQC analysis. (A) NCI-H1299 cells lacking endogenous PON2 expression depleted ¹³C-glucose at a reduced rate compared to vector cells. (B) PON2-deficient cells secreted ¹³C-lactate more slowly than their control counterparts. The consumption of the essential amino acids valine (C) and threonine (D) were unaffected by PON2 expression. Lines are linear regression fits.

3.3.10 Loss of PON2 disrupts oxidative metabolism in lung adenocarcinoma cells

To obtain detailed insight into PON2's role in oxidative metabolism within lung adenocarcinoma cells, we analyzed the abundance of radiolabeled metabolites produced from [U-^{13}C]-glucose by 2D TOCSY analysis. The abundance of ^{13}C-labeled metabolites represents *de novo* biosynthesis from glucose as a carbon source and is reflective of glycolysis, TCA cycle, PPP activity, and nucleotide biosynthesis reactions. As shown in Fig. 3.11A, alanine displayed the characteristic square pattern of ^{13}C satellites surrounding a central resonance that represents unlabeled molecule, demonstrating that alanine was synthesized directly from glucose through glycolysis [124], [126], [128]. In PON2-deficient NCI-H1299 cells, we found a decreased abundance of ^{13}C-alanine. Additionally, NCI-H1299 cells lacking PON2 expression exhibited an increased abundance of ^{13}C-lactate (Table 3.1). Since the production of extracellular ^{13}C-lactate was decreased in CRISPR-PON2 cells (Fig. 3.10), an increased relative abundance of intracellular ^{13}C-lactate suggests that PON2 may facilitate secretion of lactate. Given the findings that enhanced lactate secretion may promote tumorigenic phenotypes [133], this phenomenon is worthy of further investigation. Together, these labelling patterns suggest that glycolytic activity was altered in CRISPR-PON2 cells.

To assess TCA cycle activity, the relative abundances of radiolabeled glutamate, glutamine, and aspartate were also assessed. For glutamate and glutamine, we detected a complex labeling pattern in which 4 separate species of each were present: unlabeled, ^{13}C labeling at both positions (C2 and C4), and ^{13}C at only one position (C2 or C4) (Fig. 3.11A). While unlabeled glutamate/glutamine

are present in culture medium, labeled species are produced from α-ketoglutarate (α-KG), an intermediate metabolite in TCA cycle, via transaminases (α-KG → glutamate) and glutamine synthetase (glutamate → glutamine). The degree of ^{13}C-labeling present in α-KG dictates whether one or both positions in glutamate/glutamine possess ^{13}C atoms. Similarly, ^{13}C-labeled species of aspartate are derived from the TCA cycle intermediate oxaloacetate (OAA). This conversion occurs in mitochondria via the activity of aspartate aminotransferase (AAT) as part of the malate-aspartate shuttle. CRISPR-PON2 cells had reduced relative abundance of all ^{13}C-labeled glutamate, glutamine, and aspartate species compared to CRISPR-vector cells, suggesting PON2 deficiency impairs TCA cycle activity (Table 3.1).

The results of this experimental approach also provided insight into PON2's role in *de novo* pyrimidine nucleotide biosynthesis by monitoring the incorporation of ^{13}C atoms in uracil in UTP. In non-proliferating cells, the majority of pyrimidine nucleotides are generated through the salvage pathway, in which nucleotides are continuously recycled. In proliferating cells, such as tumor cells, the existing pool of nucleotides is insufficient and must be synthesized *de novo*. In mitochondria, the TCA cycle intermediate OAA can be converted to aspartate and eventually to uracil base (Fig. 3.9). Therefore, observing the labeling patterns of uracil in UTP is an effective surrogate for *de novo* pyrimidine biosynthesis. In this SIRM analysis, we found that the ^{13}C labeling of uracil in UTP was decreased in CRISPR-PON2 cells (Table 3.1). This may be due to reduced TCA cycle activity, since OAA is required for the production of aspartate and subsequently uracil base.

Finally, we explored the role of PON2 in PPP activity, via the labeling patterns of UTP-ribose (Fig. 3.11B). CRISPR-PON2 cells had higher relative abundance of ^{13}C-labeled UTP-ribose (Table 3.1), although the difference was slight. This indicates that PPP activity is elevated following loss of PON2 expression. Since PPP activity is involved in the production of reducing equivalents, such as NADPH, and nucleotide precursors, it is conceivable that cells deficient in PON2 expression maintain PPP activity to support cellular proliferation and redox status within cells.

Taken together, the results of the SIRM analysis reveal that loss of endogenous PON2 expression impairs key aspects of oxidative metabolism in lung adenocarcinoma cells, including glycolysis, TCA cycle activity, pyrimidine biosynthesis, and PPP activity.
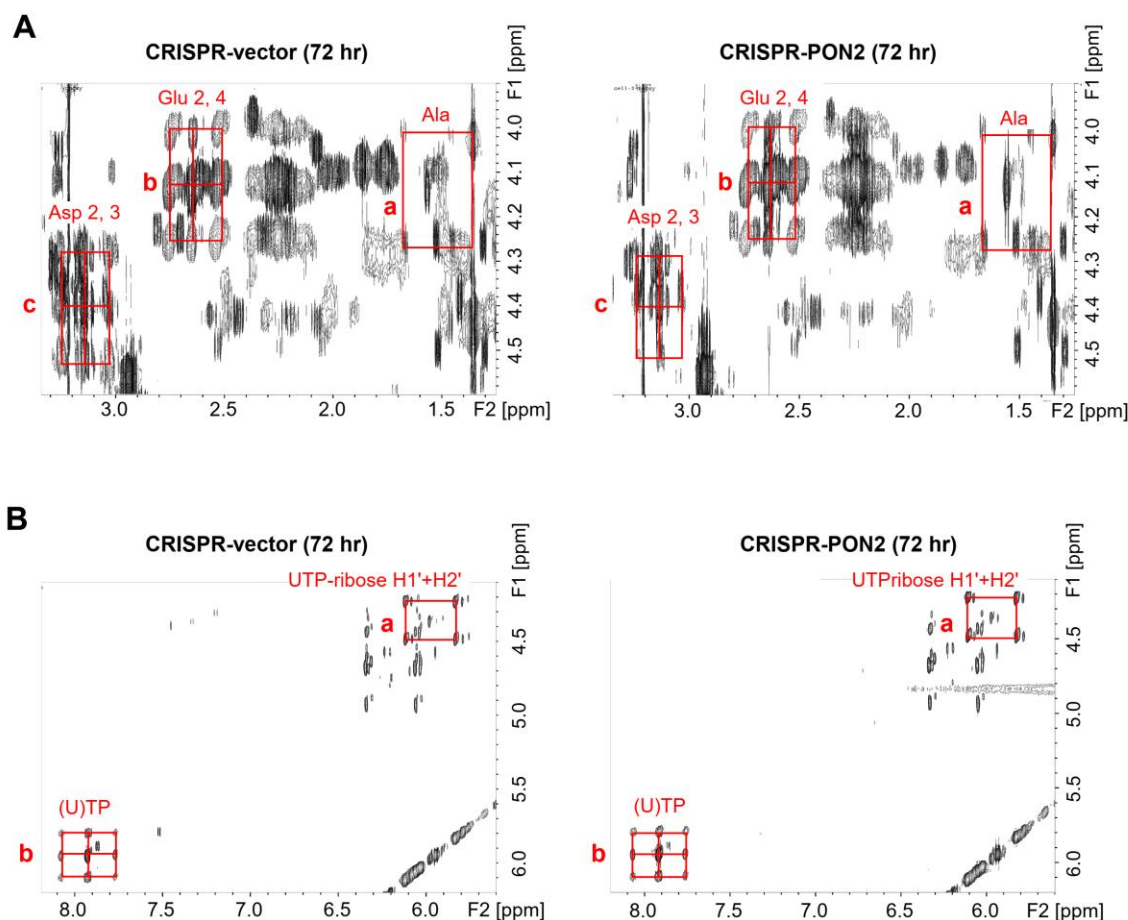
Figure 3.11. Key ¹³C-labeled soluble metabolites in NCI-H1299 cells were detected by SIRM. CRISPR-vector and CRISPR-PON2 NCI-H1299 cells were cultured in medium containing 5 mM [U-¹³C]-glucose for 72 hours. (A) ¹³C-labeling of amino acids in NCI-H1299 cells was evaluated by TOCSY. The box "a" shows the ¹³C satellite peaks of alanine, which surrounds the central peak representing unlabeled alanine. Similarly, Box "b" shows the satellite peaks of the C-2H and C-4H resonances of glutamate and the glutamate moiety of reduced glutathione, and box "c" shows the satellite peaks of aspartate C-2 and C-3. (B) Nucleotide labelling in vector control and PON2-CRISPR NCI-H1299 cells was revealed by TOCSY. Box "a" shows the ¹³C satellite peaks of the ribose moieties of UTP. Box "b" shows doubly labelled uracil as well as the two singly labelled species derived directly from aspartate. All boxes are highlighted in red.

Table 3.1. PON2 deficiency compromises nucleotide biosynthesis and pentose phosphate pathway activity in H1299 cells as revealed by 2D-NMR. Total correlation spectroscopy (TOCSY) analysis was used to quantify the relative abundance of the indicated intracellular metabolites. ^{13}C-labeling was reduced in cellular alanine, uracil in UTP, glutamine, glutamate, and aspartate (highlighted in red) in CRISPR-PON2 cells compared to vector control cells.

Molecule	Site	CRISPR-vector	CRISPR-PON2
Lactate	$^{12}C2^{12}C3$	36.3	**21.9**
	$^{13}C2^{13}C3$	63.7	78.1
Alanine	$^{12}C2^{12}C3$	33.3	**49.9**
	$^{13}C2^{13}C3$	66.7	50.1
UTP	$^{12}C1^{12}C2$	11.7	6.5
	$^{13}C1^{13}C2$	88.3	93.5
Uracil in UTP	$^{12}C6^{12}C5$	52.5	**62.5**
	$^{12}C6^{13}C5$	17.2	12.7
	$^{13}C6^{12}C5$	15.2	12.6
	$^{13}C6^{13}C5$	15.2	12.1
Glutamine	$^{12}C2^{12}C4$	46.4	**63.7**
	$^{12}C2^{13}C4$	3.5	3.7
	$^{13}C2^{12}C4$	30.6	19.6
	$^{13}C2^{13}C4$	19.5	13.0
Glutamate	$^{12}C2^{12}C4$	43.8	**55.8**
	$^{12}C2^{13}C4$	6.6	4.8
	$^{13}C2^{12}C4$	32.8	27.6
	$^{13}C2^{13}C4$	16.9	11.8
Aspartate	$^{12}C2^{12}C3$	39.2	**64.2**
	$^{12}C2^{13}C3$	24.6	20.8
	$^{13}C2^{12}C3$	14.4	15
	$^{13}C2^{13}C3$	21.8	0

3.4 DISCUSSION

A growing body of evidence in the past decade has identified a pro-tumorigenic role for PON2 in promoting cell survival and chemotherapeutic resistance. Researchers have suggested various mechanisms by which PON2 achieves these phenotypes in cancer cells, either through direct antioxidant action in mitochondria and ER [38], [131], [134], or through regulatory interactions of pro-oncogenic effectors such as Wnt/β-catenin[40], p53, and GLUT1 [41]. Despite these recent advances, further work is needed to explore PON2's role in tumor cell physiology in the context of other prevalent human cancers. To address this deficit, we examined the influence of PON2 expression in cellular proliferation, cell cycle progression, ROS production, nutrient utilization, and oxidative metabolism in lung adenocarcinoma cells.

In the present study, we demonstrated that PON2 is upregulated in HBE cells following oncogenic transformation, and in tumor samples from patients with NSCLC compared to corresponding non-malignant lung tissues (Fig. 3.1). Furthermore, we showed that PON2 expression was required for murine and human lung adenocarcinoma cell proliferation (Fig. 3.2 & 3.3), independent of lactonase activity (Fig. 3.5). In contrast, PON2 was unable to impact cell proliferation in non-transformed HBE and HEK-293T cells (Fig. 3.4). Loss of PON2 expression arrested cell cycle progression in G1 phase (Fig 3.6) and exacerbated ROS production (Fig. 3.7) in A549 and NCI-H1299 cells. Further, SIRM analysis (summarized in Fig. 3.8) revealed disruption of endogenous PON2 expression

impairs nutrient utilization, specifically, extracellular glucose uptake and lactate secretion (Fig. 3.9 & 3.10). These studies also demonstrated that PON2 deficiency disrupts key aspects of oxidative metabolism, including glycolysis, TCA cycle, PPP, and nucleotide biosynthesis in lung adenocarcinoma cells (Fig. 3.11 and Table 3.1). Overall, this report is the first, to our knowledge, to thoroughly delineate PON2's impact on lung adenocarcinoma cellular physiology and metabolism.

The relationship between PON2 activity and oxidative stress is bidirectional: PON2 expression governs ROS production and *vice versa*. Some of the earliest studies into PON2 biology revealed that PON2 prevents the formation and propagation of superoxide anion within mitochondria and ER [36], [131], [134]. Reciprocally, PON2 has a well-established role as a redox sensor. Rosenblat et al. reported that oxidative stress enhances PON2 expression in murine peritoneal macrophages (MPMs) [26]. It was further revealed that as monocytes differentiate into macrophages, PON2 mRNA and protein expression is elevated in accordance with rising production of intracellular superoxide anion [135]. Similar observations were reported in multiple vascular cells, whose PON2 expression is upregulated to protect against unfolded protein response (UPR)- induced cell death in response to ROS production [131]. These findings highlight a pivotal role of PON2 in the maintenance of cellular redox status in cells under normal and oncogenic conditions.

Management of oxidative stress is a crucial aspect of lung tumorigenesis [132]. At low levels, ROS can stimulate cell proliferation, whereas excessive rates of ROS production can impair basic cellular functions [136]. Furthermore, ROS

may initiate and fuel lung tumor growth through direct oxidation of DNA bases that result in persistent oncogenic mutations [137]. Therefore, a plausible scenario is that expression of PON2 is increased during tumorigenesis as a protective factor against excessive oxidative damage to cellular macromolecules, including DNA. Microarray experiments have demonstrated PON2 mRNA is elevated in a number of tumor types, including leukemias, hepatocellular carcinoma, pancreatic ductal adenocarcinoma, prostate carcinoma, renal carcinoma, esophageal cancer, and gastric carcinoma [33], [138]–[140]. Subsequent studies confirmed PON2 mRNA and protein is upregulated in samples collected from over 10,000 patients with 31 separate cancer types [42]. In the present study, we analyzed PON2 protein expression levels in normal and cancerous lung tissues from patients with NSCLC (Figure 3.1B & C). Our data provide strong evidence that PON2 expression is elevated in tumor samples from patients with lung adenocarcinoma. Furthermore, elevated PON2 expression is essential for lung adenocarcinoma cell proliferation (Fig. 3.2 & 3.3), but not for untransformed epithelial cells (Fig 3.4). While further work is needed to uncover the exact mechanisms responsible for upregulation of PON2 in lung adenocarcinoma, this phenomenon is likely due to increasing oxidative stress as a consequence of malignant transformation.

As a multifunctional enzyme, PON2 is involved in many aspects of cellular physiology. However, the degree of functional overlap among PON2's lactonase, arylesterase, and antioxidant activities has not been fully delineated. Earlier studies, in conjunction with our current research, has shown the lactonase activity of PON2 is required to mediate the cytotoxic properties of the bacterial quorum-

sensing molecule N-(3-oxododecanoyl)-l-homoserine lactone (C12; Fig. 3.2B & 3.5B) [83], [122]. As a freely diffusible acyl-homoserine lactone, C12 readily enters mitochondria and is hydrolyzed via PON2 lactonase activity to a cytotoxic carboxylic acid metabolite (C12-COOH) [90]. In the present study, we demonstrated that PON2 lactonase activity was not a functional requirement to stimulate proliferation of lung adenocarcinoma cells (Fig. 3.5C). Therefore, it is unlikely that PON2 mediates oxidative metabolism through its lactonase function. In support of this hypothesis, Pan et al. reported that PON2 expression modulated glucose uptake and bioenergetics independent of its lactonase activity [122].

In contrast to normal eukaryotic cells, which meet their energetic demands through mitochondrial oxidative phosphorylation, most cancer cells instead preferentially undergo glycolysis to fuel their rapid proliferation, even under aerobic conditions. This phenomenon, "the Warburg effect," was described nearly 100 years ago by Otto Warburg and was hypothesized to be a consequence of impaired mitochondrial function. Subsequent studies in the past decades have revealed that cancer cells have intact mitochondrial function and, instead, reprogram their metabolism to elevate so-called "aerobic glycolysis" as an adaptive mechanism to generate nucleotides, amino acids, and fatty acids sufficient for cell division [141]. This is not to say that mitochondrial function is expendable for cancer cell proliferation. For example, oncogenic transformation of human mesenchymal stem cells increases their dependency on mitochondrial oxidative metabolism for energy production [142], and mitochondrial oxidative metabolism is critical for oncogenic Kras-driven cell proliferation and mouse lung

adenocarcinoma tumorigenesis [143]. Herein, we have systematically evaluated major aspects of cellular bioenergetics, including nutrient utilization, lactic acid production, and *de novo* biosynthesis of intracellular metabolites in lung adenocarcinoma cells with or without endogenous PON2 expression (Figure 3.8-3.11; Table 3.1). These studies have revealed comprehensive information about metabolic changes caused by deficiency in PON2 expression, thus validating the pivotal role of PON2 in maintaining oxidative metabolism in human lung adenocarcinoma cells. As such, a major conclusion of this work is that elevated PON2 expression serves to promote cellular proliferation by enhancing lung adenocarcinoma mitochondrial bioenergetics. Future studies are warranted to uncover the detailed regulatory mechanisms that govern PON2 expression and activity in lung adenocarcinoma.

CHAPTER 4

PON2 PLAYS A LIMITED ROLE IN LUNG TUMOR DEVELOPMENT IN VIVO

4.1 INTRODUCTION

Paraoxonase 2 (PON2) is an intracellular lactonase/arylesterase enzyme with antioxidant properties [1], [33], [36]. The current body of research into PON2 biology has revealed that tumor cells exploit PON2 activity to counteract oxidative stress and escape apoptosis. Consistent with these observations, PON2 is upregulated in various solid tumors and hematologic cancers [38], [42]. A limited but growing number of studies have also demonstrated that PON2 expression negatively correlates with cancer patient prognoses. In a cohort of pediatric and adult patients with B cell acute lymphoblastic leukemia (B-ALL), high PON2 mRNA expression was associated with reduced overall survival and relapse-free survival [122]. In patients with cutaneous melanoma and basal cell carcinoma, higher expression of PON2 protein was correlated with important prognostic indicators, including Breslow thickness, Clark level, regression, lymph node metastases, and pathological stage [144]. Similarly, Wang et al. reported that elevated PON2 expression in patients with gastric cancer was unfavorably associated with clinical stage, invasion, lymph node metastasis, distant metastasis, and overall patient survival [145]. The prognostic value of PON2 expression was also explored in

patients with bladder cancer (BC), which revealed that PON2 was upregulated in early stage tumors and fell in later stage tumors, suggesting a potentially important role for PON2 in different stages of tumorigenesis [146].

Recent research efforts have implemented murine models of tumorigenesis to explore PON2's influence on malignant growth *in vivo* with somewhat mixed results. In two murine models of B-ALL driven by the oncogenic fusion protein BRC-ABL1 or constitutively-active NRAS^{G12D}, loss of PON2 expression impaired disease progression and drastically improved survival duration in transplant recipient mice [122]. Researchers also investigated PON2's role in pancreatic ductal adenocarcinoma (PDAC) tumor growth and metastasis using multiple murine tumor models [41]. This report demonstrates that PON2 expression is necessary for subcutaneously- and orthotopically-implanted xenografts of the PDAC cell line PANC1. Furthermore, knockdown of PON2 reduced PDAC metastases to liver (from splenic injection) and lung (from tail vein injection) compared to PDAC cells with normal PON2 expression. Conversely, a tumor suppressor role for PON2 was identified in the context of ovarian cancer (OC) [123]. In this study, elevated PON2 expression blunted OC cellular proliferation and xenograft tumor growth in mice through inhibition of insulin like growth factor-1 (IGF-1) expression and signaling [123]. These reported discrepancies suggest PON2's influence on tumor growth *in vivo* likely depends on microenvironmental factors that correspond to distinct organs and tissues that give rise to neoplastic growth.

Several studies within the past decade have reported that PON2 is upregulated in lung tumors [38], including lung adenocarcinoma [42], [84]. However, the effects of PON2 on lung adenocarcinoma initiation and development are unknown. Therefore, we conducted studies to investigate how PON2 influences lung tumorigenesis using a variety of murine models. These studies were performed in immunocompetent mice of both sexes to also address the potential interplay of PON2 expression and host factors in mediating lung tumorigenesis.

4.2 MATERIALS AND METHODS

4.2.1 Cell lines and reagents

Dulbecco's Modified Eagle's Medium (DMEM), penicillin/streptomycin, trypsin, and L-glutamine were obtained from Mediatech (Manassas, VA); Glucose-free DMEM was purchased from Thermo Fisher (Waltham, MA) fetal bovine serum was purchased from Gemini (Broderick, CA); Polybrene and puromycin were purchased from Sigma-Aldrich (St. Louis, MO). Antibodies (Abs) for western blot were anti-β-actin mAb (A5441; Millipore Sigma; Burlington, MA), anti-Mouse PON2 pAb (ABIN1573944; antibodies-online.com; Atlanta, GA), peroxidase-conjugated goat anti-rabbit IgG (65-6120; Thermo Fisher; Waltham, MA) and peroxidase-conjugated goat anti-mouse IgG (65-6520; Thermo Fisher). Ad5-CMV-Cre was purchased from the Baylor College of Medicine gene vector core.

4.2.2 Cell culture

LLC cells were purchased from ATCC (Manassas, VA) and cultured in DMEM containing 10% FBS, 100 units/mL penicillin, and 100 µg/mL streptomycin in a 5% CO_2 humidified incubator at 37°C. Cells were passaged at approximately 1:5–1:10 dilutions and were continuously cultured no longer than 3 weeks. Stocks were from thawed vials frozen at passage two following receipt from ATCC and were authenticated by ATCC cell bank using the Short Tandem Repeat (STR) profiling.

4.2.3 Generation of cell lines

For retrovirus production, human embryonic kidney (HEK)-293T cells were transfected with the retroviral plasmid pBABE-IRES-EGFP (Addgene, 14430) with the helper plasmids pUVMC (8449) and pMD2.G (12259) using the transfection reagent Lipofectamine2000® (Thermo Fisher). Retroviral supernatant was collected 48-72 hours after transfection with the addition of 10 µg/ml polybrene (Sigma-Aldrich) to increase infection efficiency. GFP protein was expressed in LLC cells expressing control- or PON2-shRNA by culturing cells with retrovirus-containing medium. Nearly all infected cells (>95%) were GFP positive as evaluated by flow cytometry (FACScalibur).

4.2.4 Western blot analysis

Whole cell extracts of LLC cells were prepared using RIPA buffer (Thermo Fisher) supplemented with protease inhibitors (cOmplete; Roche). Protein

concentration was measured by bicinchoninic acid (BCA assay) (Thermo Fisher). Total protein (30 µg) was electrophoresed in 4-12% Bis/Tris gels (Bio-Rad; Hercules, CA). Separated proteins were transferred to a polyvinylidene difluoride (PVDF) membrane (Millipore) and incubated with indicated primary or secondary antibodies in blotting buffer (1X phosphate-buffered saline [PBS] with 0.2% Tween-20 and 10% (w/v) non-fat dry milk (Bio-Rad). The enhanced chemiluminescence detection system (Thermo Fisher) was used to detect proteins as previously described [84]. ImageJ software (NIH, Bethesda, MA) was used to quantify optical density (OD) values of immunoblot bands.

4.2.5 Cellular proliferation experiments

For cell proliferation measurement, $5*10^3$ LLC cells/well were plated in 12-well tissue culture plates and the number of the cells in each well was determined using a hemocytometer 24, 48, 72, and 96 h after plating.

4.2.6 In vivo animal studies

Animals were housed in an AALAC- (Association for Assessment and Accreditation of Laboratory Animal Care) accredited pathogen-free barrier facility. All procedures were in accordance with the University of Louisville Institute for Animal Care and Use Committee (IACUC). Eight-week old male and female Kras$^{LSL-G12D}$ (B6.129S4-Kras^{tm4Tyj}/J) mice were purchased from Jackson laboratories. Mice were selectively bred with PON2-KO mice to generate PON2-heterozygous mice harboring the mutant Kras$^{LSL-G12D}$ allele. These mice were

subsequently bred to generated mice homozygous for either wild type PON2 or mutant PON2 alleles that also possessed a single Kras$^{LSL-G12D}$ allele. PON2 genotypes were confirmed by Sanger sequencing of mouse genomic DNA. Kras$^{LSL-G12D}$ genotypes were confirmed by PCR amplification of genomic DNA using the following primers: Kras y116-common, 5′-TCC GAA TTC AGT GAC TAC AGA TG-3′; Kras y117-LSL, 5′-CTA GCC ACC ATG GCT TGA GT-3′; and Kras y118-wt, 5′-ATG TCT TTC CCC AGC ACA GT-3′. PCR reaction conditions are as follows: 35 cycles of 95°C for 30 seconds, 60° C for 30 seconds, and 72°C for 30 seconds. PCR products were resolved on a 4% agarose gel. The expected product size of y117/y116 is 327 bp (LSL), and y116/y118 is 450 bp (wild type).

4.2.7 Subcutaneous tumor injection

LLC cells (control- and PON2-shRNA; $1*10^5$ cells in 100 μL sterile 1X PBS) were subcutaneously into the right flank of WT and PON2-KO mice. Tumor volume ($V = L*W^2/2$) was measured every other day using dull-edged Vernier calipers. Experiment endpoint was considered tumors exceeding 1000 mm^3 in volume, per IACUC guidelines. At endpoint, mice were euthanized via CO_2 inhalation.

4.2.8 Orthotopic allograft lung tumor model

GFP-positive LLC cells expressing either control- or PON2-shRNA were percutaneously injected into the pleural cavity of WT or PON2-KO mice of both sexes according to a published report, with minor modifications [147]. Briefly, mice were anesthetized via inhalation of vaporized isoflurane (3% with 1.5L/min oxygen

flow). Anesthetic depth was confirmed by toe pinch reflex. Cells ($2*10^5$) were suspended in 1:1 PBS:Matrigel and percutaneously injected into the left lateral thorax using one-mL syringes with 26-gauge hypodermic needles. Following injection, mice were monitored for 10 min to confirm recovery.

After 10 days, mice were euthanized by CO_2 inhalation. Thoracic cavity was exposed using surgical instruments, and lungs were perfused by injecting 10 mL 1X PBS with 10 U/mL Heparin into the right ventricle of the heart with a 22-guage needle. Perfused lung and tumor tissue was dissected and minced with surgical scissors in a 10 cm petri dish. Minced tissue was incubated for 30 min in 10 mL 0.25% trypsin-EDTA supplemented with 300 U/mL collagenase in a 37°C water bath. Suspension was agitated using a 1000 µL pipette, followed by a 22-gauge needle, and passed through a 0.4 µm filter. GFP positivity of single cell suspension was determined by flow cytometry.

4.2.9 Mutant Kras-driven primary lung tumor model

Details of the Kras$^{LSL-G12D}$ mouse model of primary lung tumorigenesis have been previously described [148]. Tumor initiation was accomplished by intratracheal instillation of Adenovirus expressing Cre-recombinase ($2.5*10^7$ PFU/mouse). Briefly, mouse anesthesia was initiated and maintained via inhalation of vaporized isoflurane (3% in 1.5 L/min O_2). Anesthetic depth was confirmed by absence of toe reflex prior to surgery. Once anesthetized, mice were subcutaneously administered 200 µL meloxicam (0.5 mg/mL). Surgery was performed on a slide warmer covered with sterile paper towels and maintained at

37°C. Mice were affixed with surgical tape to expose the ventral surface, and Nair depilatory cream was applied to remove hair at surgical site. Exposed area was swabbed with alternating applications of iodine followed by isopropyl alcohol for three cycles. Tracheas were exposed using sterile surgical instruments, and Ad-Cre ($2.5*10^7$ PFU/mL in 60 µL DMEM supplemented with 10 mM $CaCl_2$) was administered with an insulin syringe directly into the tracheal lumen. Surgical incision was closed with surgical staples, and anesthesia was withdrawn to allow animal to recover. Mice were subcutaneously administered meloxicam 200 µL meloxicam (0.5 mg/mL) 24 and 48 h after surgery. Mice were euthanized 28 weeks after tumor initiation and lung tissues were collected for histological examination.

4.2.10 Histological analysis of lung tissues

Lung tissue sections were prepared as previously described, with some modifications [149]. Briefly, lung tissues were fixed in 10% neutral phosphate buffered formalin for 24 h at room temperature. After paraffin processing (TEK VIP; Sakura Finetek; Torrance, CA) and embedding (EG1160; Leica Biosystems; Buffalo Grove, IL), paraffin microtomy (RM2135; Leica Biosystems) was performed at 5 µm thickness per section. 5 sections were processed with 200 µm between each to assure detection of tumorigenesis in a whole lung. Slides of sections were deparaffinized and rehydrated in xylene, ethanol, and deionized water. Slides were stained with hematoxylin (95057-844; VWR; Radnor, PA) and eosin (HT110232; Thermo Fisher) according to a published protocol [149]. Stained slides were dehydrated in ethanol and xylene and coverslips were affixed to slide using xylene-

based Permount™ mounting medium (SP15-500; Thermo Fisher; Waltham, MA). Slides were dried overnight in a chemical hood, scanned using an Aperio Imagescope (Leica Biosystems), and analyzed with the onboard software (version 12.3.3). CaseViewer software was used to outline and measure lung/tumor cross-sectional area. Tumor burden was calculated for all sections as the sum of tumor cross-sectional area divided by the cross-sectional area of the whole lung section.

4.2.11 Statistical analysis

Statistical significance was determined by Student's t-test and/or two-way ANOVA as indicated. A p-value of < 0.05 was considered significant.

4.3 RESULTS

4.3.1 PON2 plays a limited role in the growth of lung adenocarcinoma tumors in a subcutaneous allograft model of tumorigenesis

To expand upon the limited research on PON2's role in tumorigenesis *in vivo*, we employed the use of a subcutaneous allograft lung tumor model in which LLCs with or without PON2 expression were subcutaneously implanted in the rear flanks of mice (Fig. 4.1). Recently, a study demonstrated that PON2 promotes an M2 anti-inflammatory phenotype in murine peritoneal macrophages (MPMs) [150]. Because M2-polarized macrophages can promote tumor progression [151], we hypothesized that mice lacking PON2 expression would be protected from

subcutaneous tumor growth through enhanced phagocytosis of implanted tumor cells. Furthermore, we sought to explore the influence of host sex in modulating lung adenocarcinoma tumorigenesis. These experiments, to our knowledge, are the first to explore whether PON2 expression status in host organisms can alter tumor growth *in vivo*. To this purpose, WT and PON2-KO mice of both sexes were administered LLC cells with or without PON2 expression (Fig. 4.1A) and subcutaneous tumor volume was measured over 24 days (Fig. 4.1B & C). In WT animals, subcutaneous tumor growth was similar between control- and PON2-shRNA groups (Fig. 4.1B). A similar pattern was observed in mice lacking PON2 expression, in that the rate of tumor growth was unaffected by the PON2 status of injected LLC cells (Fig. 4.1C). Furthermore, tumor growth in WT vs. PON2-KO animals was uniform, suggesting that PON2 host status does not affect the subcutaneous growth of LLC cells. Finally, no differences were observed in tumor growth between male and female mice. These results were unexpected, as loss of PON2 expression hindered the growth of lung adenocarcinoma cell lines, including LLC, A549, and NCI-H1299 cells, *in vitro*.
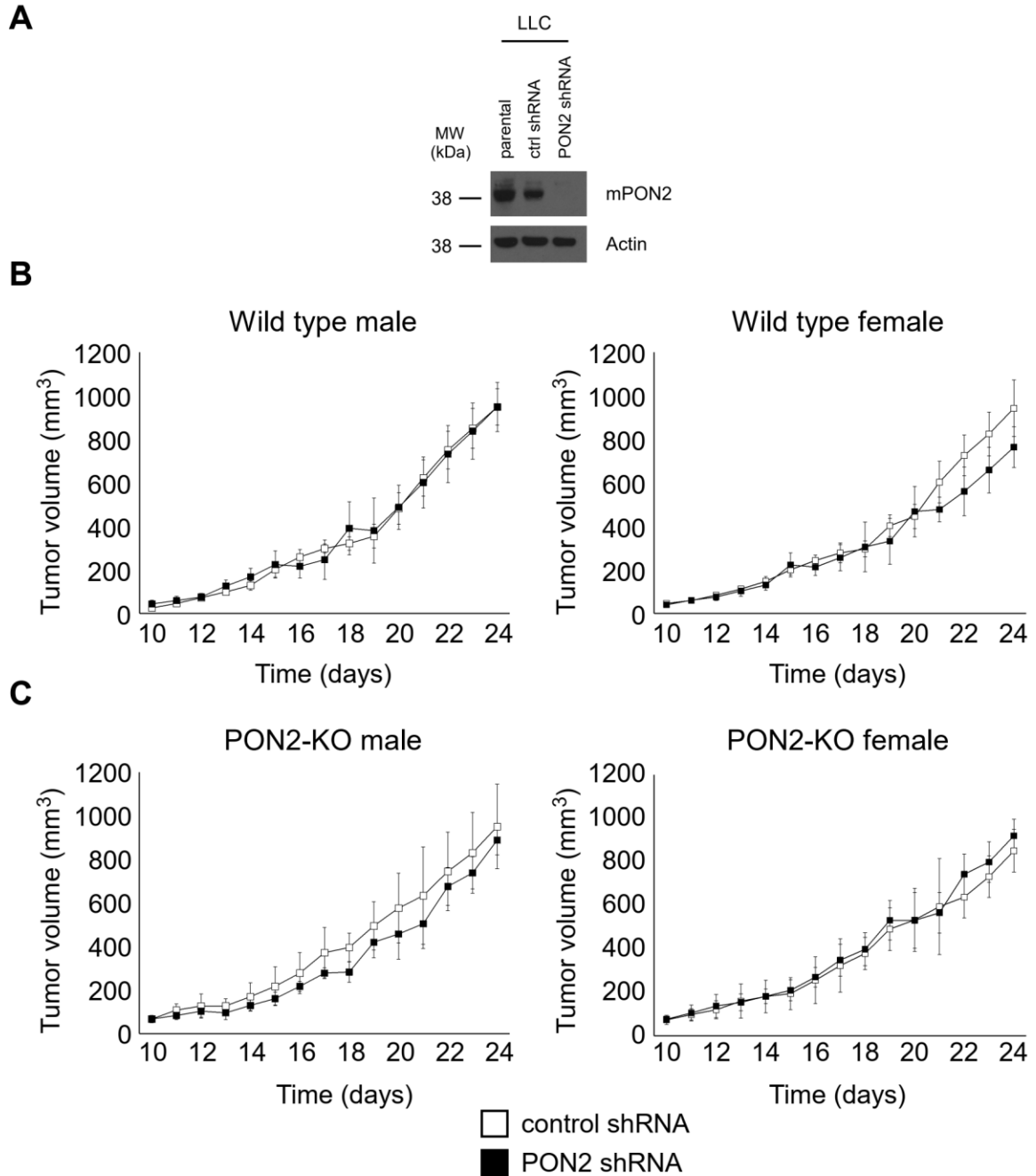
Figure 4.1. Subcutaneous LLC tumor growth is unaffected by PON2 expression status. (A) PON2 expression was determined by western blot analysis. LLC cells ($1*10^5$) with normal or reduced PON2 expression were injected into the rear flanks of WT (B) and PON2-KO (C) mice of both sexes, and tumor burden was monitored over 24 days. Data are mean ± SD for 5 mice per sex per genotype. No statistically significant differences were observed as related to PON2 status of injected LLCs, sex, or host PON2 status (unpaired Student's t-test).

4.3.2 Orthotopically-implanted lung tumor growth is unaffected by PON2 expression

We next sought to interrogate the influence of PON2 on lung adenocarcinoma growth in an orthotopic allograft murine model of lung cancer. In this approach, lung tumor cells are directly seeded into the pleural cavity, which more accurately resembles the tumor microenvironment of primary lung tumors compared to subcutaneous models of tumorigenesis. One disadvantage of the intrathoracic tumor model is that quantification of tumor burden is more difficult than directly measuring subcutaneous tumor size, because of differences in tumor multiplicity and location. To overcome this obstacle, we engineered LLC cells to express GFP, so that fluorescence could be used to distinguish tumor cells from non-malignant lung cells (Fig. 4.2). Following retroviral infection of control- and PON2-shRNA LLCs (Fig. 4.2A), fluorescence intensity was measured using flow cytometry (Fig. 4.2B), which revealed a similar GFP positivity between cell types. To functionally confirm loss of PON2 expression, we monitored cellular proliferation as before (Fig. 4.3B).

Once GFP-positive cells were generated and characterized, they were percutaneously injected into the thoracic cavity of WT and PON2-KO mice of both sexes in a PBS:matrigel (1:1 v/v) solution according to a published protocol (Fig. 4.3) [147]. Tumors were allowed to develop for 10 days, at which point animals were euthanized and lung and tumor tissues were harvested (Fig. 4.4). To quantify tumor burden, whole lung and tumor tissues were mechanically separated and enzymatically digested to generate a single cell suspension, and GFP positivity

114

was assessed by flow cytometry (Fig. 4.5). Tumor burden was measured as the % of GFP-positive cells present in each sample. This experimental approach revealed that intrathoracic tumor burden was similar among experimental conditions (Fig. 4.6). At experimental endpoint, tumors formed by LLCs lacking PON2 expression were similar in size to their control counterparts. Furthermore, host status conditions, including PON2 expression status and sex, failed to alter the growth of intrathoracic tumors. These results were in contrast to the deficits in LLC cellular proliferation following knockdown of PON2 expression and highlight the major differences between *in vitro* tumor cell proliferation and *in vivo* tumorigenesis.
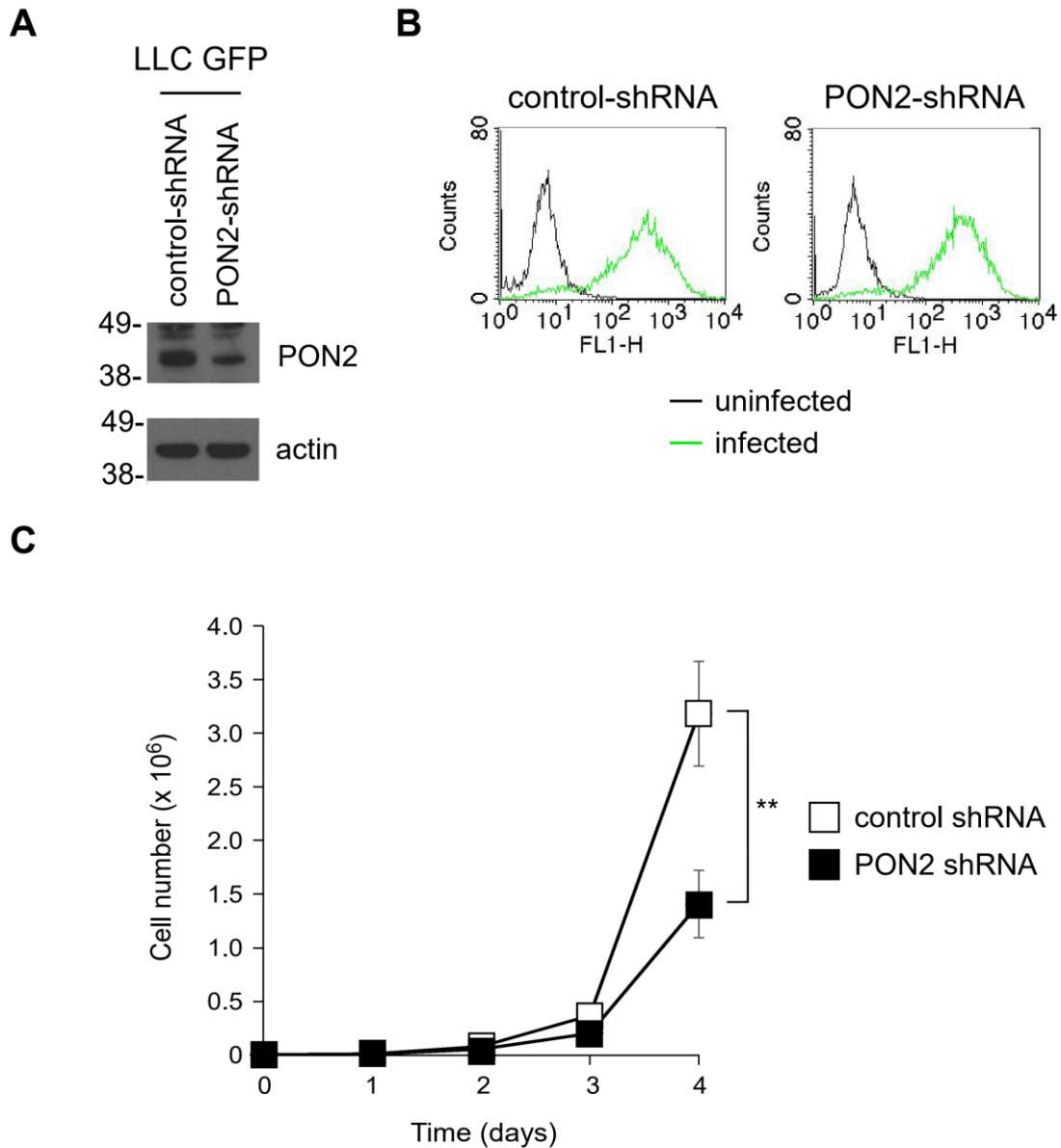
Figure 4.2. PON2 expression is required for the proliferation of murine lung adenocarcinoma cells expressing GFP. (A) GFP protein was expressed in control shRNA and PON2 shRNA LLC cells by retroviral expression, and PON2 expression was determined by western blot. (B) Fluorescence intensity of GFP in control shRNA and PON2 shRNA LLC cells was determined by FACS. (C) The proliferation of LLC cells expressing control- or PON2-shRNA was evaluated. The data shown are mean ± SD of three independent experiments. Asterisks indicate p-values of < 0.01 (**) by Student's unpaired t test.
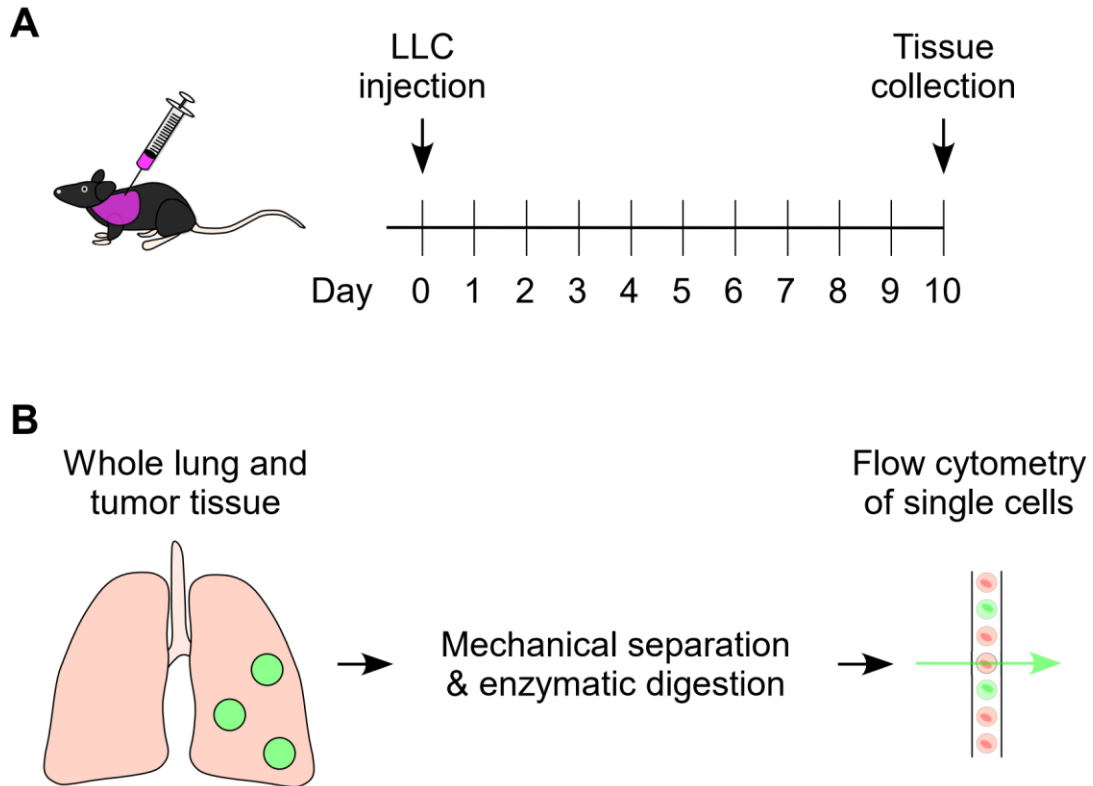
Figure 4.3. Experimental overview of orthotopic allograft model using LLC cells. (A) GFP-positive LLCs ($2*10^5$) expressing either control- or PON2-shRNA were injected directly into the thoracic cavity of WT and PON2-KO mice. After 10 days, lung and tumor tissue was collected by dissection. (B) Following mechanical separation with surgical instruments, mouse lung and tumor tissue were enzymatically digested in a trypsin and collagenase solution to create a single-cell suspension. GFP positivity (%) was determined by flow cytometry to quantify tumor burden.
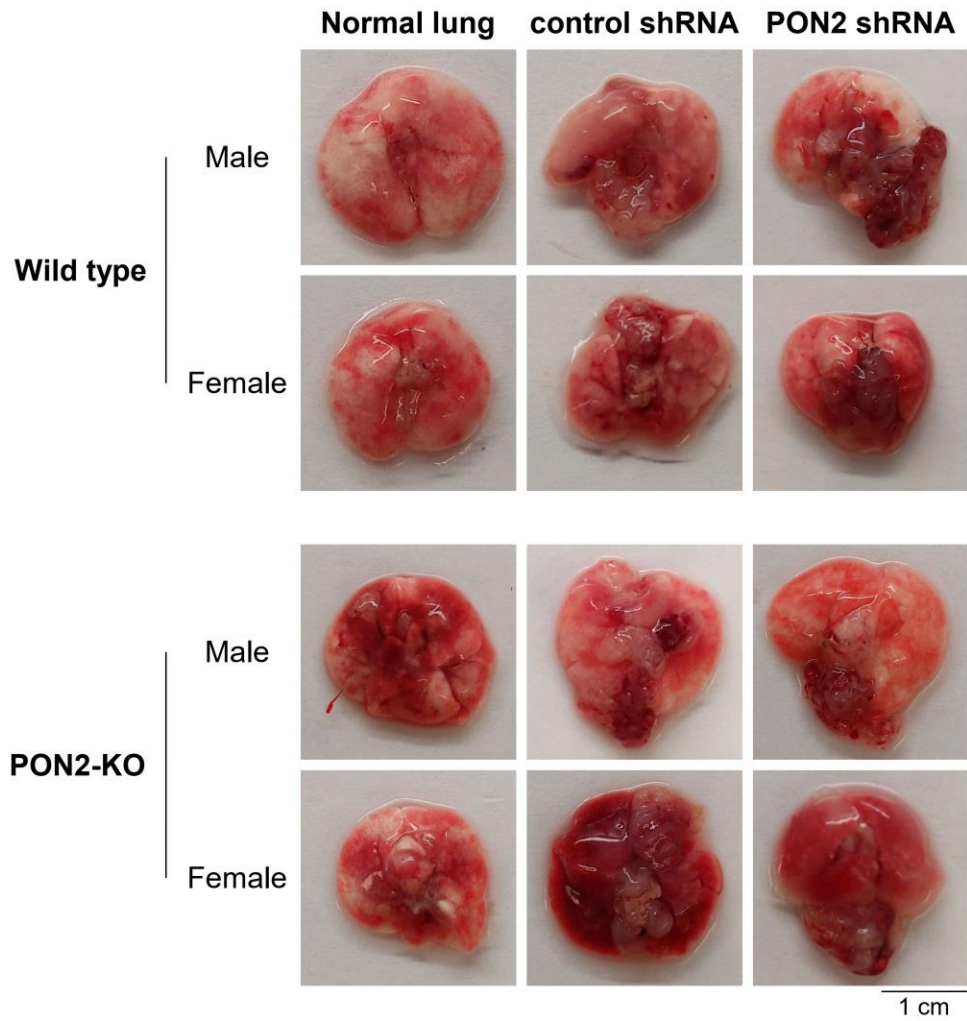
Figure 4.4. WT and PON2-KO mice develop intrathoracic tumors following administration of GFP-positive LLC cells. Representative images of lung and tumor tissue dissected from WT and PON2-KO mice of both sexes following administration of control- or PON2-shRNA LLC cells.
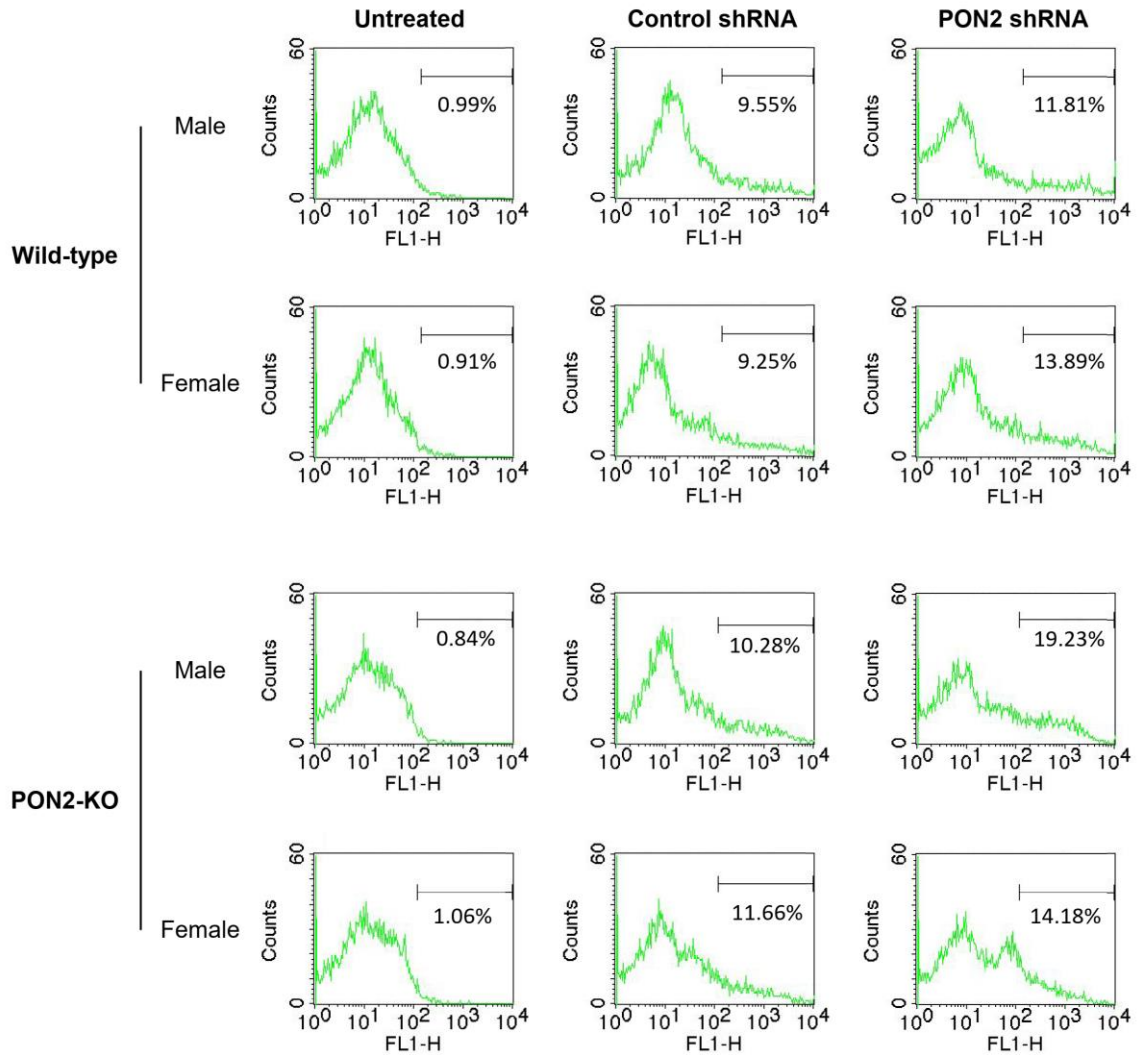
Figure 4.5. Evaluating orthotopic lung tumor burden by determining GFP-positivity of mouse lung and tumor tissue. GFP-expressing control-shRNA or PON2-shRNA LLC cells were percutaneously injected into the pleural cavity of WT or PON-KO mice. Ten days after administering LLC cells, lung tissues bearing GFP-expressing LLC adenocarcinoma were collected. Single-cell suspension of pulmonary cells were acquired and GFP fluorescence was evaluated by flow cytometry. Representative flow cytometry plots are shown.
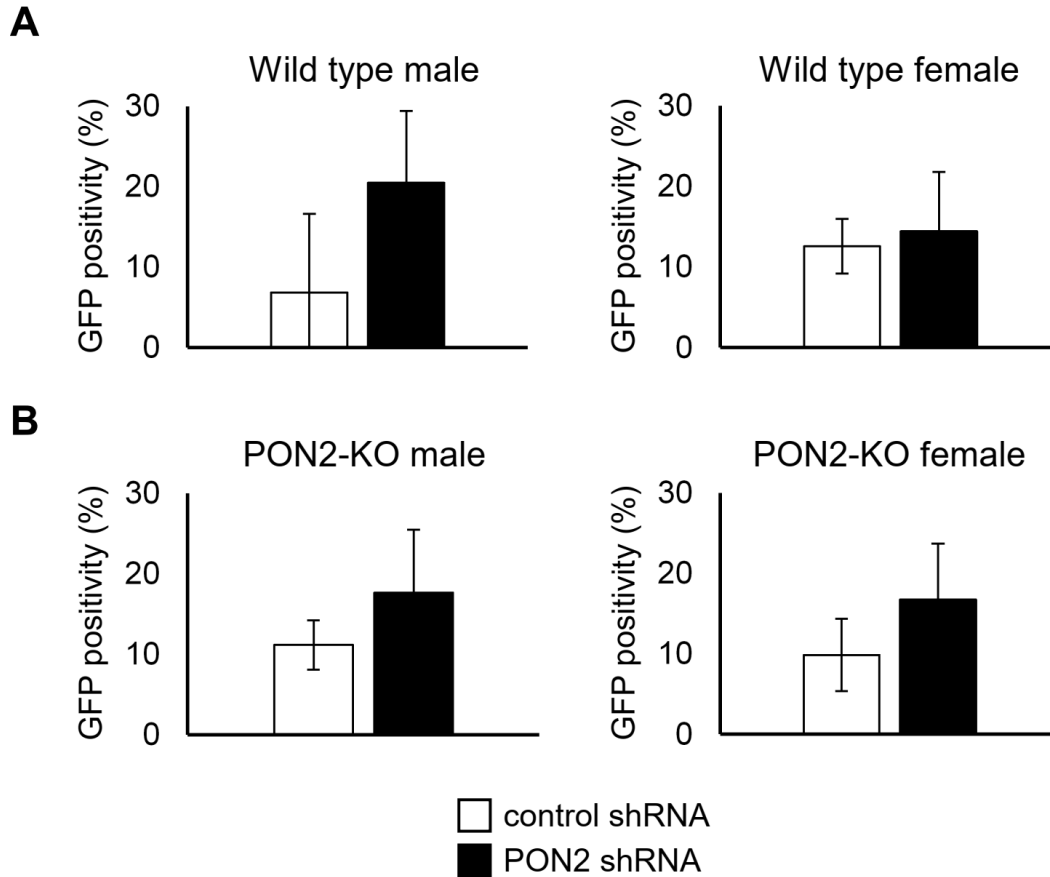
Figure 4.6. Intrathoracic LLC tumor burden is similar regardless of PON2 expression or host status. GFP positivity of mouse lung and tumor tissue was determined by flow cytometry in WT (A) and PON2-KO (B) mice of both sexes 10 days following administration of GFP-positive LLCs expressing control- or PON2-shRNA. Data are mean ± SD of 5 mice per group. Statistical significance was determined by two-way ANOVA. No significant difference was observed as related to PON2 expression status of LLCs, genetic background of host, or mouse sex.

4.3.3 Activation of a mutant Kras allele induces primary lung tumor growth in WT and PON2-KO mice.

A major focus of this body of work was to investigate PON2's role in lung tumorigenesis using physiologically-relevant animal models. As such, we employed the use of a primary tumor model driven by oncogenic Kras in mice proficient or deficient in PON2 expression. Kras is among the most frequently mutated oncogenes in lung adenocarcinoma [152], [153]. As such, much attention has been given to developing clinically-relevant animal models of lung tumorigenesis involving mutant Kras. An earlier study first reported the use of a genetically engineered mouse strain with an inducible Kras^{G12D} allele, which is activated by delivery of Cre recombinase to lung tissue to drive primary lung tumor formation [154]. This mutant allele contains an activating G12D mutation downstream of a stop codon flanked by LoxP sites. These sites can be cleaved by Cre recombinase, thereby removing the stop codon and permitting expression of the Kras^{G12D} oncoprotein. Research in the past decade has expanded the utility of this strain through selective breeding with other genetically engineered mouse strains harboring additional oncogenes [155]. In the present study, we sought to investigate PON2's role in primary tumorigenesis using a similar approach. Specifically, we endeavored to generate Kras$^{LSL-G12D}$ mice with or without PON2 expression to elucidate whether PON2 influences mutant-Kras driven primary lung tumor development. To this purpose, we selectively bred PON2-deficient mice with Kras$^{LSL-G12D}$ mice (Fig. 4.7), which yielded PON2-heterozygous mice with or without a mutant Kras allele. These mice were subsequently bred to generate mice

homozygous wild type or homozygous PON2-KO mice harboring a single copy of Kras$^{LSL-G12D}$ (WT^{Kras} and PON2-KO^{Kras}, respectively).

In the present study, we aimed to thoroughly monitor the development of lung adenocarcinoma in mice with or without PON2 expression (Fig. 4.8). To this purpose, WT^{Kras} and PON2-KO^{Kras} mice of both sexes were administered adenovirus expressing Cre recombinase (Ad-Cre) intratracheally at 6-8 weeks of age. Twenty-eight weeks following tumor induction, formalin-fixed, paraffin-embedded (FFPE) lungs were sectioned at five equidistant intervals spanning half of each lung to observe tumor prevalence at multiple depths. Each group comprised 6 males and 6 females, yielding 120 slides for quantification. Prepared sections were stained with Hematoxylin and Eosin (H&E) to aid in tumor visualization (Fig. 4.8C & D). The summed cross-sectional areas of tumors were compared to total lung cross-sectional area to determine tumor burden (%). As predicted, administration of Ad-Cre was sufficient to induce the formation of primary lung tumors in mice harboring the inducible mutant Kras allele (Fig. 4.9). Tumor burden for male and female mice with or without PON2 expression was calculated using 3DHISTECH CaseViewer software, which is shown in Fig. 4.10. The results of this analysis revealed that PON2 expression does not influence the formation and growth of mutant Kras-driven lung tumors. Furthermore, the tumor burden of male and female mice was comparable. These observations are similar to our previously documented experiments utilizing LLC cells with or without PON2 expression in subcutaneous and intrathoracic tumor models, but are unexpected compared to our *in vitro* observations that demonstrate that PON2 is required for

lung adenocarcinoma cellular proliferation. This discrepancy suggests an important context dependency for PON2's role in regulating tumor cell physiology which warrants further investigation.
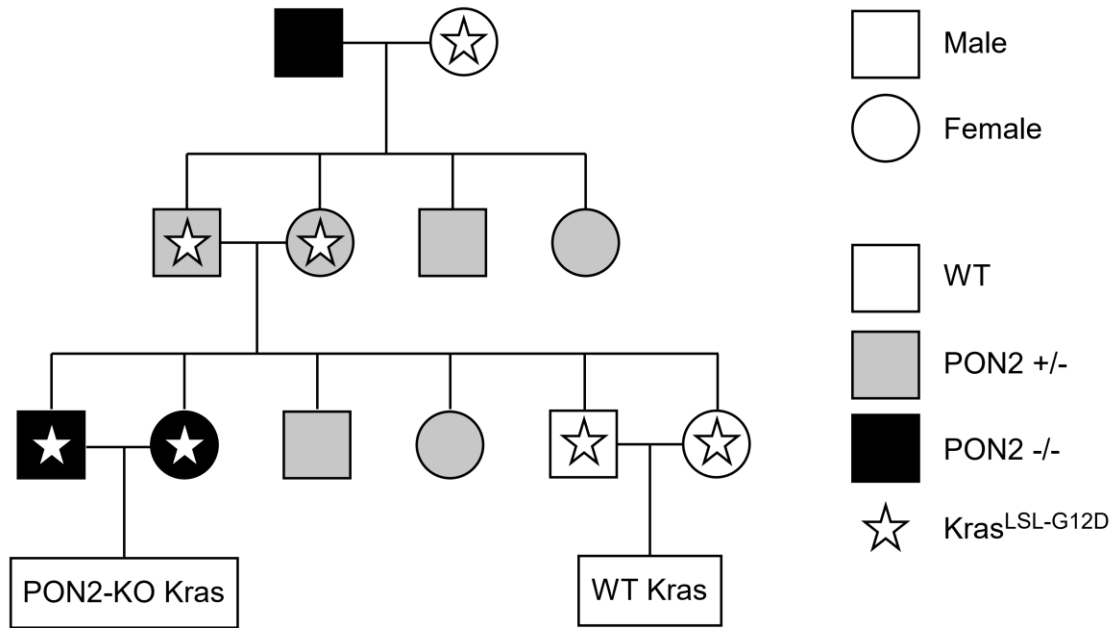
Figure 4.7. Generation of WT and PON2-deficient mice harboring an inducible mutant Kras^G12D allele. Kras^LSL-G12D mice (Jackson) were bred with PON2-KO mice to generate PON2-heterozygous mice with or without a mutant Kras allele. Kras-mutant PON2-heterozygous individuals were then selectively bred to generate Kras-mutant mice with wild type PON2 expression (WT Kras) or homozygous for PON2 deletion (PON2-KO Kras).
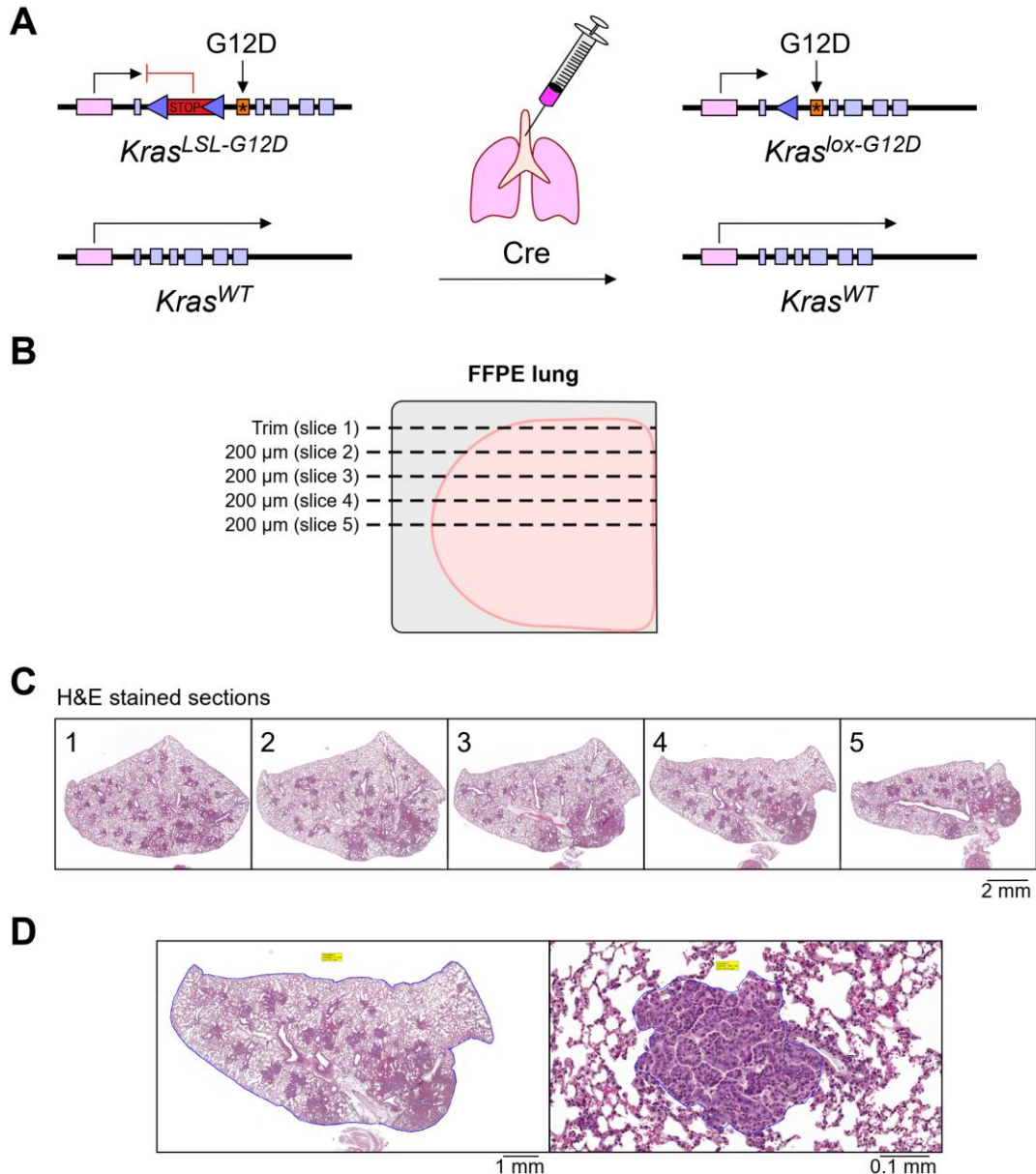
Figure 4.8. Experimental overview of Kras-driven primary tumor model. (A) The Kras[LSL-G12D] allele carries a G12D point mutation whose expression is prevented by a stop codon flanked by loxP sites. Intratracheal instillation of adenovirus expressing Cre recombinase (Ad-Cre) leads to excision of the stop codon and expression of the Kras[G12D] oncogenic protein. (B) At experimental endpoint (28 weeks post-administration of Ad-Cre), whole lungs were dissected, fixed in formalin, and embedded in paraffin. Five serial sections separated by 200 µm and spanning half formalin-fixed, paraffin-embedded (FFPE) lung tissue samples were prepared by tissue microtomy. (C) Serial FFPE sections were stained with Hematoxylin and Eosin (H&E), and (D) tumor burden (%) was quantified by comparing tumor cross-sectional area to whole lung cross-sectional area.

125
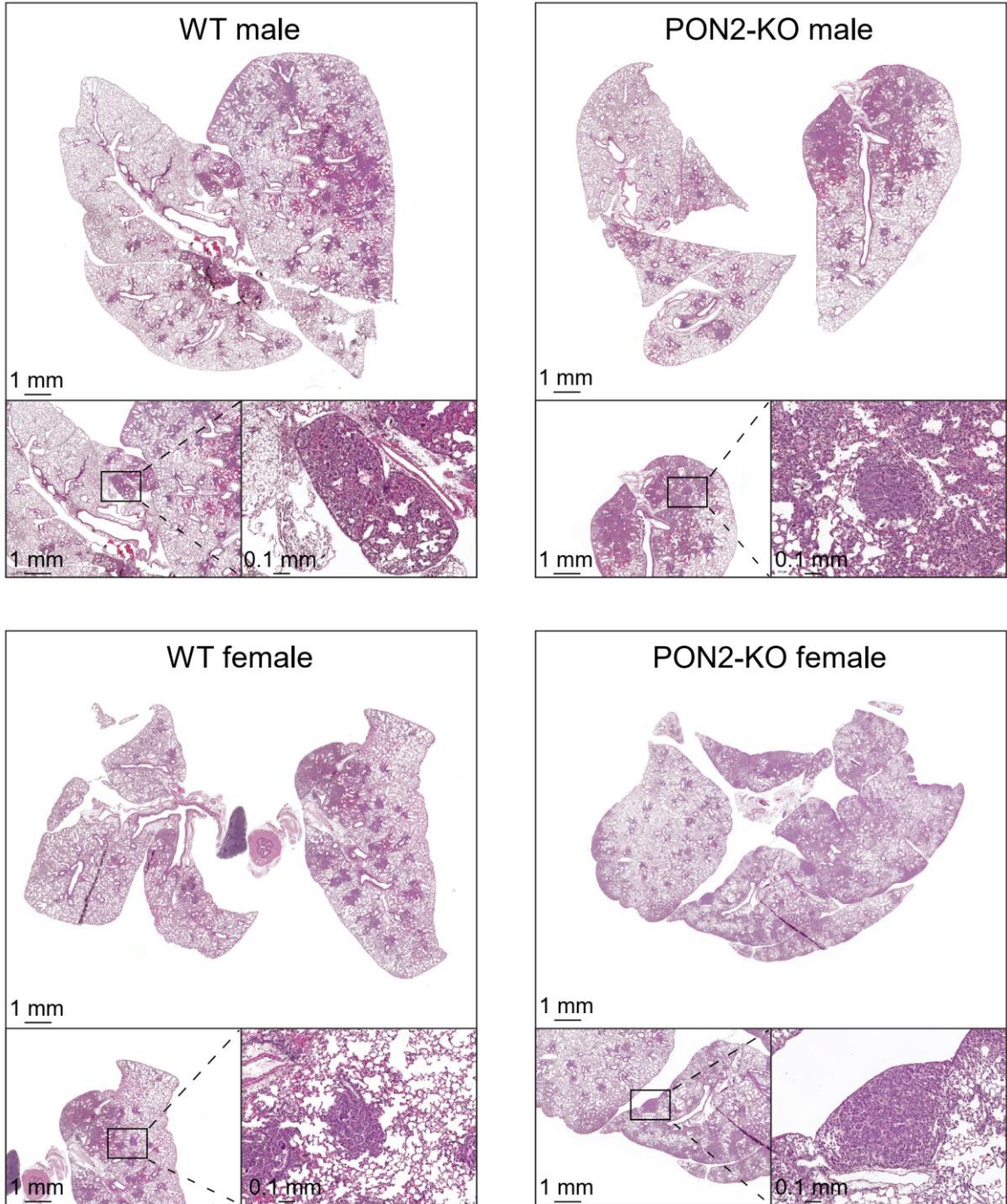
Figure 4.9. Development of Kras-driven lung adenocarcinoma in WT and PON2-KO mice. Representative digital slide images of H&E-stained lungs collected 28 weeks after tumor initiation from WT and PON2-deficient mice. Inlets show select adenocarcinoma tumors at 10X magnification.
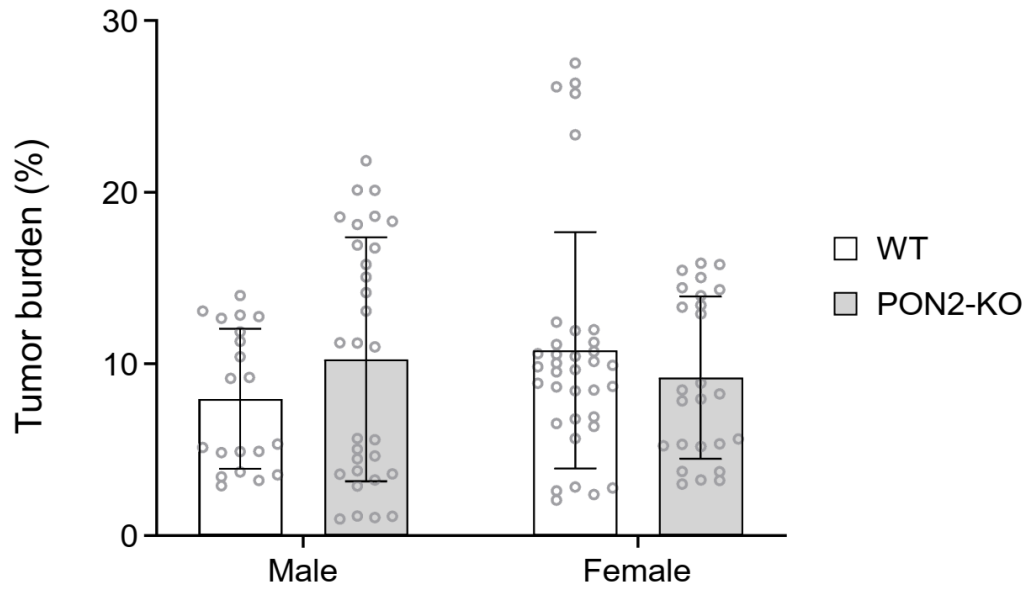
Figure 4.10. Primary lung tumor burden is similar between WT and PON2-KO mice. Tumor burden (%) was determined at 5 depths per lung in WT and PON2-KO mice of both sexes (n=5 per group). No significant differences in tumor burden were observed between WT and PON2-deficient mice of either sex. Data are mean ±SD; each point represents an individual section. A two-way ANOVA was used to determine statistical significance.

4.4 DISCUSSION

Research efforts by other laboratories have interrogated the effects of PON2 expression on tumor growth using murine models with somewhat inconsistent findings. For instance, PON2 expression had a positive correlation with mouse tumor growth and metastasis in models of PDAC, as reported by Nagarajan and colleagues [41]. This study revealed that PON2 promoted the proliferation of PDAC cells *in vitro* by enhancing GLUT1-mediated glucose transport, thereby protecting against the cellular starvation response and promoting anoikis. Further, PON2 expression was required for PDAC growth and distant metastasis to liver and lung tissues. An important revelation of this work was that PON2 is transcriptionally repressed by the tumor suppressor p53, providing mechanistic insight into how tumors may favorably upregulate PON2 expression. In a separate study, PON2 was shown to promote B-ALL leukemogenesis mice driven by two oncogenic drivers, the BCR-ABL1 tyrosine kinase and mutant NRAS^{G12D} [122]. Using PON2-deficient murine and human B-ALL cells, it was revealed that loss of PON2 resulted in compromised leukemogenesis through defective glucose uptake and ATP production. In accordance with the study conducted in PDAC cells, these experiments demonstrated that PON2 enabled glucose uptake by preventing stomatin-mediated inhibition of GLUT1. Converse to the pro-tumorigenic role thoroughly demonstrated in these studies, a recent study by Devarajan et al. uncovered a tumor suppressor role for PON2 in the context of ovarian cancer (OC) [123].

Overexpression of PON2 in an OC cell line decreased cellular proliferation via inhibition of IGF-1 expression and signaling. This phenotype was due to PON2's ability to prevent mitochondrial superoxide generation, which increases c-Jun-mediated transcriptional activation of the IGF-1 gene. Furthermore, the researchers determined PON2 expression at various stages of OC progression and found that PON2 was more abundant in early stages of OC compared to samples from patients with late-stage OC. Taken together, these results paint a complicated picture of PON2's role in tumorigenesis broadly and suggest conflicting roles in different tumor types and early vs. late-stage neoplastic growth.

In the present study, we investigated PON2's role in lung adenocarcinoma development and growth *in vivo*. A major focus of these experiments was to elucidate the extent to which PON2 host status and sex may also interact with tumor PON2 expression to affect lung neoplastic growth. First, we examined PON2's role in lung adenocarcinoma tumor growth using subcutaneously-implanted LLCs with normal or reduced PON2 expression, which were administered to WT or PON2-deficient immunocompetent mice of both sexes (Fig. 4.1). These experiments revealed that LLCs formed subcutaneous tumors in host animals independent of tumor cell PON2 expression, host PON2 status, or recipient mouse sex. Since the tissue microenvironment of subcutaneous flank tumors may not accurately represent the extracellular factors present in lung tissue, we also employed the use of an orthotopic allograft model of lung tumorigenesis (Fig. 4.2). In this model, LLCs with normal or reduced PON2 expression were percutaneously implanted directly into the thoracic cavity,

allowing lung tumors to form in a manner more comparable to primary tumor development. These experiments also utilized WT and PON2-KO hosts of both sexes to probe the dynamics that mediate the growth of lung tumors with altered PON2 expression. Like the results observed in the subcutaneous tumor model, intrathoracic tumor burden was similar among all study conditions, suggesting that LLC tumor growth *in vivo* is not affected by cellular PON2 expression or host factors (Fig. 4.6). Finally, we sought to evaluate PON2's role in lung adenocarcinoma development using a primary tumor model in which male and female mice proficient or deficient in endogenous PON2 expression spontaneously develop lung tumors via Cre-mediated activation of oncogenic Kras^{G12D} (Fig. 4.8). At experimental endpoint, tumor burden was similar among all study groups, indicating that PON2 does not impact the initiation and progression of primary lung adenocarcinoma tumors (Fig. 4.10). Together, these findings were unexpected when considered in the context of our *in vitro* studies, which demonstrated that PON2 was required for the proliferation of human and murine lung adenocarcinoma cells.

The previous results reported by our laboratory herein suggest that PON2 promotes lung adenocarcinoma cell proliferation *in vitro* by modulating mitochondrial oxidative metabolism (Fig. 3.8-11, Table 3.1). However, PON2 expression failed to impact lung adenocarcinoma initiation and progression in several mouse models (Fig. 4.1, 4.6, & 4.10). Clearly, there is a discrepancy between PON2's roles in cancer cell proliferation in *vitro* and lung tumor growth *in vivo.* Although cancer cell culture models provide valuable tools for understanding

cancer progression and treatment, the physiological relevance of *in vitro* cell cultures is, unfortunately, limited [156]. Therefore, the results of *in vitro* tissue culture experiments are unable to be directly extrapolated to *in vivo* animal studies, particularly for the complex and dynamic pathophysiological processes underlying tumorigenesis.

The non-cancerous cellular and noncellular factors surrounding tumors are collectively known as the tumor microenvironment (TME) [157], [158]. The vital components of the TME include fibroblasts, neuroendocrine cells, adipocytes, immune cells, vasculature, lymphatic networks, and extracellular matrix (ECM). Accumulating evidence indicates that TME plays an essential role in the initiation, progression, and metastasis of human tumors [159]. Tumor physiology is modulated by different aspects of the tumoral niche, including intrinsic properties of tumor cell metabolism, genetic heterogeneity, metabolic interplays between tumor cells and nontumorous cells, oxygen availability, as well as whole-body nutrient homeostasis [160], [161]. In contrast, *in vitro* cell culture models rely on studying single homogenous cell types cultured in the presence of abundant oxygen and nutrients uncomplicated by the involvement of TME components. Thus, it is not uncommon that significant differences are encountered between the metabolism of tumors and the metabolism of corresponding malignant cells cultured *in vitro* [162]. These considerations may account for the discrepancy between PON2's role in cultured cells and lung adenocarcinoma in mice.

Given the heterogenicity of intrinsic (e.g., oncogenic profiles of tumor cells) and extrinsic properties (e.g., nutrient supply and oxygen availability) of the tumor

niche, the effects of PON2 on tumorigenesis are likely vastly different among various cancer types. Indeed, PON2 is found to promote initiation and progression of PDAC and B-ALL, whereas it functions as a tumor suppressor for ovarian cancer [41], [122], [123] . It is conceivable that the interaction of lung adenocarcinoma and microenvironmental factors in our animal studies are distinct from those of PDAC, B-ALL, and OC, yielding different impacts of PON2 on tumorigenesis. Overall, prudence is required for extrapolating *in vitro* cancer cell studies to animal research. As such, future exploration is warranted to elucidate the role of PON2 in initiation, progression, and metastasis of lung adenocarcinoma.

CHAPTER 5

CONCLUSIONS AND FUTURE DIRECTIONS

5.1 Overall Summary

Paraoxonase 2 (PON2) is a multifunctional intracellular enzyme that has received growing attention for its ability to modulate various aspects of normal and malignant cellular physiology. Work by our laboratory and others has revealed that PON2 utilizes its lactonase activity to hydrolyze the bacterial quorum sensing molecule N-(3-oxododecanoyl)-l-homoserine lactone (C12) to disrupt bacterial intercellular communication [83], [85], [90]. In addition, PON2 is upregulated in various human cancers [38], [42], likely due to its ability to mitigate oxidative stress and protect against apoptotic stimuli. However, the mechanistic details underlying these phenomena are not fully understood. Therefore, we sought to explore the functional implications of PON2 expression in the context of airway cellular physiology, lung tumor cell proliferation, and lung adenocarcinoma tumorigenesis *in vivo*.

We first investigated PON2's role in mediating the cytotoxic and anti-proliferative activity of a bacterial quorum-sensing molecule, N-(3-oxododecanoyl)-l-homoserine lactone (C12), produced by the opportunistic pathogen *Pseudomonas aeruginosa*. To thoroughly study these interactions, we first generated PON2-deficient mice using a CRISPR-Cas9 approach. This approach

enabled systemic depletion of endogenous PON2 expression in mice, which was confirmed by genomic sequencing, protein immunoblotting, and enzymatic assays. Furthermore, mice deficient in PON2 grew and developed normally compared to wild type (WT) counterparts. Since a primary site of *P. aeruginosa* infections is the conducting airway, we generated tracheal epithelial cells (TECs) immortalized by expression of SV40-Large T antigen to thoroughly study C12's impact on airway epithelial physiology. Importantly, the molecular phenotype of immortalized TECs was similar to their primary counterparts. We demonstrated that PON2 mediates the cytotoxic effects of C12 in TECs at concentrations at or above 30 µM, and that concentrations of C12 below this threshold hinder TEC cellular proliferation in a PON2-dependent manner. Because C12 primarily exerts its effects on eukaryotic cells through PON2 in mitochondria, we monitored key aspects of mitochondrial function in response to C12 including membrane polarization ($\Delta\psi_{mito}$) and network morphology using fluorescent microscopy. This analysis revealed that C12 induces rapid depolarization of $\Delta\psi_{mito}$ at 100 µM, but not 20 µM. Since depolarization of $\Delta\psi_{mito}$ is an early event in the intrinsic apoptotic cascade in mitochondria, these results are consistent with observations herein that C12 is cytotoxic to TECs above a threshold concentration of 30 µM. Furthermore, C12 induced mitochondrial fission in WT TECs at both 20 and 100 µM, which suggests that C12 may impair mitochondrial function without causing overt cell death. To investigate this hypothesis, we monitored oxygen consumption and extracellular acidification in TECs treated with 20 µM C12 and observed marked reductions to key metrics of mitochondrial respiration, including basal respiration, maximal

respiration, ATP-linked respiration, and spare respiratory capacity. Together, these results indicate that physiological concentrations of C12 impairs mitochondrial function and morphology in a PON2-dependent manner.

Another major focus of this work was to investigate PON2's role in lung adenocarcinoma cellular proliferation. Recent research has revealed that PON2 is upregulated in tissues from patients with various types of solid tumors and hematologic cancers, likely due to PON2's ability to suppress oxidative stress and evade apoptosis. Lesser known, however, is how PON2 expression modulates lung tumor cellular proliferation and oxidative metabolism. In the present study, we demonstrated that PON2 is upregulated in oncogenically-transformed human bronchial epithelial cells, as well as tissue samples from patients with non-small cell lung carcinoma. Further, PON2 expression is required for murine and human lung adenocarcinoma cell proliferation, independent of its lactonase activity. In contrast, loss of PON2 expression failed to alter non-transformed cellular proliferation. Furthermore, loss of PON2 expression exacerbated the production of ROS in human lung adenocarcinoma cells. To thoroughly investigate the impact of altered PON2 expression on lung adenocarcinoma oxidative metabolism, we employed the use of a stable isotope-resolved metabolomics (SIRM) approach. In this study, we tracked the presence of extracellular and intracellular metabolites derived from radiolabeled-glucose by high-resolution nuclear magnetic resonance (NMR), which provided insights into key aspects of oxidative metabolism, including glycolysis, TCA cycle, pentose phosphate pathway (PPP), and nucleotide biosynthesis. The results of this detailed analysis revealed that loss of PON2

expression reduces extracellular glucose depletion and lactate production, likely as a result of reduced glycolysis. Furthermore, PON2 deficiency impaired tricarboxylic acid cycle (TCA) cycle, pentose phosphate pathway (PPP), and nucleotide biosynthetic activity in lung adenocarcinoma cells. Taken together, these studies highlight PON2 as a potentially important factor in promoting the rapid proliferation of human lung adenocarcinoma cells.

The final aim of this work was to evaluate how PON2 expression may mediate lung tumorigenesis *in vivo*. Specifically, we were interested in exploring the interplay between tumor PON2 expression, host PON2 status, and host sex on murine lung tumor growth. In a subcutaneous allograft model, murine Lewis lung carcinoma cells (LLCs) with normal or reduced PON2 expression exhibited similar tumor growth independent of PON2 status or sex of host recipient animals. Using an orthotopic allograft model of tumorigenesis, intrathoracically-injected LLCs generated lung tumors independent of PON2 expression or host status. Finally, we generated WT and PON2-KO mice harboring an inducible oncogenic Kras[12D] allele to study PON2's effect on primary lung tumor development. In accordance with implanted tumors, Kras-driven primary lung tumorigenesis was similar between WT and PON2-KO mice. Together, these results suggest PON2 plays a limited role in murine lung tumor initiation and development *in vivo*. These findings were unexpected considered alongside our *in vitro* experimentation, which demonstrated that PON2 is essential for lung adenocarcinoma cell proliferation.

5.2 Significance of Findings

The present study highlights PON2 as an important factor in mediating lung cell physiology with respect to *P. aeruginosa* infections and malignant transformation. This is the first report, to our knowledge, directly linking PON2 activity to disruptions to mitochondrial morphology and function in response to the bacterial quorum sensing molecule C12 at physiologically-relevant concentrations. Furthermore, our data underscore PON2 as essential for lung adenocarcinoma cell proliferation through its ability to promote oxidative metabolism and mitigate the production of ROS. Finally, the *in vivo* experimentation performed by us is the first to explore PON2 host status in the initiation and development of lung tumors in mice. Together, these findings expand our knowledge of PON2 biology as it relates opportunistic lung infection and lung tumorigenesis and serve as a springboard for future investigations.

5.3 Future Directions

Despite an increased focus on PON2's role in infection in cancer, further work is warranted to fully understand the mechanisms by which PON2 may modulate various (patho)physiological processes. We are interested in progressing the field of PON2 biology in the following future studies.

5.3.1 Investigate the functional implications of PON2 expression on gut-derived sepsis in an ethanol binge-drinking mouse model

While the major site of *P. aeruginosa* infection is the lungs of compromised patients [163], the intestinal tract is considered the primary reservoir for this bacterium [164]. As such, many of these infections occur through hematogenous colonization from the intestine to the lungs. Alcohol abuse has been shown to increase intestinal permeability [165], thereby increasing the risk of bacterial infections and sepsis. Given PON2's role in disrupting bacterial quorum sensing, we hypothesize that mice deficient in PON2 will be more susceptible to gut-derived sepsis following a bolus administration of ethanol. To evaluate this hypothesis, we will examine the intestinal microbiome composition, intestinal permeability, and bloodborne pathogen burden in WT and PON2-KO mice following ethanol administration.

5.3.2 Explore PON2's contribution to liver tumorigenesis using hepatoxicant-induced models of murine hepatocellular carcinoma

Recent research has begun to explore PON2's role in tumorigenesis using murine models of B-cell acute lymphoblastic leukemia (B-ALL), pancreatic ductal adenocarcinoma (PDAC), and ovarian cancer (OC). While these studies were thorough in their experimental approaches, further work is needed to understand how aberrant PON2 expression influences neoplastic growth. Furthermore, the conflicting results of these studies suggest a context-dependent role for PON2 in

either promoting or suppressing tumorigenesis, contingent upon the contribution of specific oncogenic drivers or microenvironmental factors. To address this gap, we are interested in utilizing other mouse models congenic to the C57BL/6J strain. PON2 is overexpressed in liver hepatocellular carcinoma (HCC) and correlates with poor patient prognoses [42]. Furthermore, PON2 is upregulated as part of the antioxidant response in HCC cells treated with the novel cytotoxic small molecule agent 5hc2 [166]. Given these observations, we hypothesize that PON2 plays an important role in HCC tumorigenesis. To address this hypothesis, we will employ a murine model of HCC induced by hepatotoxicants such as diethylnitrosamine (DEN) or thioacetamide (TAA) in WT and PON2-KO mice maintained on a high-fat diet. [167]. We will evaluate incidence and progression of HCC using histopathological analysis in tandem with overall survival. The results of this study will elucidate PON2's influence on HCC tumorigenesis *in vivo*.

REFERENCES

[1] D. I. Draganov, J. F. Teiber, A. Speelman, Y. Osawa, R. Sunahara, and B. N. La Du, "Human paraoxonases (PON1, PON2, and PON3) are lactonases with overlapping and distinct substrate specificities," *J. Lipid Res.*, vol. 46, no. 6, pp. 1239–1247, Jun. 2005.

[2] C. Moya and S. Manez, "Paraoxonases: metabolic role and pharmacological projection," *Naunyn Schmiedebergs Arch Pharmacol*, vol. 391, no. 4, pp. 349–359, 2018.

[3] N. Martinelli, L. Consoli, D. Girelli, E. Grison, R. Corrocher, and O. Olivieri, "Paraoxonases: ancient substrate hunters and their evolving role in ischemic heart disease," *Adv Clin Chem*, vol. 59, pp. 65–100, 2013.

[4] S. L. Primo-Parmo, R. C. Sorenson, J. Teiber, and B. N. L. Du, "The Human Serum Paraoxonase/Arylesterase Gene (PON1) Is One Member of a Multigene Family," *Genomics*, vol. 33, no. 3, pp. 498–507, May 1996.

[5] M. Elias and D. S. Tawfik, "Divergence and convergence in enzyme evolution: parallel evolution of paraoxonases from quorum-quenching lactonases.," *J. Biol. Chem.*, vol. 287, no. 1, pp. 11–20, Jan. 2012.

[6] C. E. Furlong, J. Marsillach, G. P. Jarvik, and L. G. Costa, "Paraoxonases-1, -2 and -3: What are their functions?," 2016.

[7] W. N. ALDRIDGE, "Serum esterases. I. Two types of esterase (A and B) hydrolysing p-nitrophenyl acetate, propionate and butyrate, and a method for their determination.," *Biochem. J.*, vol. 53, no. 1, pp. 110–7, Jan. 1953.

[8] A. Devarajan, D. Shih, and S. T. Reddy, "Inflammation, infection, cancer

and all that...the role of paraoxonases," *Adv Exp Med Biol*, vol. 824, pp. 33–41, 2014.

[9]   B. M. P. N. D. A. M. F. J. B. A. J. L. M. N. D. S. G. C. F. Michael I. Mackness, "Paraoxonase and coronary heart disease," *Curr. Opin. Lipidol.*, vol. 9, no. 4, pp. 319–324, Aug. 1998.

[10]   M. Mackness and B. Mackness, "Targeting paraoxonase-1 in atherosclerosis," *Expert Opin. Ther. Targets*, vol. 17, no. 7, pp. 829–837, Oct. 2013.

[11]   A. García-Heredia *et al.*, "Paraoxonase-1 Inhibits Oxidized Low-Density Lipoprotein-Induced Metabolic Alterations and Apoptosis in Endothelial Cells: A Nondirected Metabolomic Study," *Mediators Inflamm.*, vol. 2013, pp. 1–9, 2013.

[12]   A. Tward *et al.*, "Decreased Atherosclerotic Lesion Formation in Human Serum Paraoxonase Transgenic Mice," *Circulation*, vol. 106, no. 4, pp. 484–490, Jul. 2002.

[13]   D. M. Shih *et al.*, "Combined serum paraoxonase knockout/apolipoprotein E knockout mice exhibit increased lipoprotein oxidation and atherosclerosis.," *J. Biol. Chem.*, vol. 275, no. 23, pp. 17527–35, Jun. 2000.

[14]   J. Camps, J. Marsillach, and J. Joven, "Pharmacological and lifestyle factors modulating serum paraoxonase-1 activity.," *Mini Rev. Med. Chem.*, vol. 9, no. 8, pp. 911–20, Jul. 2009.

[15]   D. A. Chistiakov, A. A. Melnichenko, A. N. Orekhov, and Y. V Bobryshev,

"Paraoxonase and atherosclerosis-related cardiovascular diseases,"
Biochimie, vol. 132, pp. 19–27, 2017.

[16] C. K. Chun, E. A. Ozer, M. J. Welsh, J. Zabner, and E. P. Greenberg, "Inactivation of a Pseudomonas aeruginosa quorum-sensing signal by human airway epithelia.," *Proc. Natl. Acad. Sci. U. S. A.*, vol. 101, no. 10, pp. 3587–90, Mar. 2004.

[17] M. Marchesani *et al.*, "New Paraoxonase 1 Polymorphism I102V and the Risk of Prostate Cancer in Finnish Men," *JNCI J. Natl. Cancer Inst.*, vol. 95, no. 11, pp. 812–818, Jun. 2003.

[18] V. L. Stevens, C. Rodriguez, A. L. Pavluck, M. J. Thun, and E. E. Calle, "Association of Polymorphisms in the Paraoxonase 1 Gene with Breast Cancer Incidence in the CPS-II Nutrition Cohort," *Cancer Epidemiol. Biomarkers Prev.*, vol. 15, no. 6, pp. 1226–1228, Jun. 2006.

[19] M. B. D. Aldonza *et al.*, "Paraoxonase-1 (PON1) induces metastatic potential and apoptosis escape via its antioxidative function in lung cancer cells.," *Oncotarget*, vol. 8, no. 26, pp. 42817–42835, Jun. 2017.

[20] M. Zhang *et al.*, "Paraoxonase 1 (PON1) Q192R Gene Polymorphism and Cancer Risk: A Meta-Analysis Based on 30 Publications," *Asian Pac. J. Cancer Prev.*, vol. 16, no. 10, pp. 4457–4463, 2015.

[21] S. T. Reddy *et al.*, "Human paraoxonase-3 is an HDL-associated enzyme with biological activity similar to paraoxonase-1 protein but is not regulated by oxidized lipids," *Arterioscler. Thromb. Vasc. Biol.*, vol. 21, no. 4, pp. 542–547, Apr. 2001.

[22] D. I. Draganov, P. L. Stetson, C. E. Watson, S. S. Billecke, and B. N. La Du, "Rabbit serum paraoxonase 3 (PON3) is a high density lipoprotein-associated lactonase and protects low density lipoprotein against oxidation.," *J. Biol. Chem.*, vol. 275, no. 43, pp. 33435–42, Oct. 2000.

[23] E.-M. M. Schweikert *et al.*, "PON3 is upregulated in cancer tissues and protects against mitochondrial superoxide-mediated cell death," *Cell Death Differ*, vol. 19, no. 9, pp. 1549–1560, Sep. 2012.

[24] L. Rothem, C. Hartman, A. Dahan, J. Lachter, R. Eliakim, and R. Shamir, "Paraoxonases are associated with intestinal inflammatory diseases and intracellularly localized to the endoplasmic reticulum," *Free Radic. Biol. Med.*, vol. 43, no. 5, pp. 730–739, Sep. 2007.

[25] T. Bacchetti, G. Ferretti, and A. Sahebkar, "The role of paraoxonase in cancer," *Semin Cancer Biol*, 2017.

[26] M. Rosenblat, D. Draganov, C. E. Watson, C. L. Bisgaier, B. N. La Du, and M. Aviram, "Mouse macrophage paraoxonase 2 activity is increased whereas cellular paraoxonase 3 activity is decreased under oxidative stress," *Arterioscler. Thromb. Vasc. Biol.*, vol. 23, no. 3, pp. 468–474, Mar. 2003.

[27] M. Aviram and M. Rosenblat, "Paraoxonases 1, 2, and 3, oxidative stress, and macrophage foam cell formation during atherosclerosis development," *Free Radic. Biol. Med.*, vol. 37, no. 9, pp. 1304–1316, Nov. 2004.

[28] S. Porntadavity, T. Permpongpaiboon, and W. Sukketsiri, "Human paraoxonase 2," *Excli j*, vol. 9, pp. 159–172, 2010.

[29] H. Hagmann *et al.*, "Breaking the chain at the membrane: paraoxonase 2 counteracts lipid peroxidation at the plasma membrane," *FASEB J.*, vol. 28, no. 4, pp. 1769–1779, Apr. 2014.

[30] A. Devarajan *et al.*, "Macrophage paraoxonase 2 regulates calcium homeostasis and cell survival under endoplasmic reticulum stress conditions and is sufficient to prevent the development of aggravated atherosclerosis in paraoxonase 2 deficiency/apoE-/- mice on a Western diet," *Mol Genet Metab*, vol. 107, no. 3, pp. 416–427, 2012.

[31] A. Devarajan *et al.*, "Paraoxonase 2 deficiency alters mitochondrial function and exacerbates the development of atherosclerosis," *Antioxid Redox Signal*, vol. 14, no. 3, pp. 341–351, 2011.

[32] C. J. Ng *et al.*, "Paraoxonase-2 deficiency aggravates atherosclerosis in mice despite lower apolipoprotein-B-containing lipoproteins: anti-atherogenic role for paraoxonase-2.," *J. Biol. Chem.*, vol. 281, no. 40, pp. 29491–500, Oct. 2006.

[33] I. Witte, U. Foerstermann, A. Devarajan, S. T. Reddy, and S. Horke, "Protectors or Traitors: The Roles of PON2 and PON3 in Atherosclerosis and Cancer," *J Lipids*, vol. 2012, p. 342806, 2012.

[34] O. Frank *et al.*, "Gene expression signature of primary imatinib-resistant chronic myeloid leukemia patients," *Leukemia*, vol. 20, no. 8, pp. 1400–1407, Aug. 2006.

[35] H. Kang *et al.*, "Gene expression classifiers for relapse-free survival and minimal residual disease improve risk classification and outcome prediction

in pediatric B-precursor acute lymphoblastic leukemia," *Blood*, vol. 115, no. 7, pp. 1394–1405, Feb. 2010.

[36] S. Altenhöfer *et al.,* "One enzyme, two functions: PON2 prevents mitochondrial superoxide formation and apoptosis independent from its lactonase activity.," *J. Biol. Chem.*, vol. 285, no. 32, pp. 24398–403, Aug. 2010.

[37] V. E. Kagan *et al.,* "Cytochrome c/cardiolipin relations in mitochondria: a kiss of death," *Free Radic. Biol. Med.*, vol. 46, no. 11, pp. 1439–1453, Jun. 2009.

[38] I. Witte *et al.*, "Beyond reduction of atherosclerosis: PON2 provides apoptosis resistance and stabilizes tumor cells," *Cell Death Dis*, vol. 2, p. e112, 2011.

[39] M. Kruger, A. M. Pabst, B. Al-Nawas, S. Horke, and M. Moergel, "Paraoxonase-2 (PON2) protects oral squamous cell cancer cells against irradiation-induced apoptosis," *J Cancer Res Clin Oncol*, vol. 141, no. 10, pp. 1757–1766, 2015.

[40] M. Kruger *et al.*, "The anti-apoptotic PON2 protein is Wnt/beta-catenin-regulated and correlates with radiotherapy resistance in OSCC patients," *Oncotarget*, vol. 7, no. 32, pp. 51082–51095, 2016.

[41] A. Nagarajan *et al.*, "Paraoxonase 2 Facilitates Pancreatic Cancer Growth and Metastasis by Stimulating GLUT1-Mediated Glucose Transport," *Mol Cell*, vol. 67, no. 4, pp. 685-701.e6, 2017.

[42] M. I. Shakhparonov *et al.*, "Expression and Intracellular Localization of

Paraoxonase 2 in Different Types of Malignancies.," *Acta Naturae*, vol. 10, no. 3, pp. 92–99, 2018.

[43] G. Giordano, T. B. Cole, C. E. Furlong, and L. G. Costa, "Paraoxonase 2 (PON2) in the mouse central nervous system: A neuroprotective role?," *Toxicol. Appl. Pharmacol.*, vol. 256, no. 3, pp. 369–378, 2011.

[44] J. M. Garrick *et al.*, "Developmental expression of paraoxonase 2," *Chem. Biol. Interact.*, vol. 259, pp. 168–174, Nov. 2016.

[45] L. G. Costa, R. de Laat, K. Dao, C. Pellacani, T. B. Cole, and C. E. Furlong, "Paraoxonase-2 (PON2) in brain and its potential role in neuroprotection.," *Neurotoxicology*, vol. 43, pp. 3–9, Jul. 2014.

[46] A. Kumar, A. Singh, and Ekavali, "A review on Alzheimer's disease pathophysiology and its management: an update," *Pharmacol. Rep.*, vol. 67, no. 2, pp. 195–203, 2015.

[47] J. Shi *et al.*, "Possible association between Cys311Ser polymorphism of paraoxonase 2 gene and late-onset Alzheimer's disease in Chinese," *Brain Res. Mol. Brain Res.*, vol. 120, no. 2, pp. 201–204, Jan. 2004.

[48] Z. Janka, A. Juhász, A. Rimanóczy, K. Boda, J. Márki-Zay, and J. Kálmán, "Codon 311 (Cys --> Ser) polymorphism of paraoxonase-2 gene is associated with apolipoprotein E4 allele in both Alzheimer's and vascular dementias," *Mol. Psychiatry*, vol. 7, no. 1, pp. 110–112, 2002.

[49] Y. Nie *et al.*, "A Meta-Analysis on the Relationship of the PON Genes and Alzheimer Disease," *J. Geriatr. Psychiatry Neurol.*, vol. 30, no. 6, pp. 303–310, Nov. 2017.

[50] H. Khan, H. Ullah, M. Aschner, W. S. Cheang, and E. K. Akkol, "Neuroprotective Effects of Quercetin in Alzheimer's Disease," *Biomolecules*, vol. 10, no. 1, Jan. 2020.

[51] L. G. Costa *et al.*, "Modulation of paraoxonase 2 (PON2) in mouse brain by the polyphenol quercetin: a mechanism of neuroprotection?," *Neurochem. Res.*, vol. 38, no. 9, p. 1809, Sep. 2013.

[52] W. Dauer and S. Przedborski, "Parkinson's disease: mechanisms and models," *Neuron*, vol. 39, no. 6, pp. 889–909, Sep. 2003.

[53] E. C. Hirsch, P. Jenner, and S. Przedborski, "Pathogenesis of Parkinson's disease," *Mov. Disord.*, vol. 28, no. 1, pp. 24–30, Jan. 2013.

[54] M. Parsanejad *et al.*, "DJ-1 Interacts with and Regulates Paraoxonase-2, an Enzyme Critical for Neuronal Survival in Response to Oxidative Stress," *PLoS One*, vol. 9, no. 9, p. e106601, Sep. 2014.

[55] V. Bonifati *et al.*, "Mutations in the DJ-1 gene associated with autosomal recessive early-onset parkinsonism," *Science*, vol. 299, no. 5604, pp. 256–259, Jan. 2003.

[56] D. Shih *et al.*, "PON2 Deficiency Leads to Increased Susceptibility to Diet-Induced Obesity," *Antioxidants*, vol. 8, no. 1, p. 19, Jan. 2019.

[57] D. Qujeq, A. Mahrooz, A. Alizadeh, and R. Boorank, "Paraoxonase-2 variants potentially influence insulin resistance, beta-cell function, and their interrelationships with alanine aminotransferase in type 2 diabetes.," *J. Res. Med. Sci.*, vol. 23, p. 107, 2018.

[58] Z. Yang *et al.*, "The Ser311Cys variation in the paraoxonase 2 gene

increases the risk of type 2 diabetes in northern Chinese."

[59]   H. Ren, S.-L. Tan, M.-Z. Liu, H. L. Banh, and J.-Q. Luo, "Association of
        PON2 Gene Polymorphisms (Ser311Cys and Ala148Gly) With the Risk of
        Developing Type 2 Diabetes Mellitus in the Chinese Population," vol. 9, p.
        495, Aug. 2018.

[60]   F. Parween and R. Devi Gupta, "Review Insights into the role of
        paraoxonase 2 in human pathophysiology," *J Biosci*, vol. 46, no. 4, 2021.

[61]   G. Manco, E. Porzio, and T. M. Carusone, "Human Paraoxonase-2
        (PON2): Protein Functions and Modulation," *Antioxidants*, vol. 10, no. 2,
        pp. 1–28, Feb. 2021.

[62]   M. Shiner, B. Fuhrman, and M. Aviram, "A biphasic U-shape effect of
        cellular oxidative stress on the macrophage anti-oxidant paraoxonase 2
        (PON2) enzymatic activity," *Biochem. Biophys. Res. Commun.*, vol. 349,
        no. 3, pp. 1094–1099, Oct. 2006.

[63]   B. Fuhrman *et al.*, "Urokinase activates macrophage PON2 gene
        transcription via the PI3K/ROS/MEK/SREBP-2 signalling cascade
        mediated by the PDGFR-beta," *Cardiovasc Res*, vol. 84, no. 1, pp. 145–
        154, 2009.

[64]   L.-P. Précourt *et al.*, "Antioxidative properties of paraoxonase 2 in intestinal
        epithelial cells," *Am. J. Physiol. Liver Physiol.*, vol. 303, no. 5, pp. G623–
        G634, Sep. 2012.

[65]   D. A. Stoltz *et al.*, "A common mutation in paraoxonase-2 results in
        impaired lactonase activity," *J Biol Chem*, vol. 284, no. 51, pp. 35564–

35571, 2009.

[66] L. Mandrich, M. Cerreta, and G. Manco, "An Engineered Version of Human PON2 Opens the Way to Understand the Role of Its Post-Translational Modifications in Modulating Catalytic Activity," *PLoS One*, vol. 10, no. 12, p. e0144579, 2015.

[67] T. M. Carusone *et al.*, "WTAP and BIRC3 are involved in the posttranscriptional mechanisms that impact on the expression and activity of the human lactonase PON2," *Cell Death Dis.*, vol. 11, no. 5, May 2020.

[68] S. L. Gellatly and R. E. W. Hancock, "Pseudomonas aeruginosa: new insights into pathogenesis and host defenses," *Pathog. Dis.*, vol. 67, no. 3, pp. 159–173, 2013.

[69] C. S. Curran, T. Bolig, and P. Torabi-Parizi, "Mechanisms and targeted therapies for pseudomonas aeruginosa lung infection," *Am. J. Respir. Crit. Care Med.*, vol. 197, no. 6, pp. 708–727, Mar. 2018.

[70] J. B. Lyczak, C. L. Cannon, and G. B. Pier, "Lung infections associated with cystic fibrosis," *Clinical Microbiology Reviews*, vol. 15, no. 2. American Society for Microbiology Journals, pp. 194–222, 01-Apr-2002.

[71] S. Malhotra, D. Hayes, and D. J. Wozniak, "Cystic fibrosis and pseudomonas aeruginosa: The host-microbe interface," *Clinical Microbiology Reviews*, vol. 32, no. 3. American Society for Microbiology, 01-Jul-2019.

[72] M. B. Miller and B. L. Bassler, "Quorum sensing in bacteria," *Annual Review of Microbiology*, vol. 55. Annu Rev Microbiol, pp. 165–199, 2001.

[73]   R. S. Smith and B. H. Iglewski, "P. aeruginosa quorum-sensing systems and virulence," *Current Opinion in Microbiology*, vol. 6, no. 1. Elsevier Ltd, pp. 56–60, 01-Feb-2003.

[74]   E. Drenkard, "Antimicrobial resistance of Pseudomonas aeruginosa biofilms," *Microbes and Infection*, vol. 5, no. 13. Elsevier Masson SAS, pp. 1213–1219, 01-Nov-2003.

[75]   T. S. Charlton *et al.*, "A novel and sensitive method for the quantification of N-3-oxoacyl homoserine lactones using gas chromatography-mass spectrometry: Application to a model bacterial biofilm," *Environ. Microbiol.*, vol. 2, no. 5, pp. 530–541, Oct. 2000.

[76]   D. L. Erickson *et al.,* "Pseudomonas aeruginosa quorum-sensing systems may control virulence factor expression in the lungs of patients with cystic fibrosis," *Infect. Immun.*, vol. 70, no. 4, pp. 1783–1790, 2002.

[77]   C. E. Chambers, M. B. Visser, U. Schwab, and P. A. Sokol, "Identification of N-acylhomoserine lactones in mucopurulent respiratory secretions from cystic fibrosis patients," *FEMS Microbiol. Lett.*, vol. 244, no. 2, pp. 297–304, Mar. 2005.

[78]   J. Guo, K. Yoshida, M. Ikegame, and H. Okamura, "Quorum sensing molecule N-(3-oxododecanoyl)-L-homoserine lactone: An all-rounder in mammalian cell modification," *Journal of Oral Biosciences*, vol. 62, no. 1. Japanese Association for Oral Biology, pp. 16–29, 01-Mar-2020.

[79]   K. Tateda *et al.*, "The Pseudomonas aeruginosa autoinducer N-3-oxododecanoyl homoserine lactone accelerates apoptosis in macrophages

and neutrophils," *Infect. Immun.*, vol. 71, no. 10, pp. 5785–5793, Oct. 2003.

[80] C. A. Jacobi *et al.*, "Effects of bacterial N-acyl homoserine lactones on human Jurkat T lymphocytes-OdDHL induces apoptosis via the mitochondrial pathway," *Int. J. Med. Microbiol.*, vol. 299, no. 7, pp. 509–519, Nov. 2009.

[81] C. Schwarzer *et al.*, "Pseudomonas aeruginosa biofilm-associated homoserine lactone C12 rapidly activates apoptosis in airway epithelia," *Cell. Microbiol.*, vol. 14, no. 5, pp. 698–709, May 2012.

[82] C. Schwarzer *et al.*, "Pseudomonas aeruginosa homoserine lactone triggers apoptosis and Bak/Bax-independent release of mitochondrial cytochrome C in fibroblasts," *Cell. Microbiol.*, vol. 16, no. 7, pp. 1094–1104, Jul. 2014.

[83] C. Schwarzer *et al.*, "Paraoxonase 2 serves a proapopotic function in mouse and human cells in response to the Pseudomonas aeruginosa quorum-sensing molecule N-(3-Oxododecanoyl)-homoserine lactone," *J Biol Chem*, vol. 290, no. 11, pp. 7247–7258, 2015.

[84] G. Zhao *et al.*, "N-(3-oxo-acyl) homoserine lactone inhibits tumor growth independent of Bcl-2 proteins," *Oncotarget*, vol. 7, no. 5, pp. 5924–5942, 2016.

[85] A. M. Neely *et al.*, "N-(3-Oxo-acyl)-homoserine lactone induces apoptosis primarily through a mitochondrial pathway in fibroblasts," *Cell Microbiol*, vol. 20, no. 1, 2018.

[86] E. Vikström, L. Bui, P. Konradsson, and K. E. Magnusson, "Role of calcium

signalling and phosphorylations in disruption of the epithelial junctions by Pseudomonas aeruginosa quorum sensing molecule," *Eur. J. Cell Biol.*, vol. 89, no. 8, pp. 584–597, Aug. 2010.

[87] E. Vikström, L. Bui, P. Konradsson, and K. E. Magnusson, "The junctional integrity of epithelial cells is modulated by Pseudomonas aeruginosa quorum sensing molecule through phosphorylation-dependent mechanisms," *Exp. Cell Res.*, vol. 315, no. 2, pp. 313–326, Jan. 2009.

[88] E. Vikström, F. Tafazoli, and K. E. Magnusson, "Pseudomonas aeruginosa quorum sensing molecule N-(3 oxododecanoyl)-l-homoserine lactone disrupts epithelial barrier integrity of Caco-2 cells," *FEBS Lett.*, vol. 580, no. 30, pp. 6921–6928, Dec. 2006.

[89] S. Y. Eum, D. Jaraki, L. Bertrand, I. E. András, and M. Toborek, "Disruption of epithelial barrier by quorum-sensing N-3-(oxododecanoyl)-homoserine lactone is mediated by matrix metalloproteinases," *Am. J. Physiol. - Gastrointest. Liver Physiol.*, vol. 306, no. 11, p. G992, Jun. 2014.

[90] S. Horke *et al.*, "Novel Paraoxonase 2-Dependent Mechanism Mediating the Biological Effects of the Pseudomonas aeruginosa Quorum-Sensing Molecule N-(3-Oxo-Dodecanoyl)-L-Homoserine Lactone," vol. 83, no. 9, Sep. 2015.

[91] R. AJ, W. C, L. JJ, C. SR, P. DI, and C. MA, "The immunomodulatory Pseudomonas aeruginosa signalling molecule N-(3-oxododecanoyl)-L-homoserine lactone enters mammalian cells in an unregulated fashion," *Immunol. Cell Biol.*, vol. 85, no. 8, pp. 596–602, Nov. 2007.

[92] J. F. Teiber *et al.*, "Dominant Role of Paraoxonases in Inactivation of the Pseudomonas aeruginosa Quorum-Sensing Signal N-(3-Oxododecanoyl)-l-Homoserine Lactone," *Infect. Immun.*, vol. 76, no. 6, p. 2512, Jun. 2008.

[93] M. E. Durkin, X. Qian, N. C. Popescu, and D. R. Lowy, "Isolation of Mouse Embryo Fibroblasts," *Bio-protocol*, vol. 3, no. 18, p. e908, 2013.

[94] Y. You, E. J. Richer, T. Huang, and S. L. Brody, "Growth and differentiation of mouse tracheal epithelial cells: Selection of a proliferative population," *Am. J. Physiol. - Lung Cell. Mol. Physiol.*, vol. 283, no. 6 27-6, Dec. 2002.

[95] H. C. Lam, A. M. Choi, and S. W. Ryter, "Isolation of mouse respiratory epithelial cells and exposure to experimental cigarette smoke at air liquid interface," *J Vis Exp*, no. 48, 2011.

[96] E. Eenjes *et al.*, "A novel method for expansion and differentiation of mouse tracheal epithelial cells in culture," *Sci. Rep.*, vol. 8, no. 1, p. 7349, Dec. 2018.

[97] J. F. Teiber *et al.*, "Dominant role of paraoxonases in inactivation of the Pseudomonas aeruginosa quorum-sensing signal N-(3-oxododecanoyl)-L-homoserine lactone," *Infect. Immun.*, vol. 76, no. 6, pp. 2512–2519, Jun. 2008.

[98] S. Horke *et al.*, "Paraoxonase 2 is down-regulated by the Pseudomonas aeruginosa quorumsensing signal N-(3-oxododecanoyl)-L-homoserine lactone and attenuates oxidative stress induced by pyocyanin.," *Biochem. J.*, vol. 426, no. 1, pp. 73–83, Jan. 2010.

[99] O. SG, C. NS, O. GK, and D. MW, "The fluorescent protein color palette,"

Curr. Protoc. cell Biol., vol. Chapter 21, no. 1, Sep. 2007.

[100] J. Schindelin *et al.*, "Fiji: An open-source platform for biological-image analysis," *Nature Methods*, vol. 9, no. 7. Nat Methods, pp. 676–682, Jul-2012.

[101] A. Chaudhry, R. Shi, D. S. Luciani, C. A, S. R, and L. DS, "A pipeline for multidimensional confocal analysis of mitochondrial morphology, function, and dynamics in pancreatic β-cells," vol. 318, no. 2, pp. E87–E101, Feb. 2020.

[102] B. Li, J. R. Dedman, and M. A. Kaetzel, "Intron disruption of the annexin IV gene reveals novel transcripts.," *J. Biol. Chem.*, vol. 278, no. 44, pp. 43276–83, Oct. 2003.

[103] C. J. Ng, S. Y. Hama, N. Bourquard, M. Navab, and S. T. Reddy, "Adenovirus mediated expression of human paraoxonase 2 protects against the development of atherosclerosis in apolipoprotein E-deficient mice," *Mol Genet Metab*, vol. 89, no. 4, pp. 368–373, 2006.

[104] J. R. Rock, S. H. Randell, and B. L. M. Hogan, "Airway basal stem cells: a perspective on their roles in epithelial homeostasis and remodeling.," *Dis. Model. Mech.*, vol. 3, no. 9–10, pp. 545–56, Sep. 2010.

[105] J. R. Rock *et al.*, "Basal cells as stem cells of the mouse trachea and human airway epithelium.," *Proc. Natl. Acad. Sci. U. S. A.*, vol. 106, no. 31, pp. 12771–5, Aug. 2009.

[106] K. U. Hong, S. D. Reynolds, S. Watkins, E. Fuchs, and B. R. Stripp, "Basal Cells Are a Multipotent Progenitor Capable of Renewing the Bronchial

Epithelium," *Am. J. Pathol.*, vol. 164, no. 2, pp. 577–588, 2004.

[107] A. S. Lundberg *et al.*, "Immortalization and transformation of primary human airway epithelial cells by gene transfer," *Oncogene*, vol. 21, no. 29, pp. 4577–4586, 2002.

[108] J. C. Snyder, R. M. Teisanu, and B. R. Stripp, "Endogenous Lung stem cells and contribution to disease," *Journal of Pathology*, vol. 217, no. 2. NIH Public Access, pp. 254–264, Jan-2009.

[109] G. Ferone *et al.*, "SOX2 Is the Determining Oncogenic Switch in Promoting Lung Squamous Cell Carcinoma from Different Cells of Origin," *Cancer Cell*, vol. 30, no. 4, pp. 519–532, Oct. 2016.

[110] A. Satelli and S. Li, "Vimentin in cancer and its potential as a molecular target for cancer therapy," *Cellular and Molecular Life Sciences*, vol. 68, no. 18. NIH Public Access, pp. 3033–3046, Sep-2011.

[111] N. M. Maurice *et al.*, "Pseudomonas aeruginosa Induced Host Epithelial Cell Mitochondrial Dysfunction," *Sci. Rep.*, vol. 9, no. 1, Dec. 2019.

[112] H. Josephson, M. Ntzouni, C. Skoglund, S. Linder, M. V. Turkina, and E. Vikström, "Pseudomonas aeruginosa N-3-Oxo-Dodecanoyl-Homoserine Lactone Impacts Mitochondrial Networks Morphology, Energetics, and Proteome in Host Cells," *Front. Microbiol.*, vol. 11, May 2020.

[113] S. Tao *et al.*, "N-(3-oxododecanoyl)-L-homoserine lactone modulates mitochondrial function and suppresses proliferation in intestinal goblet cells," *Life Sci.*, vol. 201, pp. 81–88, May 2018.

[114] P. K. Singh, A. L. Schaefer, M. R. Parsek, T. O. Moninger, M. J. Welsh,

and E. P. Greenberg, "Quorum-sensing signals indicate that cystic fibrosis lungs are infected with bacterial biofilms," *Nature*, vol. 407, no. 6805, pp. 762–764, Oct. 2000.

[115] A. Atlante, L. De Bari, A. Bobba, E. Marra, P. Calissano, and S. Passarella, "Cytochrome c, released from cerebellar granule cells undergoing apoptosis or excytotoxic death, can generate protonmotive force and drive ATP synthesis in isolated mitochondria," *J. Neurochem.*, vol. 86, no. 3, pp. 591–604, Aug. 2003.

[116] W. C and Y. RJ, "The role of mitochondria in apoptosis*," *Annu. Rev. Genet.*, vol. 43, pp. 95–118, Dec. 2009.

[117] R. J. Youle and A. M. Van Der Bliek, "Mitochondrial fission, fusion, and stress," *Science*, vol. 337, no. 6098. American Association for the Advancement of Science, pp. 1062–1065, 31-Aug-2012.

[118] J. Ferlay *et al.*, "Global Cancer Observatory: Cancer Today.," *International Agency for Research on Cancer*, 2020. [Online]. Available: https://gco.iarc.fr/today. [Accessed: 11-Feb-2022].

[119] J. Lortet-Tieulent, I. Soerjomataram, J. Ferlay, M. Rutherford, E. Weiderpass, and F. Bray, "International trends in lung cancer incidence by histological subtype: adenocarcinoma stabilizing in men but still increasing in women," *Lung Cancer*, vol. 84, no. 1, pp. 13–22, Apr. 2014.

[120] Z. Chen, C. M. Fillmore, P. S. Hammerman, C. F. Kim, and K.-K. Wong, "Non-small-cell lung cancers: a heterogeneous set of diseases," *Nat. Rev. Cancer*, vol. 14, no. 8, pp. 535–546, Aug. 2014.

[121] M. Saito, H. Suzuki, K. Kono, S. Takenoshita, and T. Kohno, "Treatment of lung adenocarcinoma by molecular-targeted therapy and immunotherapy," *Surg. Today*, vol. 48, no. 1, Jan. 2018.

[122] L. Pan *et al.*, "PON2 subverts metabolic gatekeeper functions in B cells to promote leukemogenesis," *Proc. Natl. Acad. Sci.*, vol. 118, no. 7, p. e2016553118, Feb. 2021.

[123] A. Devarajan *et al.*, "Paraoxonase 2 overexpression inhibits tumor development in a mouse model of ovarian cancer," *Cell Death Dis*, vol. 9, no. 3, p. 392, 2018.

[124] T. W. M. Fan *et al.*, "Altered regulation of metabolic pathways in human lung cancer discerned by (13)C stable isotope-resolved metabolomics (SIRM).," *Mol. Cancer*, vol. 8, no. 1, p. 41, Jun. 2009.

[125] X. Wang *et al.*, "ER stress modulates cellular metabolism.," *Biochem. J.*, vol. 435, no. 1, pp. 285–96, Apr. 2011.

[126] T. W. M. Fan *et al.*, "Rhabdomyosarcoma cells show an energy producing anabolic metabolic phenotype compared with primary myocytes," *Mol. Cancer*, vol. 7, Oct. 2008.

[127] A. N. Lane, T. W.-M. Fan, and R. M. Higashi, "Stable isotope-assisted metabolomics in cancer research," *IUBMB Life*, vol. 60, no. 2, pp. 124–129, Feb. 2008.

[128] A. N. Lane, T. W. M. W. -M. Fan, and R. M. Higashi, "Isotopomer-Based Metabolomic Analysis by NMR and Mass Spectrometry," *Methods Cell Biol.*, vol. 84, pp. 541–588, Jan. 2008.

[129] S. Klebe and D. W. Henderson, "Facts and fiction: premalignant lesions of lung tissues.," *Pathology*, vol. 45, no. 3, pp. 305–15, Apr. 2013.

[130] D. Sulaiman *et al.*, "Paraoxonase 2 protects against acute myocardial ischemia-reperfusion injury by modulating mitochondrial function and oxidative stress via the PI3K/Akt/GSK-3β RISK pathway," *J. Mol. Cell. Cardiol.*, vol. 129, pp. 154–164, Apr. 2019.

[131] S. Horke, I. Witte, P. Wilgenbus, M. Kruger, D. Strand, and U. Forstermann, "Paraoxonase-2 reduces oxidative stress in vascular cells and decreases endoplasmic reticulum stress-induced caspase activation," *Circulation*, vol. 115, no. 15, pp. 2055–2064, 2007.

[132] G. Y. Liou and P. Storz, "Reactive oxygen species in cancer," *Free Radic. Res.*, vol. 44, no. 5, pp. 479–496, 2010.

[133] R. Pérez-Tomás and I. Pérez-Guillén, "Lactate in the Tumor Microenvironment: An Essential Molecule in Cancer Progression and Treatment," *Cancers (Basel).*, vol. 12, no. 11, pp. 1–29, Nov. 2020.

[134] S. Horke *et al.*, "Protective effect of paraoxonase-2 against endoplasmic reticulum stress-induced apoptosis is lost upon disturbance of calcium homoeostasis.," *Biochem. J.*, vol. 416, no. 3, pp. 395–405, Dec. 2008.

[135] M. Shiner, B. Fuhrman, and M. Aviram, "Paraoxonase 2 (PON2) expression is upregulated via a reduced-nicotinamide-adenine-dinucleotide-phosphate (NADPH)-oxidase-dependent mechanism during monocytes differentiation into macrophages," *Free Radic Biol Med*, vol. 37, no. 12, pp. 2052–2063, 2004.

[136] W. Dröge, "Free radicals in the physiological control of cell function," *Physiol. Rev.*, vol. 82, no. 1, pp. 47–95, 2002.

[137] U. S. Srinivas, B. W. Q. Tan, B. A. Vellayappan, and A. D. Jeyasekharan, "ROS and the DNA damage response in cancer," *Redox Biol.*, vol. 25, Jul. 2019.

[138] Y. Li *et al.*, "Discovery and analysis of hepatocellular carcinoma genes using cDNA microarrays," *J. Cancer Res. Clin. Oncol.*, vol. 128, no. 7, pp. 369–379, Jul. 2002.

[139] T. Ribarska, M. Ingenwerth, W. Goering, R. Engers, and W. A. Schulz, "Epigenetic inactivation of the placentally imprinted tumor suppressor gene TFPI2 in prostate carcinoma," *Cancer Genomics and Proteomics*, vol. 7, no. 2, pp. 51–60, 2010.

[140] M. E. Ross *et al.*, "Classification of pediatric acute lymphoblastic leukemia by gene expression profiling," *Blood*, vol. 102, no. 8, pp. 2951–2959, Oct. 2003.

[141] R. J. DeBerardinis and N. S. Chandel, "We need to talk about the Warburg effect," *Nat. Metab.*, vol. 2, no. 2, pp. 127–129, Feb. 2020.

[142] J. M. Funes *et al.*, "Transformation of human mesenchymal stem cells increases their dependency on oxidative phosphorylation for energy production," *Proc. Natl. Acad. Sci. U. S. A.*, vol. 104, no. 15, p. 6223, Apr. 2007.

[143] F. Weinberg *et al.*, "Mitochondrial metabolism and ROS generation are essential for Kras-mediated tumorigenicity," *Proc. Natl. Acad. Sci. U. S. A.*,

vol. 107, no. 19, pp. 8788–8793, May 2010.

[144] T. Bacchetti *et al.*, "Paraoxonase-2: A potential biomarker for skin cancer aggressiveness," *Eur. J. Clin. Invest.*, vol. 51, no. 5, May 2021.

[145] X. Wang *et al.*, "The clinical and prognostic significance of paraoxonase-2 in gastric cancer patients: immunohistochemical analysis," *Hum. Cell*, vol. 32, no. 4, pp. 487–494, Oct. 2019.

[146] T. Bacchetti, D. Sartini, V. Pozzi, T. Cacciamani, G. Ferretti, and M. Emanuelli, "Exploring the role of paraoxonase-2 in bladder cancer: analyses performed on tissue samples, urines and cell cultures," *Oncotarget*, vol. 8, no. 17, pp. 28785–28795, 2017.

[147] A. Onn *et al.*, "Development of an orthotopic model to study the biology and therapy of primary human lung cancer in nude mice," *Clin Cancer Res*, vol. 9, no. 15, pp. 5532–5539, Nov. 2003.

[148] M. DuPage, A. L. Dooley, and T. Jacks, "Conditional mouse lung cancer models using adenoviral or lentiviral delivery of Cre recombinase," *Nat. Protoc.*, vol. 4, no. 7, pp. 1064–1072, Jul. 2009.

[149] A. H. Fischer, K. A. Jacobson, J. Rose, and R. Zeller, "Hematoxylin and eosin staining of tissue and cell sections," *CSH Protoc.*, vol. 2008, no. 5, May 2008.

[150] M. Koren-Gluzer, M. Rosenblat, and T. Hayek, "Paraoxonase 2 Induces a Phenotypic Switch in Macrophage Polarization Favoring an M2 Anti-Inflammatory State," *Int J Endocrinol*, vol. 2015, p. 915243, Dec. 2015.

[151] Y. Pan, Y. Yu, X. Wang, and T. Zhang, "Tumor-Associated Macrophages in

Tumor Immunity," *Front. Immunol.*, vol. 11, Dec. 2020.

[152] E. A. Collisson *et al.*, "Comprehensive molecular profiling of lung adenocarcinoma," *Nature*, vol. 511, no. 7511, pp. 543–550, 2014.

[153] M. Imielinski *et al.*, "Mapping the hallmarks of lung adenocarcinoma with massively parallel sequencing," *Cell*, vol. 150, no. 6, pp. 1107–1120, Sep. 2012.

[154] E. L. Jackson *et al.*, "Analysis of lung tumor initiation and progression using conditional expression of oncogenic K-ras," *Genes Dev.*, vol. 15, no. 24, pp. 3243–3248, Dec. 2001.

[155] A. Arnal-Estapé, G. Foggetti, J. H. Starrett, D. X. Nguyen, and K. Politi, "Preclinical Models for the Study of Lung Cancer Pathogenesis and Therapy Development," *Cold Spring Harb. Perspect. Med.*, vol. 11, no. 12, 2021.

[156] P. Mirabelli, L. Coppola, and M. Salvatore, "Cancer Cell Lines Are Useful Model Systems for Medical Research," *Cancers (Basel).*, vol. 11, no. 8, Aug. 2019.

[157] N. M. Anderson and M. C. Simon, "Tumor Microenvironment," *Curr. Biol.*, vol. 30, no. 16, p. R921, Aug. 2020.

[158] P. I. Ribeiro Franco, A. P. Rodrigues, L. B. de Menezes, and M. Pacheco Miguel, "Tumor microenvironment components: Allies of cancer progression," *Pathol. Res. Pract.*, vol. 216, no. 1, Jan. 2020.

[159] R. Baghban *et al.*, "Tumor microenvironment complexity and therapeutic implications at a glance," *Cell Commun. Signal.*, vol. 18, no. 1, Apr. 2020.

[160] M. Reina-Campos, J. Moscat, and M. Diaz-Meco, "Metabolism shapes the tumor microenvironment," *Curr. Opin. Cell Biol.*, vol. 48, pp. 47–53, Oct. 2017.

[161] C. A. Lyssiotis and A. C. Kimmelman, "Metabolic Interactions in the Tumor Microenvironment," *Trends Cell Biol.*, vol. 27, no. 11, pp. 863–875, Nov. 2017.

[162] A. N. Lau and M. G. Vander Heiden, "Metabolism in the Tumor Microenvironment," *Annu. Rev. Cancer Biol.*, vol. 4, pp. 17–40, Mar. 2020.

[163] R. T. Sadikot, T. S. Blackwell, J. W. Christman, and A. S. Prince, "Pathogen–Host Interactions in Pseudomonas aeruginosa Pneumonia," *https://doi.org/10.1164/rccm.200408-1044SO*, vol. 171, no. 11, pp. 1209–1223, Dec. 2012.

[164] O. Zaborina *et al.*, "Identification of multi-drug resistant Pseudomonas aeruginosa clinical isolates that are highly disruptive to the intestinal epithelial barrier," *Ann. Clin. Microbiol. Antimicrob.*, vol. 5, Jun. 2006.

[165] F. Bishehsari *et al.*, "Alcohol and Gut-Derived Inflammation," *Alcohol Res.*, vol. 38, no. 2, p. 163, 2017.

[166] X. Zhang *et al.*, "Indolyl-chalcone derivatives induce hepatocellular carcinoma cells apoptosis through oxidative stress related mitochondrial pathway in vitro and in vivo," *Chem. Biol. Interact.*, vol. 293, pp. 61–69, Sep. 2018.

[167] J. M. Henderson *et al.*, "Multiple liver insults synergize to accelerate experimental hepatocellular carcinoma," *Sci. Rep.*, vol. 8, no. 1, Dec. 2018.

ABBREVIATIONS

α-KG	Alpha-ketoglutarate
Δy_{mito}	Mitochondrial membrane potential
AALAC	Association for Assessment and Accreditation of Laboratory Animal Care
Ab	Antibody
AD	Alzheimer's disease
AHL	Acyl-homoserine lactone
ALL	Acute lymphoblastic leukemia
AMPK	AMP-activated protein kinase
ANOVA	Analysis of variance
ATCC	American Type Culture Collection
ATP	Adenosine triphosphate
B-ALL	B-cell acute lymphoblastic leukemia
BC	Bladder cancer
BCA	Bicinchoninic acid
BEGM	Bronchial Epithelial Cell Growth Medium
C12	N-(3-oxododecanoyl)-l-homoserine lactone
C12-COOH	N-(3-oxododecanoyl)-l-homoserine lactone acid
cDNA	Complementary DNA
CF	Cystic fibrosis
ChIP	Chromatin immunoprecipitation
CHOP	CCAAT/-enhancer-binding protein homologous protein
CML	Chronic myelogenous leukemia
CoQ10	Coenzyme Q10
CRISPR	Clustered randomly interspaced short palindromic repeats
C_T	Threshold cycle
DAPT	N-[N-(3,5-Difluorophenacetyl-L-alanyl)]-(S)-phenylglycine t-butyl ester
DCF	Dichlorofluorescein
DEN	Diethylnitrosamine
DEVD	Aspartate-Glutamate-Valine-Aspartate
DMEM	Dulbecco's Modified Eagle Medium
DMNQ	2,3-dimethoxy-1,4-naphthalenedione
DMSO	Dimethylsulfoxide
DSB	Double strand break

DSS	Sodium trimethylsilylpropanesulfonate
ECAR	Extracellular acidification rate
EDTA	Ethylenediaminetetraacetic acid
ER	Endoplasmic reticulum
ERK1/2	extracellular signal-regulated protein kinase 1 and 2
ETC	Electron transport chain
FACS	Fluorescence-activated cell sorting
FBS	Fetal bovine serum
FFPE	Formalin-fixed, paraffin-embedded
GFP	Green fluorescent protein
GLUT1	Glucose transporter 1
H&E	Hematoxylin and Eosin
H_2DCFDA	2',7'-dichlorodihydrofluorescein diacetate
HBE	Human bronchial epithelial cell
HBSS	Hank's Balanced Salt Solution
HCC	Hepatocellular carcinoma
HDL	High density lipoprotein
HPLC	High-performance liquid chromatography
hPON2	Human paraoxonase 2
HSQC	Heteronuclear single quantum coherence
IACUC	Institute for Animal Care and Use Committee
IGF-1	Insulin like growth factor 1
IgG	Immunoglobulin G
KRT5	Cytokeratin 5
LC-MS	Liquid chromatography-mass spectrometry
LDL	Low density lipoprotein
LLC	Lewis lung carcinoma
MEF	Mouse embryonic fibroblast
MeOH	Methanol
MPM	Mouse peritoneal macrophage
mPON2	Mouse paraoxonase 2
mPON3	Mouse paraoxonase 3
mRNA	Messenger RNA
NADPH	Nicotinamide adenine dinucleotide phosphate
NMR	Nuclear magnetic resonance
NSAID	Non-steroidal anti-inflammatory drug
NSCLC	Non-small cell lung carcinoma
nt	nucleotide
OAA	Oxaloacetate
OC	Ovarian cancer
OCR	Oxygen consumption rate
OD	Optical density

OS	Overall survival
OSCC	Oral squamous cell carcinoma
PBS	Phosphate-buffered saline
PCR	Polymerase chain reaction
PD	Parkinson's disease
PDAC	Pancreatic ductal adenocarcinoma
PGC-1α	Peroxisome proliferator-activated receptor-γ coactivator-1α
PI	Propidium iodide
PON1	Paraoxonase 1
PON2	Paraoxonase 2
PON2-KO	Paraoxonase 2 knockout
PON3	Paraoxonase 3
PPP	Pentose phosphate pathway
PTM	Post-translational modification
PVDF	polyvinylidene difluoride
Rb	Retinoblastoma
RFS	Relapse-free survival
RFU	Relative fluorescence units
RNAi	RNA interference
ROCK	Rho-associated, coiled-coil containing protein kinase
ROS	Reactive oxygen species
RT-PCR	Quantitative reverse transcriptase polymerase chain reaction
SD	Standard deviation
sgRNA	Single guide RNA
shRNA	Small hairpin RNA
SIRM	Stable isotope-resolved metabolomics
siRNA	Small interfering RNA
SNP	Single nucleotide polymorphism
SOX2	Sex determining region Y-box 2,
SREBP-2	Sterol regulatory binding protein-2
STR	Short tandem repeat
SV-40	Simian virus 40
T2DM	Type 2 diabetes mellitus
TAA	Thioacetamide
TCA cycle	Tricarboxylic acid cycle
TCGA	The Cancer Genome Atlas
TEC	Tracheal epithelial cell
TME	Tumor microenvironment
TMRE	Tetramethylrhodamine
TOCSY	Total correlation spectroscopy
TP63	Tumor protein 63
uPa	Urokinase plasminogen activator
UPR	Unfolded protein response

UTP	Uridine triphosphate
UV	Ultraviolet
VLDL	Very low density lipoprotein
WT	Wild type

CURRICULUM VITAE

Aaron G. Whitt

University of Louisville School of Medicine
Dept. of Pharmacology and Toxicology
505 S Hancock Street
CTRB 433A
Louisville, KY 40202
agwhit05@louisville.edu
Phone: (606) 356-3754

EDUCATION

2017-Present   University of Louisville
Ph.D., Pharmacology and Toxicology

2006-2010   Morehead State University
B.S., Biology

HONORS AND AWARDS

2019-2021   NIEHS T32 Training Grant Fellowship

2020   University of Louisville. Research! Louisville. Second place poster award, Doctoral Basic Science Graduate Student category.

2020   NIEHS Superfund Research Program annual meeting. Top poster award.

2020   University of Louisville. Graduate Student Regional Research Conference. Honorable mention poster award.

2018   University of Louisville. Research! Louisville. Second place poster award, Master's Basic Science Graduate Student category.

2017-2019   University of Louisville Integrated Programs in Biomedical Sciences (IPIBS) fellowship award.

PROFESSIONAL EXPERIENCE

2014-2017   Research Technician, University of Louisville Brown Cancer Center, Louisville, KY.

2012-2014   Laboratory Analyst I, Microbac Laboratories, Louisville Division, Louisville, KY.

2011-2012   Laboratory Analyst I, Microbac Laboratories, Lexington Division, Lexington, KY.

2009-2011   Laboratory Technician, Morehead State University Water Testing Laboratory, Morehead, KY.

2008   Research Assistant, Morehead State University Dept. of Psychology, Morehead, KY.

PROFESSIONAL MEMBERSHIPS

2015-Present   Society of Toxicology (OVSOT)

2015-Present   American Association for the Advancement of Science

2019-Present   American Society of Microbiology

ABSTRACTS

1. <u>Whitt, A.</u>, Jiu-Zhen, J., Arumugam, S., Burlison, J., Li, C. Investigating the role of paraoxonase 2 in non-small cell lung carcinoma. Research! Louisville. November 2021.

2. <u>Whitt, A.</u>, Dela Cerna, M., Burlison, J., Lee, D., Li, C. Inhibiting lung adenocarcinoma by a bacterial quorum-sensing molecule. Ohio Valley Society of Toxicology summer meeting. July 2021.

3. <u>Whitt, A.</u>, Jiu-Zhen, J., Burlison, J., Hill, B., White, C., Li, C. Paraoxonase 2 mediates metabolic reprogramming of murine tracheal epithelial cells in response to the quorum-sensing molecule n-(3-oxododecanoyl)-l-

homoserine lactone. American Society of Pharmacology and Experimental Therapeutics annual meeting. April 2021.

4. Whitt, A., Jiu-Zhen, J., Burlison, J., Hill, B., White, C., Li, C. Paraoxonase 2 mediates disruptions to mitochondrial function in response to the quorum-sensing molecule N-(3-oxododecanoyl)-l-homoserine lactone. University of Louisville Graduate Student Regional Research Conference. March 2021.

5. Whitt, A., Jiu-Zhen, J., Arumugam, S., Burlison, J., Li, C. Exploring the role of paraoxonase 2 in non-small cell lung carcinoma. National Institute of Environmental Health Sciences Superfund Research annual meeting. December 2020.

6. Whitt, A., Jiu-Zhen, J., Arumugam, S., Burlison, J., Li, C. Investigating the role of paraoxonase 2 in non-small cell lung carcinoma. Ohio Valley Society of Toxicology fall meeting. November 2020.

7. Whitt, A., Jiu-Zhen, J., Arumugam, S., Burlison, J., Li, C. The role of paraoxonase 2 in non-small cell lung carcinoma. Ohio Valley Society of Toxicology summer meeting. July 2020.

8. Whitt, A., Jiu-Zhen, J., Arumugam, S. Burlison, J. Li, C. Characterizing the role of Paraoxonase 2 in non-small cell lung carcinoma. American Society of Microbiology- Microbe. August 2020.

9. Whitt, A., Jiu-Zhen, J., Burlison, J., Li, C. Paraoxonase 2 mediates metabolic reprogramming in mouse airway epithelial cells in response to N-3-oxododecanoyl-l-homoesrine lactone. Research! Louisville. September 2019.

10. Meng, S., Whitt, A., Tu, A., Eaton, J.W., Yaddanapudi, K., Li, C. An embryonic stem cell-based vaccine in lung cancer prevention. Research! Louisville. September 2019.

11. Whitt, A., Jiu-Zhen, J., Neely, A., Li, C. Paraoxonase 2 plays a critical role in non-small cell lung carcinoma proliferation. OVSOT Summer Meeting. June 2019.

12. Meng, S., Whitt, A., Tu, A., Eaton, J.W., Yaddanapudi, K., Li, C. A novel embryonic stem cell-based vaccine for the prevention against lung cancer. OVSOT Summer Meeting. June 2019.

13. Meng, S., <u>Whitt, A.</u>, Eaton, J., Yaddanapudi, K., Li, C., Al-Rayyan, N., Tu, A. A Novel Embryonic Stem Cell-based Vaccine for the Prevention of Lung Cancer. Experimental Biology. April 2019.

14. <u>Whitt, A.</u>, Neely, A., Jiu-Zhen, J., Li, C. Paraoxonase 2 plays a critical role in non-small cell lung carcinoma proliferation. Kentucky Lung Cancer Research Program Symposium. September 2018. (Event cancelled).

15. <u>Whitt, A.</u>, Neely, A., Jiu-Zhen, J., Li, C. Paraoxonase 2 plays a critical role in non-small cell lung carcinoma proliferation. Research! Louisville. October 2018.

16. Meng, S., <u>Whitt, A.</u>, Eaton, J., Yaddanapudi, K., Li, C., Al-Rayyan, N., Tu, A. Exosomes from embryonic stem cells against lung cancer as a prophylactic vaccine. Research! Louisville. October 2018.

<u>POSTERS</u>

1. Research! Louisville. University of Louisville. October 2021.

2. Ohio Valley Society of Toxicology summer meeting. Online 3-minute thesis presentation. July 2021.

3. Research! Louisville. University of Louisville. October 2021.

4. American Society for Pharmacology and Experimental Therapeutics annual meeting. Online poster presentation. April 2021

5. University of Louisville Graduate Student Regional Research Conference. Online poster presentation. March 2021.

6. NIEHS Superfund Research Program annual meeting. Online poster presentation. December 2020.

7. Ohio Valley Society of Toxicology fall meeting. Online graphical abstract presentation. November 2020.

8. Ohio Valley Society of Toxicology summer meeting. Online graphical abstract presentation. July 2020.

9. American Society of Microbiology- Microbe annual meeting. Online poster presentation. June 2020.

10. Research! Louisville. University of Louisville. September 2019.

11. Ohio Valley Society of Toxicology Summer Meeting. June 2019.

12. Research! Louisville. University of Louisville. October 2018.

<u>PUBLICATIONS</u>

1. Whitt AG, Jiu-Zhen J, Meng S, Conroy LR, Burlison JA, Hill BG, Clem BF, White C, Li C. Paraoxonase 2 mediates mitochondrial dysfunction in response to the bacterial quorum sensing molecule N-(3-oxododecanoyl)-l-homoserine lactone. *Submitted for publication.* Dept. of Pharmacology and Toxicology, University of Louisville.

2. Meng S., Whitt AG., Tu A, Eaton JW, Li C, Yaddanapudi K. Isolation of exosome-enriched extracellular vesicles carrying granulocyte-macrophage colony-stimulating factor from embryonic stem cells. *J Vis Exp.* 2021 Nov 11;(177). doi: 10.3791/60170. PMID: 34842232.

3. Yaddanapudi K, Meng S, Whitt AG, Al Rayyan N, Richie J, Tu A, Eaton JW, Li C. Exosomes from GM-CSF expressing embryonic stem cells are an effective prophylactic vaccine for cancer prevention. *Oncoimmunology.* 2019 Jan 9;8(3):1561119. doi: 10.1080/2162402X.2018.1561119. PMID: 30723593; PMCID: PMC6350682.

4. Neely AM, Zhao G, Schwarzer C, Stivers NS, Whitt AG, Meng S, Burlison JA, Machen TE, Li C. N-(3-Oxo-acyl)-homoserine lactone induces apoptosis primarily through a mitochondrial pathway in fibroblasts. *Cell Microbiol.* 2018 Jan;20(1):10.1111/cmi.12787. doi: 10.1111/cmi.12787. Epub 2017 Oct 9. PMID: 28876505; PMCID: PMC5729120.

5. Zhao G, Neely AM, Schwarzer C, Lu H, Whitt AG, Stivers NS, Burlison JA, White C, Machen TE, Li C. N-(3-oxo-acyl) homoserine lactone inhibits tumor growth independent of Bcl-2 proteins. *Oncotarget.* 2016 Feb 2;7(5):5924-42. doi: 10.18632/oncotarget.6827. PMID: 26758417; PMCID: PMC4868731.

6. Schwarzer C, Fu Z, Morita T, Whitt AG, Neely AM, Li C, Machen TE. Paraoxonase 2 serves a proapopotic function in mouse and human cells in response to the Pseudomonas aeruginosa quorum-sensing molecule N-(3-Oxododecanoyl)-homoserine lactone. *J Biol Chem.* 2015 Mar

13;290(11):7247-58. doi: 10.1074/jbc.M114.620039. Epub 2015 Jan 27.
PMID: 25627690; PMCID: PMC4358143.